INFORMATION TO USERS

This manuscript has been reproduced from the microfilm master. UMI films the text directly from the original or copy submitted. Thus, some thesis and dissertation copies are in typewriter face, while others may be from any type of computer printer.

The quality of this reproduction is dependent upon the quality of the copy submitted. Broken or indistinct print, colored or poor quality illustrations and photographs, print bleedthrough, substandard margins, and improper alignment can adversely affect reproduction.

In the unlikely event that the author did not send UMI a complete manuscript and there are missing pages, these will be noted. Also, if unauthorized copyright material had to be removed, a note will indicate the deletion.

Oversize materials (e.g., maps, drawings, charts) are reproduced by sectioning the original, beginning at the upper left-hand corner and continuing from left to right in equal sections with small overlaps.

ProQuest Information and Learning
300 North Zeeb Road, Ann Arbor, MI 48106-1346 USA
800-521-0600

NOTE TO USERS

This reproduction is the best copy available.

UMI®

UNIVERSITY OF ALBERTA

EFFECT OF LIQUID PROPERTIES ON SEPARATION EFFICIENCY IN A RANDOMLY PACKED DISTILLATION COLUMN

by

ANDREA JACQUELINE BADER

A thesis submitted to the Faculty of Graduate Studies and Research in partial fulfillment of the requirements for the degree of Master of Science

in

CHEMICAL ENGINEERING

Department of Chemical and Materials Engineering

Edmonton, Alberta

Fall, 2005

DEDICATION

I would like to dedicate this work to my grandparents Frieda, Ken and Phyllis. They were essential in teaching me the acts of love, support and hard work. I miss you every day but I feel your love and support around me wherever I go.

ABSTRACT

The effects of the liquid properties on distillation packing efficiency were investigated experimentally. Tests were carried out using surface tension positive (methanol/water, n-heptane/toluene and isopropanol/water), negative (benzene/n-heptane, water/acetic acid and water/isopropanol) and neutral (methanol/isopropanol and cyclohexane/n-heptane) systems. Ceramic Intalox® saddles, 7 mm in diameter, were used as the packing material. The distillation column was operated under total reflux and at atmospheric pressure (94 kPa).

For the surface tension positive and negative systems, lower HETP values were observed over the middle concentration range of the more volatile component, accompanied by a sharp increase in HETP at the high concentration regions. The experimental results suggested the surface tension gradient and thermal distillation were dominant factors affecting HETP in surface tension positive systems and thermal distillation was a dominant factor in surface tension negative systems. For the cyclohexane/n-heptane system, HETP remained relatively constant over the entire concentration range investigated, and for the methanol/isopropanol system, HETP decreased with increasing methanol concentration. It was believed that liquid viscosity was the most significant factor affecting HETP for the neutral systems. It was not possible to quantify the individual effects of each factor due to the limited number of test systems used. Furthermore, the measured HETP values were also compared to Murphree Efficiency data and the results suggested that both packed and tray columns are influenced in a similar manner by the surface tension gradient, thermal distillation and viscosity.

ACKNOWLEDGEMENTS

I would like to express my appreciation to Dr. Karl T. Chuang for his guidance and support throughout this project. His expertise was a valuable asset to the success of this research. Special thanks are also extended for his financial support throughout this project.

I would like to sincerely thank Mr. Artin Afacan for his guidance, support and optimism. His technical skills, knowledge of the field of distillation and handling of benzene were greatly appreciated! Thank you for being a mentor and a friend.

I would like to extend a special thanks to Dave Sharp and Dr. Tony Yeung for their advice and assistance, and to the instrument and machine shop staff for their technical expertise.

Most importantly, I would like to thank my parents, Dan and Marilyn, and my sister, Kerri, for their love and support. Thank you for always believing in my potential to achieve...so much for beauty school eh!

TABLE OF CONTENTS

LIST OF TABLES

LIST OF FIGURES

NOMENCLATURE

D_L	Liquid phase diffusivity, m^2/s
D_P	Bubble diameter, mm
D_V	Vapor phase diffusivity, m^2/s
E_{MV}	Murphree tray efficiency, %
HETP	Height equivalent to a theoretical plate, m
L	Molar flow rate of liquid, (kmol/s)
M	Mass flow rate, kg/s
m	Slope of the equilibrium line
N_G	Number of gas phase transfer units
N_L	Number of liquid phase transfer units
N_{OG}	Number of overall gas transfer units
N_T	Number of theoretical trays
RR	Rotameter reading, %
S	Tray spacing, m
V	Molar flow rate of vapor, (kmol/s)
x	liquid mole fraction
y	Vapor mole fraction
y^*	Vapor composition in equilibrium with x
z	Height of packing, m

Greek Letters

α	Relative volatility
ΔH_{vap}	Latent heat of vaporization, kJ/kg
λ	Ratio of the slope of the equilibrium line to the slope of the operating line
μ_L	Saturated liquid viscosity, $N \cdot s/m^2$
μ_V	Saturated vapor viscosity, $N \cdot s/m^2$
ρ_L	Saturated liquid density, kg/m^3
ρ_V	Saturated vapor density, kg/m^3
σ	Surface tension, mN/m

Chapter 1

INTRODUCTION

Distillation is the most prevalent separation process used worldwide in refineries, petrochemical plants, organic chemical plants and gas processing plants. There are two main types of column internals used in industrial applications: trays and packing. Tray columns are more efficient at higher operating pressures and offer better design reliability for large diameter columns. Tray columns are suitable for fouling service, offer feed point flexibility and have low cost internals. There is moderate to high pressure drop per tray therefore tray columns are not ideal for low pressure operations or operations where low flow rates are required. Packed columns are less suitable for fouling compared to trays, however, ceramic or polymeric packing can be used in place of metal packing to reduce the degree of fouling. Packed columns offer no feed point flexibility and liquid maldistribution significantly reduces the separation efficiency of the packing therefore packed columns should be restricted to operations requiring column diameters less than 0.914 m (Coker, 1991). With low-pressure drop across the packed bed, it is ideal to carry out vacuum and low-pressure operations in a packed column. As a result of the low-pressure drop, operating expenses are lower and increasing liquid rates result in increased capacity due to low liquid holdup.

The degree of separation achievable in either type of column is a function of the interfacial area available for vapor-liquid contact. In tray columns this interfacial area is unsupported. Vapor bubbles rise up through the liquid holdup on each tray and mass transfer occurs at the vapor-liquid interface or on the bubble surfaces. The interfacial area available for mass transfer depends on bubble size and stability for a particular tray geometry. Efficiency in tray columns is largely a function of the liquid properties and, to a lesser extent, of tray design. In packed columns the interfacial area is supported. A liquid film forms on the packing surface and mass transfer occurs at the film surface as vapor rises up through the packed bed. The interfacial area available for vapor-liquid contact depends on the stability of the liquid film.

Packing efficiency, called height equivalent to a theoretic plate or HETP, is a function of packing type, size and material of construction and as well, the liquid properties. The selection of a tray or packed column for a given separation depends on the operating conditions, column dimensions, and characteristics of the system to be separated so as to maximize separation efficiency and column capacity while minimizing energy requirements and product waste.

It has been long established that tray efficiencies are system dependent. The effective interfacial area depends largely on the properties of the liquid components, specifically static surface tension, the surface tension gradient, viscosity, density and diffusivity. Extensive research has been done to investigate the effects of surface tension and the surface tension gradient on tray efficiency (van Wijk and Thijssen, 1954; Zuiderweg and Harmens, 1958; Kister 1992; Wong, 1993; Yang and Chuang, 1995; Syeda, 2002). A general consensus is the surface tension gradient has a more profound effect on separation efficiency over surface tension forces when operation is in the froth regime. Zuiderweg and Harmens (1958) classified distillation systems based on the relative surface tension of the two components that constitute a binary system as surface tension positive, surface tension negative or surface tension neutral. A mixture is surface tension positive if the more volatile component has lower surface tension; conversely, if the more volatile component has higher surface tension the mixture is surface tension negative. If both components exhibit similar surface tension, the mixture is surface tension neutral. Previous studies have found surface tension positive systems exhibit higher tray efficiencies compared to surface tension negative and neutral systems (van Wijk and Thijssen, 1954; Zuiderweg and Harmens, 1958; Wong, 1993; Syeda, 2002). The higher tray efficiencies obtained for the positive systems can be partially attributed to Marangoni forces present on the bubbles surfaces that act to stabilize the vapor bubbles and therefore aid in froth stabilization. Figure 1.1 illustrates how bubble stabilization occurs in surface tension positive systems. The bulk liquid in Figure 1.1(a) represents the liquid holdup on a typical tray and the bubbles represent vapor rising up through the liquid holdup. As mass transfer takes place on the bubble surfaces, the more volatile component is

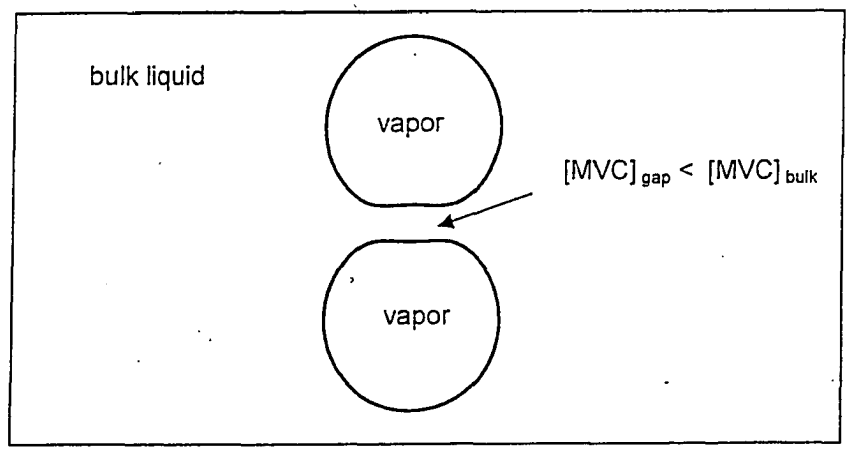

(a) MVC = More Volatile Component

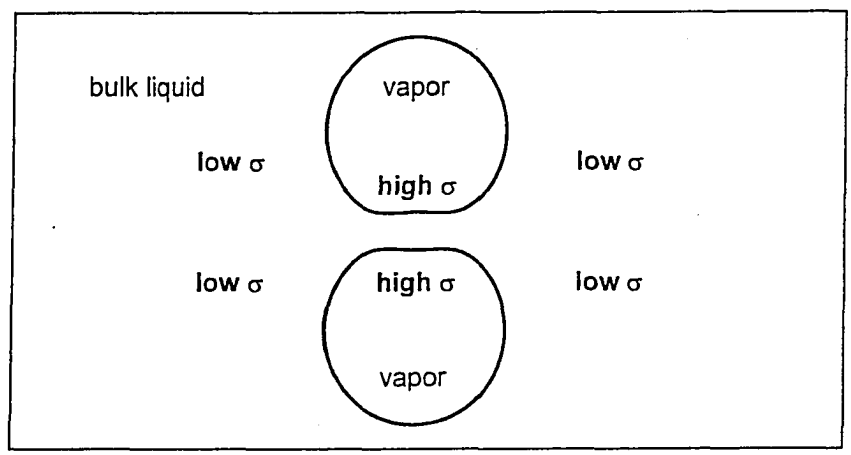

(b)

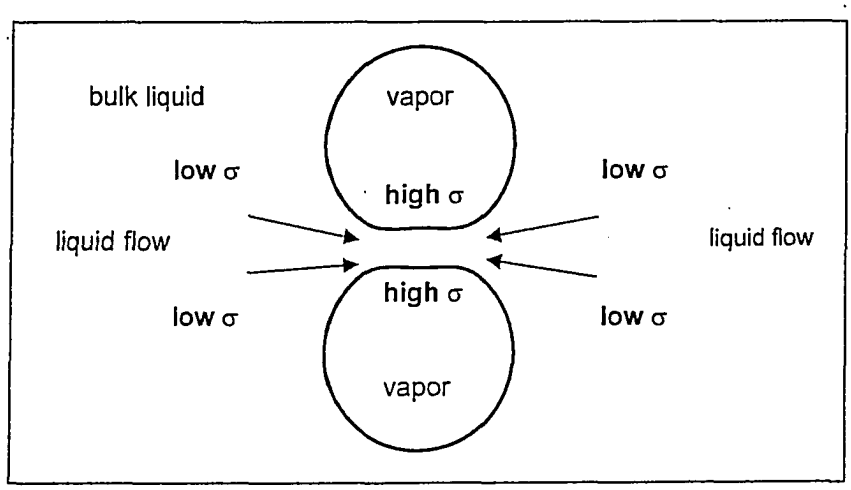

(c)

Figure 1.1 Bubble stabilization that occurs in surface tension positive systems.

removed from the thin film or gap that exists between the individual vapor bubbles. Removal of the more volatile component from the gap creates not only a concentration gradient but also a surface tension gradient, as illustrated in Figure 1.1(b). The liquid flows up the surface tension gradient, from lower surface tension to higher surface tension. As shown in Figure 1.1(c), the liquid flows into the gap and acts to stabilize the vapor bubbles by preventing coalescence. The smaller stable bubbles provide greater interfacial area available for mass transfer and therefore higher tray efficiencies result.

Sharp (2000) studied the effect of methanol concentration on bubble diameter for a methanol/water system using a 2-D bubble column. His results are presented in Figure 1.2. Smaller bubbles were observed over the middle concentration range. These smaller bubbles remain distinct and therefore provide a stabilized froth, which results in greater interfacial area available for mass transfer. The bubble size increases as the system concentration approaches pure methanol or pure water due to the coalescence of smaller bubbles. The photographs in Figure 1.3 were taken in the 2-D bubble column at pure water and pure methanol concentrations, and at various concentrations between the pure components. At pure water and methanol concentrations, larger bubbles form as a result of the coalescence of smaller unstable bubbles due to the absence of a surface tension gradient. As the system concentration is varied, an abundance of smaller, stable bubbles can be seen, which results in an obvious increase in the interfacial area available for mass transfer. Surface tension negative and neutral systems do not exhibit froth stabilization; consequently, lower tray efficiencies are obtained for these systems compared to surface tension positive systems. A typical efficiency trend for a positive system, based on surface tension gradient effects, should consist of higher tray efficiencies over the middle concentration range of the more volatile component, and efficiency should decrease as the system approaches the pure component concentrations. Over the middle concentration range, the vapor bubbles remain distinct and therefore provide greater interfacial area available for mass transfer. Marangoni forces are stronger over this range due to the larger surface tension gradient that exists between the bulk liquid and the thin liquid film present between the individual bubbles. The liquid flow into the

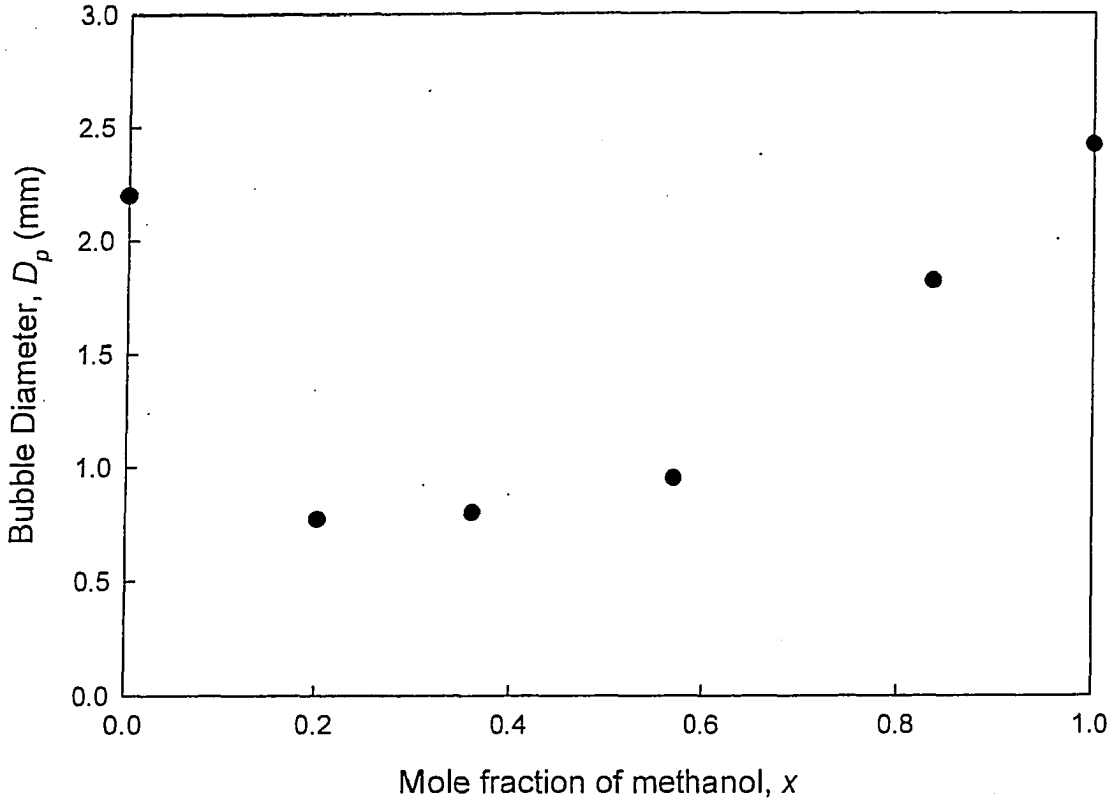

Figure 1.2 Bubble Diameter as a function of methanol concentration for a methanol/water system using a 2-D bubble column.

gap prevents coalescence of the vapor bubbles. Near pure component concentrations, the magnitude of the surface tension gradient diminishes because the bulk liquid and liquid film approach similar concentrations. The vapor bubbles coalesce because there is little force keeping them apart. This reduction in interfacial area results in lower observed tray efficiencies.

Syeda (2002) separated surface tension positive (methanol/water, n-heptane/toluene), surface tension negative (benzene/n-heptane, water/acetic acid) and surface tension neutral (methanol/isopropanol, cyclohexane/n-heptane) systems using a sieve tray column to examine the effect of the surface tension gradient on tray efficiency. She found, in accordance with literature (van Wijk and Thijssen, 1954; Zuiderweg and Harmens, 1958; Ruckenstein and Smigelschi, 1967), that much higher point efficiencies were observed over the middle concentration range of the more volatile component for the surface tension positive systems and that these systems showed a pronounced decrease in point efficiency as the system concentration

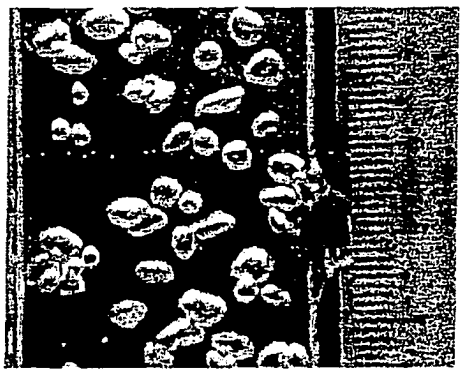

(a) Pure water

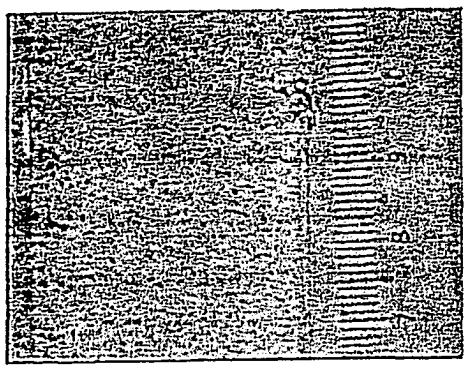

(b) 6 mole % methanol

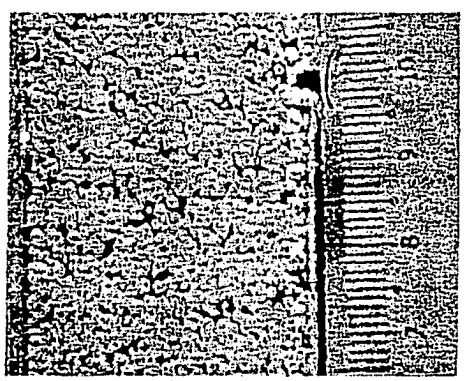

(c) 24 mole % methanol

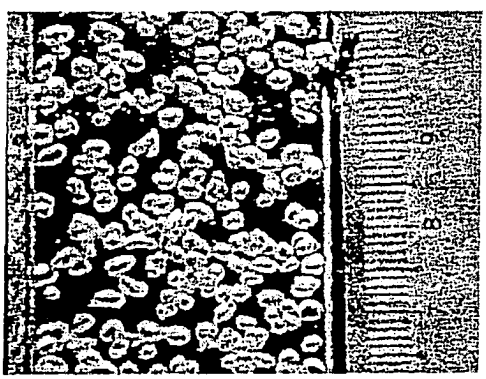

(d) 84 mole % methanol

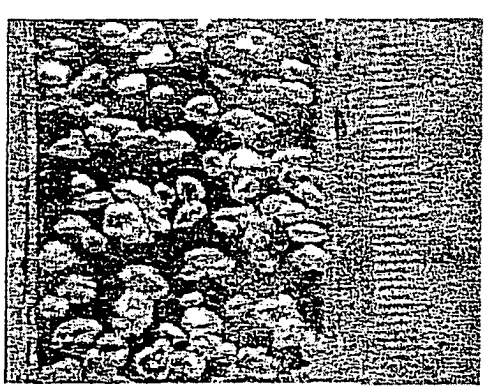

(e) Pure methanol

Figure 1.3 Photographs of the concentration effect on bubble diameter for a methanol/water system using a 2-D bubble column.

approached that of the pure components. The change in efficiency with concentration for the negative and neutral systems was not as significant compared to that for the positive system.

Kister (1992), Wong (1993) and Yang and Chuang (1995) also discussed the effects of liquid density, viscosity and diffusivity on tray efficiency. Kister (1992) reported that tray efficiency increased with decreasing viscosity, stating that lower viscosity typically implies higher liquid diffusivity and therefore lower resistance to mass transfer in the liquid phase. He also found that distillation of higher viscosity liquids results in the formation of larger bubbles, which generates less interfacial area for mass transfer. Wong (1993) separated a chloroform/toluene (surface tension neutral) system using a sieve tray column. He found that tray efficiency drastically increased with increasing chloroform concentration due to presence of a density gradient in the liquid phase. He stated that the significant density change within the system results in the formation of a density gradient, which in turn increases the liquid phase mass transfer coefficient and therefore tray efficiency. Yang and Chuang (1995) used the Chen and Chuang (1993) Model to simulate the effects of the physical properties on tray efficiency. They found that liquid viscosity, density and diffusivity significantly influence mass transfer coefficients. Their results showed that tray efficiency decreases with increasing viscosity and increases with increasing density and diffusivity.

In addition to the mass transfer resulting from contact distillation, Danckwerts et al. (1960) and Ruckenstein and Smigelschi (1967) suggest that mass transfer also occurs as a result of thermal distillation. They speculate that it is possible for vapor to condense on the liquid interface and liquid to evaporate through bubble formation or by flashing at freshly formed surfaces, explaining that the degree of mass transferred by thermal distillation depends on the rate of heat transfer between the liquid and vapor phases. They also speculate that the effect of thermal distillation should be the most significant where the temperature difference between the two bulk phases is the greatest.

Studies to date focusing on the effects of the liquid properties on separation efficiency in packed columns have proven to be incomplete and have failed to clearly define the extent to which liquid properties affect separation efficiency. Furthermore, there have been no studies found in open literature comparing tray and packing efficiencies on a similar level to determine if tray and packing efficiencies are influenced in a similar manner by the liquid properties.

The separation efficiency of a packed column is measured in terms of HETP. Obvious factors affecting HETP values include packing size, structure, material of construction and the liquid properties of the mixture. To date, three generations of random packings have evolved with the primary objective of minimizing HETP and therefore maximizing efficiency. Common packing types currently used in commercial practice include Intalox® saddles, Pall® rings and numerous other packing types based on their design (Kister, 1992). The selection of packing material, based primarily on corrosion resistance, includes metal (stainless or carbon steel), ceramic and plastic. Ideally, the optimum combination of packing type and material should provide the user with a high degree of wetting, even distribution of the liquid over the surface of the packing, good distribution of the vapor and liquid throughout the packing, sufficient renewal of the liquid on the packing surface and low liquid holdup. Common sense tells us that if static surface tension, the surface tension gradient, heat transfer effects, viscosity, density, diffusivity, or some combination thereof, influence tray efficiency, they will also influence packing efficiency, but to what extent?

Since 1939, and perhaps prior, the effect of concentration on separation efficiency in packed columns has been in question. Furnas and Taylor (1939) separated an aqueous ethanol/water system using stoneware Raschig rings and Berl saddles of different sizes to develop a better understanding of packed column design and operation. They found that packing efficiency was only slightly affected by packing type and geometry. They suggested that the wettability of the packing was affected by the alcohol concentration and by liquid viscosity. Furnas and Taylor (1939) inferred that wettability increased with increasing alcohol content due to decreased interfacial tension between the packing and the liquid film and that

wettability decreased with increasing liquid viscosity. Yoshida et al. (1954) proposed that density, viscosity and diffusivity of the liquid not only affect the liquid film coefficient but that also interfacial area was affected by the viscosity and surface tension of the liquid. It was not until 1958 that the first experimental data supporting or combating these hypotheses were published. Zuiderweg and Harmens (1958) separated three hydrocarbon systems, n-heptane/toluene, n-heptane/ methylcyclohexane (surface tension positive) and benzene/n-heptane (surface tension negative), using 6 mm porcelain Raschig rings and fine metal Fenske helices and Dixon rings. Regardless of packing size and type, higher HETP values were obtained for the surface tension negative benzene/n-heptane system, where as the positive n-heptane/toluene and n-heptane/methylcyclohexane systems exhibited lower HETP values of similar magnitude. The difference between the higher and lower HETP values was attributed to the different degrees of wetting attained by each system. Partial wetting occurs in surface tension negative systems due to destabilization of the liquid film, which results in rivulet formation. An explanation as to why the liquid film breaks is analogous to the explanation previously given regarding bubble destabilization. Liquid films on packing surfaces are not completely uniform. As mass transfer occurs, portions of the film become thinner compared to the surrounding film and are more saturated with the heavier component of lower surface tension. Liquid flows up the surface tension gradient, away from the thinner regions of lower surface tension. Rivulet flow develops from the breakup of the liquid film, which reduces the interfacial area available for mass transfer and therefore higher HETP values result. The opposite effect occurs in surface tension positive systems. The thin, weak regions become saturated with the component of higher surface tension. Liquid flows up the surface tension gradient into the thinner portions of higher surface tension, which stabilizes the liquid film. Lower HETP values were obtained for the positive systems because the liquid film is stabilized. It should be noted that for all systems studied, concentrations less than 18 mole % and greater than 90 mole % of the more volatile component were not investigated.

The pioneering work of Zuiderweg and Harmens (1958) opened a window of opportunity for several researchers. Norman and Binns (1960) studied the effects of

the liquid properties of an azeotropic n-propanol/water system on the minimum wetting rate in a wetted rod column. They found at lower alcohol concentrations, when the system behaved as surface tension positive, the liquid film was stabilized and minimum wetting rates were low. At higher alcohol concentrations, when the system behaved as surface tension negative, minimum wetting rates were higher and dry spots were visible on the rod surface. They developed a correlation to determine the minimum wetting rate, taking into account liquid surface tension, density and viscosity and included a parameter called surface tension difference. It was concluded that surface tension changes significantly affect minimum wetting rates in wetted wall columns; however, one could not assume that this statement holds for randomly packed columns. Their correlation was successful in providing a relationship between separation efficiency and wetted surface area. A few years later, Norman et al. (1963) separated the same system using graphite discs. Their results were similar to those of Norman and Binns (1960) both above and below the azeotrope concentration. When the system behaved as surface tension positive, below 43 mole % n-propanol, the packing was completely wetted with a smooth, uniform film for all flow rates. They found that height of a transfer unit, H_{OG}, values remained relatively constant between 18 mole % and 43 mole % n-propanol, and then increased rapidly at concentration less than 18 mole % n-propanol. Above 43 mole % n-propanol, where the system behaved as surface tension negative, the film was variable and uneven and H_{OG} values were much higher. In addition to the azeotropic n-propanol/water system, Norman et al. (1963) also studied surface tension positive (methanol/water, n-heptane/toluene) and surface tension negative (benzene/n-heptane) systems. Separation of the methanol/water system was carried out using ceramic discs as the packing material. They found that HETP values remained relatively constant over the middle concentration range, between 20 mole % and 95 mole % methanol, and nearly doubled as the system concentration approached pure water. They noted that irregularities in the film developed at concentrations less than 3 mole % methanol and reported that dry patches were visible on the discs at concentrations below 0.5 mole % methanol. Sawistowski (1964) and Ponter et al. (1967) obtained similar results when investigating the separation behavior of a

methanol/water system under total reflux. When evaluating minimum wetting rates using graphite discs, Sawistowski (1964) observed that H_{OG} values soared at methanol concentrations less than 0.38 mole %, resulting in significantly higher minimum wetting rates. He examined the effect of packing surface area on H_{OG} values using 25.4 mm ceramic Raschig rings and 15.9 mm mild steel Pall rings. Slightly lower H_{OG} values were obtained using Raschig rings, which is expected since ceramic is more wettable than steel. Sawistowski (1964) concluded that column efficiency was almost independent of the surface area of the packing tested and poor column performance was a result of underwetting, which occurred at lower methanol concentrations due to higher surface tension and viscosity values. Ponter et al. (1967) investigated the influence of contact angle on the determination of under wetting in a packed column. Out of all packing materials tested, brass, Teflon®, stainless steel, copper and graphite, the lowest minimum wetting rates and smallest contact angles were obtained using graphite discs, which proved to be the most wettable material. A strong relationship exists between contact angle and minimum wetting rate. As the methanol concentration decreases, contact angles become larger which results in decreased interfacial area for vapor-liquid contact, and therefore higher minimum wetting rates and higher HETP or H_{OG} values. They found that minimum wetting rates remained relatively constant over the middle concentration range of methanol and rapidly increased at concentrations less than 10 mole % and greater than 95 mole % methanol. In addition to methanol/water, an n-propanol/water system was also separated using graphite discs. The results obtained validate those of Norman et al. (1963), as similar trends were observed. When Norman et al. (1963) separated the surface tension positive and negative hydrocarbon systems; two very different sets of H_{OG} data were obtained. For the positive n-heptane/toluene system, separated using graphite discs, H_{OG} values remained constant over the entire concentration range investigated. For the negative benzene/n-heptanes system, separated using ceramic discs, H_{OG} values remained relatively constant over the middle concentration range and sharply increased at the low-end and high-end benzene concentrations. At low benzene concentrations, visual observations revealed partial wetting was responsible for the increase in H_{OG} values. However, at high benzene concentrations, the packing

appeared to be completely wetted yet H_{OG} values increased. The explanation offered was that poor visibility of wetting on the ceramic surface made it difficult to determine when the discs were wet or just damp; there was no consideration of surface tension, the surface tension gradient or viscosity effects.

In an attempt to explain the efficiency trends obtained for packed columns, such as those discussed in the previous paragraph, several papers discuss the role of the surface tension gradient on separation efficiency (Zuiderweg and Harmens, 1958; Danckwerts et al., 1960; Moens, 1972; King, 1980). It is understood the gradient formed in the liquid film acts to stabilize or destabilize the film depending on the direction of the gradient and the magnitude of the surface tension gradient significantly influences the interfacial area available for mass transfer and therefore, HETP values. Sawistowski and Smith (1959), Danckwerts et al. (1960) and Liang and Smith (1962) discuss an additional factor to consider, the possibility of mass transfer occurring as a result of condensation in the bulk vapor phase and evaporation in the bulk liquid phase caused by temperature differences between the vapor and liquid phases. As for the effects of the liquid viscosity, density and diffusivity, little literature has been found that provides a clear explanation regarding the effects of these properties on separation efficiency in packed columns. Common sense tells us liquid hold-up in a packed bed should increase with increasing liquid viscosity. Greater hold-up could mean more intimate contact between the vapor and liquid phases and therefore a higher rate of mass transfer. However, it is also known that as viscosity increases, the rate of diffusion of the more volatile component through the liquid film decreases. Zuiderweg and Harmens (1958) stated the effect of surface tension on separation efficiency was more pronounced than the effects of liquid viscosity, density and diffusivity; however they presented no data to support this theory. Onda et al. (1973) provided experimental data to support that statement, showing the effect of viscosity on the liquid spreading factor was almost negligible compared to that of the surface tension gradient. When developing correlations to calculate the effective interfacial area per unit volume of packing, a_e, the liquid-side mass transfer coefficient, k_L, and the volumetric mass transfer coefficient, $k_L a_e$, for ceramic and plastic packing, Shi and Mersmann (1985) found increased viscosity

results in a slight increase in the wettability of the packing due to higher liquid holdup. Yang and Chuang (1995) used the Onda et al. (1968) model to simulate the influence of operating conditions, hardware parameters and physical properties on the separation of an ethylbenzene/styrene system using metal Pall rings. They found increasing viscosity reduces the separation efficiency of the column and the effect of increasing density on separation efficiency was negligible. A study by Nicolaiewsky et al. (1999) focused on the effect of viscosity on the wetted area of ceramic and metallic structured packings to clarify the discrepancies found in literature regarding the influence of viscosity on interfacial area. To evaluate wetted area, three systems with similar wetting conditions and differing viscosities were selected. The solutions selected were water/glycol, ethylene glycol/(polyvinyl alcohol solution) and ethanol/acetone. Through wetting tests they showed increasing viscosity tends to form thicker films, which decreases liquid spreading on both ceramic and surface treated metallic surfaces and concluded that higher liquid holdup or improved liquid spreading does not occur as a result of increased viscosity. A general consensus is that increasing viscosity decreases the separation efficiency of a packed column by reducing the effective interfacial area of the liquid film.

In industry, it is common practice to select a packing for a given separation based on the HETP value for a particular packing. In other words, packing efficiency is thought to be largely packing-dependent. If this is not the case and packing efficiency is in fact largely system-dependent, then misguided recommendations of packings can lead to wasteful over-design or under-design and poor performance. In order to provide a clear and concise explanation as to the effects of the liquid properties on separation efficiency in a randomly packed column, the present study will attempt to validate, summarize and clarify the previous findings using experimental data.

1.1 Scope of the Investigation

The objective of this study is two-fold, to examine the effects of the liquid properties on HETP measurements in a randomly packed column and to determine if tray and packing efficiencies are affected in a similar manner by the liquid properties. Ceramic Intalox® saddles will be used as the packing material and were selected because ceramic is assumed to be a completely wettable packing material, meaning any liquid would make a contact angle of zero with the surface. This takes wettability out of the picture, leaving only the liquid properties to influence the interfacial area available for mass transfer. The test mixtures to be separated include methanol/water, n-heptane/toluene and isopropanol/water (surface tension positive), benzene/n-heptane, water/acetic acid and water/isopropanol (surface tension negative) and methanol/isopropanol and cyclohexane/n-heptane (surface tension neutral systems). These systems were selected to examine the large range liquid properties effect on HETP.

Chapter 2

EXPERIMENTAL METHOD

2.1 Equipment

A schematic diagram of the equipment used is given in Figure 2.1. The distillation column consisted of a 75 mm glass column, a thermosyphon partial reboiler and a total condenser. The column walls were made of glass to allow for visual observations. Ceramic Intalox® saddles, 7 mm in diameter, were selected as the packing material. The column dimensions and packing specifications are given in Table 2.1.

Table 2.1 Column dimensions and packing specifications.

Column diameter, mm	75.0
Packing type	Ceramic Intalox® Saddles
Size, mm	7.0
Porosity	0.723
Surface area, m^2/m^3	899
Packing height, mm	50.8

To determine the bed height required to investigate the concentration effect on HETP, 152.4 mm, 101.6 mm and 50.8 mm bed heights were tested. A packed bed height of 50.8 mm was selected in order to investigate the entire range of binary systems. The power supply to the reboiler was controlled using two variacs operated in series and cooling water was used as the cooling medium. The column pressure was maintained at atmospheric pressure by adjusting the cooling water flow rate to the condenser. A Validyne differential pressure cell, DP/Cell, was used to measure the column pressure relative to atmospheric pressure and the pressure controller adjusted the cooling water flow rate to maintain the column pressure equal to atmospheric pressure. The cooling water flow rate was measured using a pre-calibrated Fischer-Porter rotameter (tube

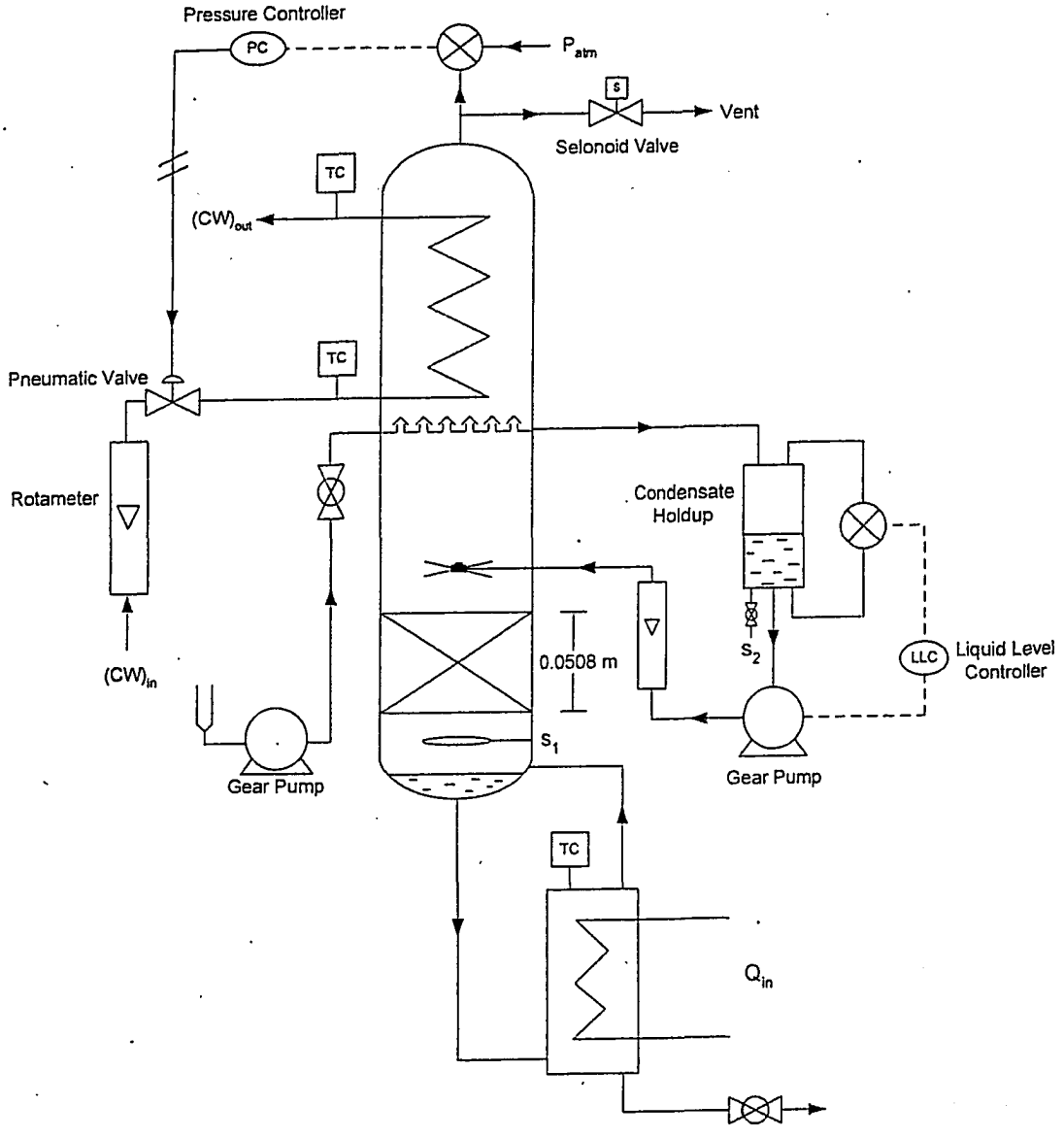

Figure 2.1 Schematic diagram of the distillation column.

number FP-1/2-35-G-10/83). The following calibration equation was used to convert percent rotameter reading to mass flow rate of cooling water:

$$M_{cooling}\,(kg/s) = 3.9053x10^{-4}(RR)$$

The reflux flow rate was maintained by ensuring that the liquid level in the condensate holdup container remained constant. The reflux was evenly distributed across the cross-sectional area of the packed bed using a cross type stainless steel distributor with five, 1 mm diameter holes. A Matheson rotameter (tube number 604), calibrated with water, was used to measure the reflux flow rate. The calibration equation used to determine mass flow rate of the reflux in terms of mass flow rate of water is given below:

$$M_{reflux}\,(kg_{H_2O}/s) = 2.4947x10^{-5}(RR) - 9.9915x10^{-5}$$

The rotameter calibration curves for the cooling water and reflux flow rates are given in Appendix C. The reflux flow rate was then converted from mass flow rate of water to mass flow rate of mixture by knowing the float density, ρ_{float}, mixture liquid density at the reflux temperature, ρ_L, and water density, ρ_{water}, at 25 °C:

$$M_{reflux}\,(kg/s) = \sqrt{\frac{(\rho_{float} - \rho_L)\rho_L}{(\rho_{float} - \rho_{water})\rho_{water}}}$$

A variable speed gear pump (Micropump®) was used to pump the reflux. A solenoid valve located at the top of the condenser was used to vent the column to atmosphere when required. The inlet and outlet cooling water temperatures and the temperature of the mixture in the reboiler were measured using J-type thermocouples.

Liquid samples were taken from sample ports located just below the packed bed, at the bottom of the condensate holdup container and from the reboiler. The liquid samples were analyzed using a Hewlett-Packard 5790A Series II gas

chromatograph (GC) equipped with a thermal conductivity detector (TCD). Table 2.2 contains the GC column specifications and operating conditions used for each system.

Table 2.2 GC column specifications and operating conditions.

System	Column	Operating Conditions	
		Temperatures	He flow rate
Methanol/Water	3% Aprezon L on W 36" 1/8 ss column	Injector: 250 °C Detector: 200 °C Oven: 68 °C	30 ml/min
n-Heptane/Toluene	20 % sp2100 80/100 supelcoport 6 ' 03605	Injector: 250 °C Detector: 200 °C Oven: 55 °C	30 ml/min
Benzene/n-Heptane	20 % sp2100 80/100 supelcoport 6 ' 03605	Injector: 250 °C Detector:200 °C Oven: 50 °C	30 ml/min
Water/Acetic acid	3% Aprezon L on W 36" 1/8 ss column	Injector: 250 °C Detector: 200 °C Oven: 115 °C	30 ml/min
Isopropanol/Water	6.6% CBX 20m 80/100 Carbopark 6' R21044	Injector: 250 °C Detector:200 °C Oven: 68 °C	30 ml/min
Methanol/Isopropanol	6.6% CBX 20m 80/100 Carbopark 6' R21044	Injector: 250 °C Detector: 200 °C Oven: 88 °C	30 ml/min
Cyclohexane/n-Heptane	20 % sp2100 80/100 supelcoport 6 ' 03605	Injector: 250 °C Detector:200 °C Oven: 70 °C	30 ml/min

The calibration equations used to determine the weight percent of the more volatile component for each system are given in Appendix C.

2.2 Systems

The test mixtures studied include the surface tension positive methanol/water and n-heptane/toluene systems, the surface tension negative benzene/n-heptane and water/acetic acid systems and the surface tension neutral methanol/isopropanol and cyclohexane/n-heptane systems. In addition, an azeotropic isopropanol/water system was studied. This mixture forms an azeotrope at 68 mole % isopropanol, therefore the system behaves as surface tension positive at concentrations less than 68 mole % isopropanol and behaves as surface tension negative at concentrations greater than 68 mole % isopropanol. The ACS grade chemicals were purchased from Fisher Scientific.

2.3 System Properties

ASPENTech simulation software was first used to verify vapor-liquid equilibrium data obtained for each system from Gmehling (1980, 1981) and was then used to obtain vapor-liquid property data for each system. The criterion for model selection was best fit of the vapor-liquid equilibrium data. Of the models tested, the NRTL with ideal gas and Henry's Law model was selected for the methanol/water, n-heptane/toluene, isopropanol/water and benzene/n-heptane systems and the Peng-Robinson equation of state with Wong-Sandler mixing rules model was selected for the water/acetic acid, methanol/isopropanol and cyclohexane/n-heptane systems. Flash calculations were then carried out at 94 kPa to obtain data for diffusivity, viscosity, density and static surface tension. The ranges of the systems properties are presented in Tables 2.3, 2.4 and 2.5 for the surface tension positive, surface tension negative and surface tension neutral systems, respectively. Appendix B contains all system property plots, equations and equilibrium data that were obtained using ASPENTech and as well, the literature vapor-liquid equilibrium data (Gmehling, 1980, 1981). The relative volatility values were calculated using the experimental data obtained from Gmehling (1980, 1981) for each mixture. Relative volatility values were calculated based on the top and bottom concentrations of the more volatile component; see Appendix E for sample calculations.

Table 2.3 System property ranges for the surface tension positive systems obtained at saturation conditions using ASPENTech.

	Methanol/Water	n-Heptane/Toluene	Isopropanol/Water
Mole fraction			
x	0.137 – 0.953	0.053 – 0.963	0.227 – 0.597
Diffusivity, (m^2/s)			
D_L	$(5.21 - 3.70)x10^{-9}$	$(5.01 - 4.45)x10^{-9}$	$(3.31 - 3.23)x10^{-9}$
D_V	$(2.34 - 1.96)x10^{-5}$	$(4.16 - 3.51)x10^{-6}$	$(1.73 - 1.59)x10^{-5}$
Viscosity, (N s/m^2)			
μ_L	$(3.34 - 3.53)x10^{-4}$	$(2.50 - 2.21)x10^{-4}$	$(3.92 - 4.61)x10^{-4}$
μ_V	$(1.24 - 1.11)x10^{-5}$	$(8.78 - 7.29)x10^{-6}$	$(1.18 - 1.04)x10^{-5}$
Density, (kg/m^3)			
ρ_L	876 – 749	772 – 528	826 – 759
ρ_V	0.61 – 1.05	2.75 – 3.06	0.86 – 1.37
Surface tension, (mN/m)			
σ	55.1 – 21.1	18.3 – 13.1	51.8 – 35.2
Relative volatility			
α	6.64 – 2.76	1.79 – 1.12	4.50 – 1.26

Table 2.4 System property ranges for the surface tension negative systems obtained at saturation conditions using ASPENTech.

	Benzene/n-Heptane	Water/Acetic acid	Water/Isopropanol
Mole fraction			
x	0.076 – 0.935	0.143 – 0.987	0.080 – 0.259
Diffusivity, (m^2/s)			
D_L	$(7.87 - 6.85)x10^{-9}$	$(9.27 - 7.86)x10^{-9}$	$(7.15 - 6.98)x10^{-9}$
D_V	$(4.41 - 4.02)x10^{-6}$	$(4.14 - 3.78)x10^{-6}$	$(1.60 - 1.59)x10^{-5}$
Viscosity, (N s/m^2)			
μ_L	$(2.27 - 3.21)x10^{-4}$	$(3.81 - 2.87)x10^{-4}$	$(5.16 - 4.90)x10^{-4}$
μ_V	$(7.35 - 8.75)x10^{-6}$	$(1.30 - 1.39)x10^{-5}$	$(9.45 - 9.95)x10^{-6}$
Density, (kg/m^3)			
ρ_L	627 – 796	936 – 917	730 – 746
ρ_V	3.03 – 2.56	1.58 – 0.57	1.82 – 1.58
Surface tension, (mN/m)			
σ	13.6 – 20.9	23.9 – 58.0	20.2 – 28.5
Relative volatility			
α	2.08 – 1.21	1.83 – 1.64	1.67 – 1.10

Table 2.5 System property ranges for the surface tension neutral systems obtained at saturation conditions using ASPENTech.

	Methanol/Isopropanol	Cyclohexane/n-Heptane
Mole fraction		
x	0.070 – 0.972	0.055 – 0.958
Diffusivity, (m^2/s)		
D_L	$(4.30 - 2.90)x10^{-9}$	$(7.09 - 6.14)x10^{-9}$
D_V	$(1.10 - 1.01)x10^{-5}$	$(4.14 - 3.79)x10^{-6}$
Viscosity, (N s/m^2)		
μ_L	$(4.85 - 3.13)x10^{-4}$	$(2.05 - 2.42)x10^{-4}$
μ_V	$9.35\ x10^{-6} - 1.10\ x10^{-5}$	$(7.32 - 8.07)x10^{-6}$
Density, (kg/m^3)		
ρ_L	698 – 643	620 – 753
ρ_V	1.91 – 1.12	3.18 – 2.81
Surface tension, (mN/m)		
σ	16.7 – 19.0	13.1 – 18.1
Relative volatility		
α	1.91 – 1.89	1.65 – 1.70

2.4 Experimental Procedure

All experiments were conducted under total reflux conditions and at atmospheric pressure. At each startup, the solenoid valve, located at the top of the column, was opened to purge air out of the column. The reboiler was then filled with the more volatile component of the system to be studied. To ensure complete wetting of the packing, the column was filled to a height just above the packed bed and was subsequently drained to the desired reboiler liquid level. Power was then introduced to the reboiler by adjusting the variacs to 1000 Watts. The column pressure was monitored until the column pressure was equivalent to atmospheric pressure, at which point the solenoid valve was closed. Power to the reboiler was increased until the desired reflux flow rate was reached on the rotameter (i.e. when the reflux was evenly distributed out of all five holes on the distributor). The column was then left running until steady state was reached. Steady state was assumed when the cooling water and reflux flow rates, the inlet and outlet cooling water temperatures and the reboiler temperature remained within ± 2 % of the average values. This took approximately 40 minutes. Once steady state was achieved, liquid samples were taken from the

bottom of the packed bed, the condensate hold up container and from the reboiler. The samples were then analyzed using gas chromatograph (GC). To confirm steady state, liquid samples were taken approximately 10 minutes later to ensure that the top and bottom concentrations remained within ± 2 % of the initial measurements. The inlet and outlet water temperatures, reboiler duty, cooling water and reflux flow rates were then recorded. The reboiler concentration was subsequently adjusted by adding the less volatile component while monitoring the reboiler temperature. The less volatile component was added such that the system concentration shifted a minimum of roughly 5 mole % each time. The integrity of the GC calibration equation was verified by injecting samples of known concentration throughout the duration of the experiment. The remaining systems were investigated using a similar procedure. The column was thoroughly cleaned between each system. The vapor rate was held relatively constant for each binary mixture. Table 2.6 contains the ranges of vapor rates used for each system.

Table 2.6 Ranges of vapor rates used for each system.

System	Vapor Rate (m/s)
Methanol/Water	0.21 – 0.29
n-Heptane/Toluene	0.09 – 0.14
Benzene/n-Heptane	0.11 – 0.15
Water/Acetic acid	0.17 – 0.41
Isopropanol/Water	0.14 – 0.22
Methanol/Isopropanol	0.19 – 0.26
Cyclohexane/n-Heptane	0.09 – 0.12

Chapter 3

RESULTS

Seven binary mixtures were employed to investigate the effect of the liquid properties on packing efficiency. At the onset of the study, the ceramic packing was heat-treated to ensure the removal of any contaminants present on the packing surface. It was important to make certain the largest possible surface area was available for mass transfer. To test for wall effects, the column was operated in the absence of packing. Liquid samples were taken from both sample ports located on the column and it was found that the column walls did not have any effect on HETP. This result was expected, since the distance between the distributor and the bottom sample port is only 101.6 mm. Liquid and vapor maldistribution can significantly affect mass transfer rates in packed columns, consequently end effects were also considered. To reduce the effects of liquid maldistribution, the distributor was designed to disperse liquid to the majority of the cross-sectional area of the packed bed and the vapor rates, given in Table 2.6, were selected for each system to ensure all holes of the distributor were operating at all times. There was enough distance between the reboiler and the bottom of the packing to eliminate maldistribution of the vapor.

The objective of this study is two-fold, first to examine the effect of the liquid properties on HETP and secondly, to determine if trays and packing are affected in a similar manner by the liquid properties. To address the first objective, HETP measurements as a function of the average concentration of the more volatile component are presented in Figures 3.1, 3.2 and 3.3 for the surface tension positive methanol/water, n-heptane/toluene and isopropanol/water systems, respectively. HETP values were calculated using the following equation (Kister, 1992):

$$HETP = \frac{z}{N_T} \qquad (1)$$

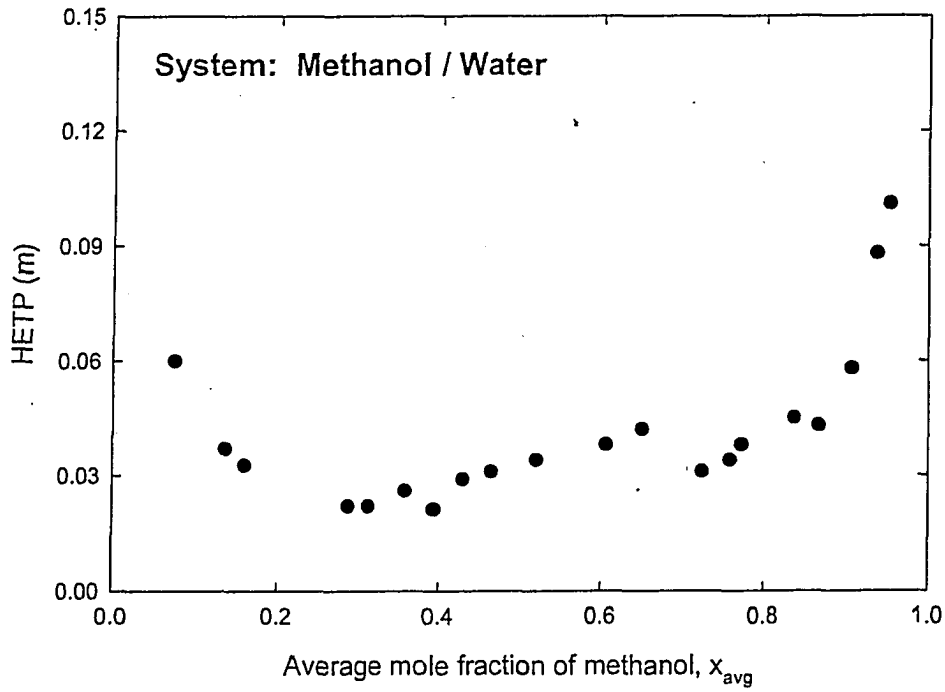

Figure 3.1 HETP as a function of average methanol concentration for the surface tension positive methanol/water system.

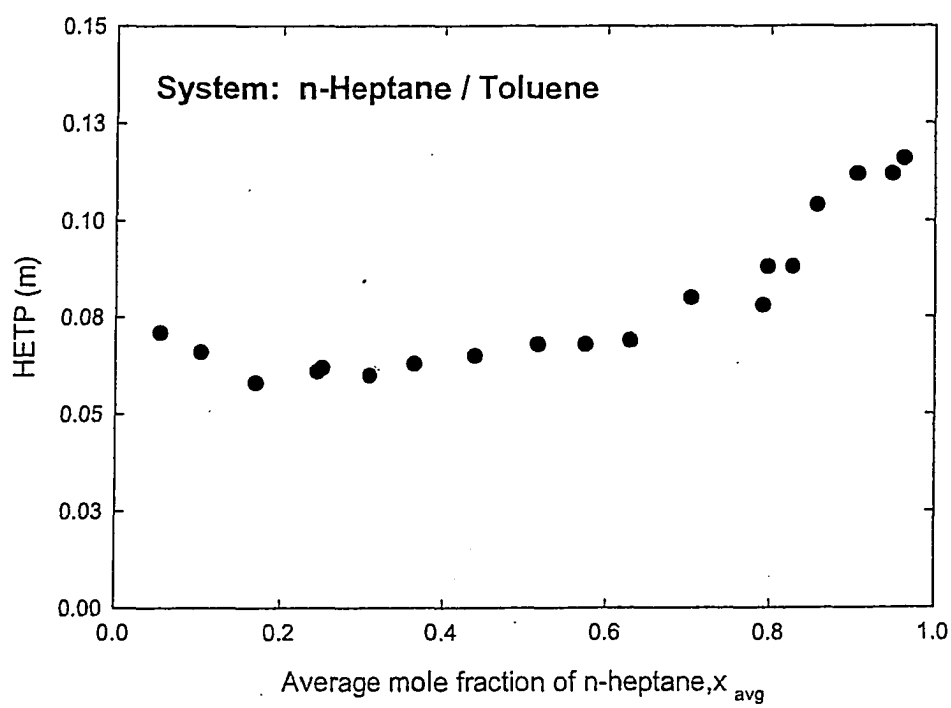

Figure 3.2 HETP as a function of average n-heptane concentration for the surface tension positive n-heptane/toluene system.

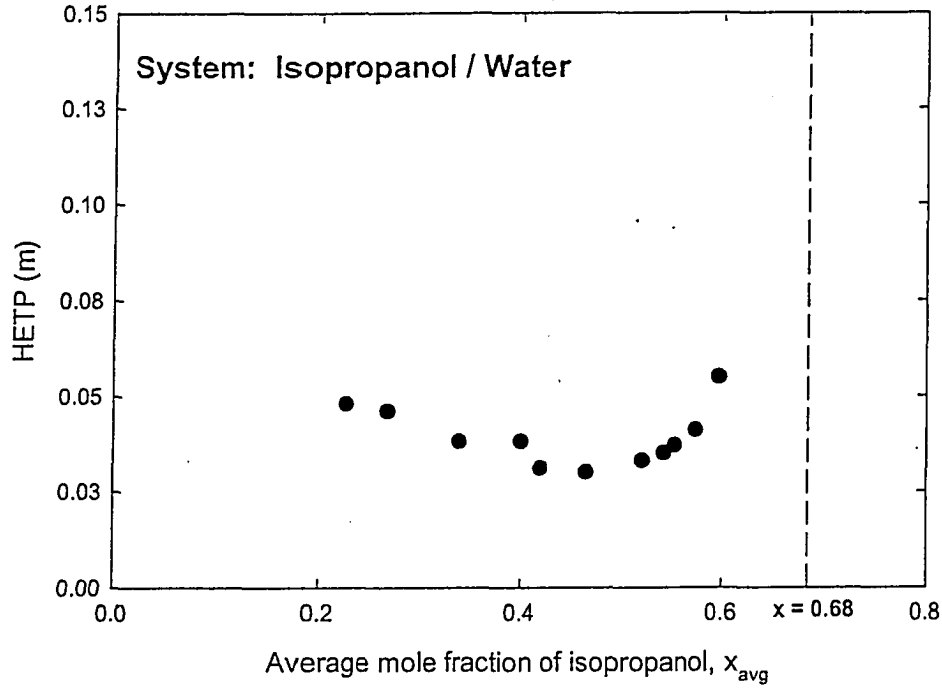

Figure 3.3 HETP as a function of average isopropanol concentration for the surface tension positive isopropanol/water system.

where z is the packing height and N_T is the number of theoretical trays. The Fenske (1932) Equation, developed specifically for total reflux operations, was used to determine the number of theoretical trays:

$$N_T = \frac{\log\left[\left(\frac{x_{Top}}{1-x_{Top}}\right)\left(\frac{1-x_{Bottom}}{x_{Bottom}}\right)\right]}{\log\left(\sqrt{\alpha_{Top}\alpha_{Bottom}}\right)} \qquad (2)$$

where is x is the mole fraction of the more volatile component at the top or bottom of the packed bed. The relative volatility, α, of the mixture at the top and bottom of the packed bed was obtained using equilibrium data in conjunction with the following equations:

$$\alpha_{Top} = \frac{\frac{y^*}{x_{Top}}}{\frac{(1-y^*)}{(1-x_{Top})}} \tag{3}$$

$$\alpha_{Bottom} = \frac{\frac{y^*}{x_{Bottom}}}{\frac{(1-y^*)}{(1-x_{Bottom})}} \tag{4}$$

where y^* is the vapor concentration that is in equilibrium with the liquid concentration. All three Figures show that similar efficiency trends were obtained for the surface tension positive systems. Over the middle concentration range, HETP values remain lower and as the system approaches the pure component concentrations, HETP values increase. This efficiency trend agrees with the findings of Norman et al. (1960) for both the methanol/water and n-heptane/toluene systems. Near the pure component concentrations, the increase in HETP is much more pronounced for the methanol/water system than it is for the isopropanol/water and n-heptane/toluene systems. These Figures also show that the lowest HETP values were obtained for the methanol/water and isopropanol/water systems, averaging between 0.030 and 0.035 m.

Figures 3.4, 3.5 and 3.6 show HETP variation as a function of concentration of the more volatile component for the surface tension negative benzene/n-heptane, water/acetic acid and water/isopropanol systems, respectively. HETP values were calculated using Equations (1) through (4). The overall efficiency trend obtained for the surface tension negative systems is comparable to that obtained for the surface tension positive systems. HETP values remain lower across the middle concentration range and increase as the system approaches the pure component concentrations. The results obtained for the benzene/n-heptane system, between 35 and 75 mole % benzene, support the findings of Zuiderweg and Harmens (1958). The increase in HETP values near the pure component concentrations is more prominent for the

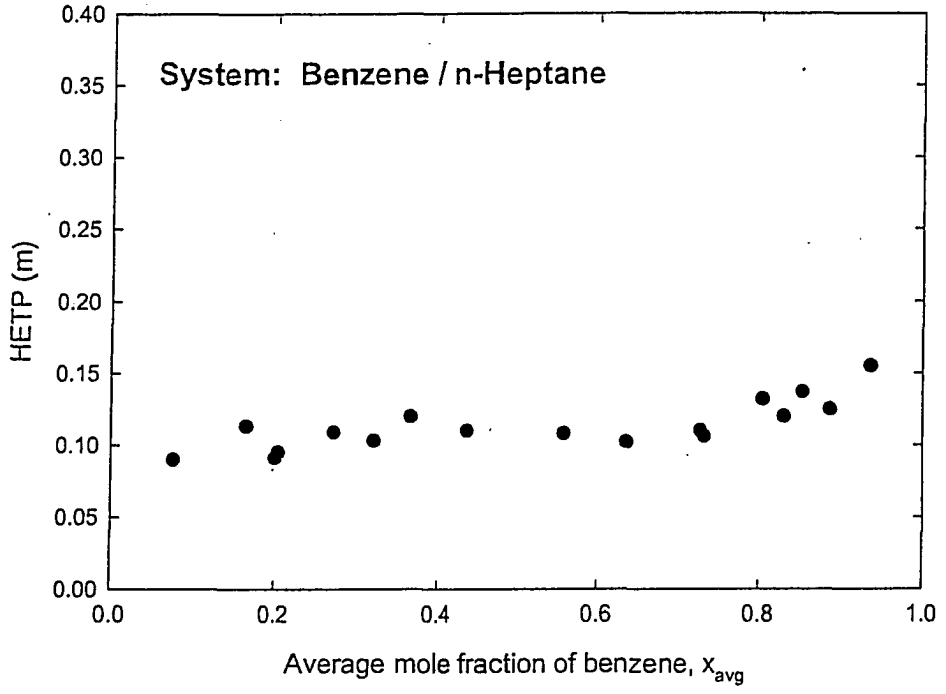

Figure 3.4 HETP as a function of average benzene concentration for the surface tension negative benzene/n-heptane system.

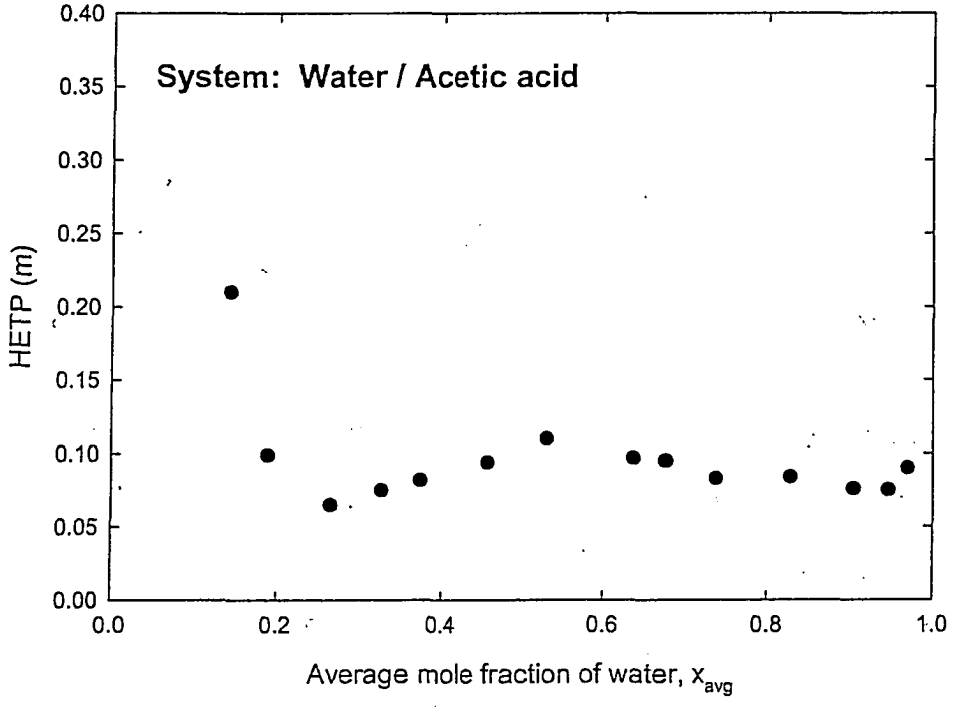

Figure 3.5 HETP as a function of average water concentration for the surface tension negative water/acetic acid system.

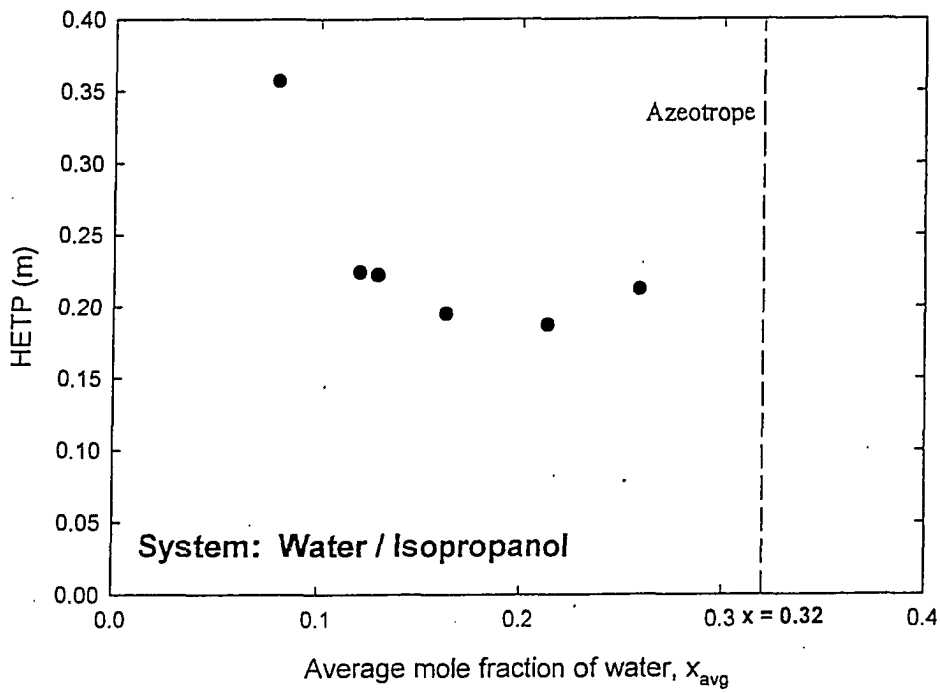

Figure 3.6 HETP as a function of average water concentration for the surface tension negative water/isopropanol system.

water/acetic acid and water/isopropanol systems compared to the benzene/n-heptane system. From these Figures, it can also be seen that HETP values remain relatively constant at approximately 0.090 m for the water/acetic acid system, 0.110 m for the benzene/n-heptane system and 0.200 m for the water/isopropanol system over the middle concentration range.

HETP variation as a function of the average concentration of the more volatile component is presented in Figures 3.7 and 3.8 for the surface tension neutral methanol/isopropanol and cyclohexane/n-heptane systems, respectively. HETP values were calculated using Equations (1) through (4). Both Figures show that no sharp increase in HETP occurred near the pure component concentrations. A decreasing HETP trend was observed for the methanol/isopropanol system, HETP decreases from 0.150 m down to 0.100 m as the system concentration approaches pure methanol. For the cyclohexane/n-heptane system, HETP values remain relatively constant near 0.090 m over the entire concentration range investigated.

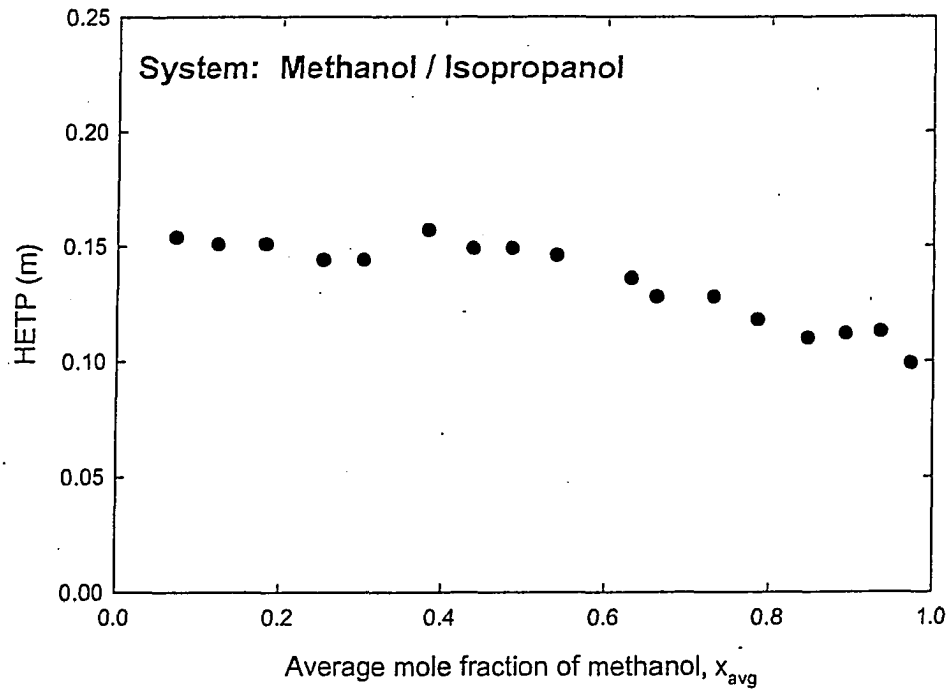

Figure 3.7 HETP as a function of average methanol concentration for the surface tension neutral methanol/isopropanol system.

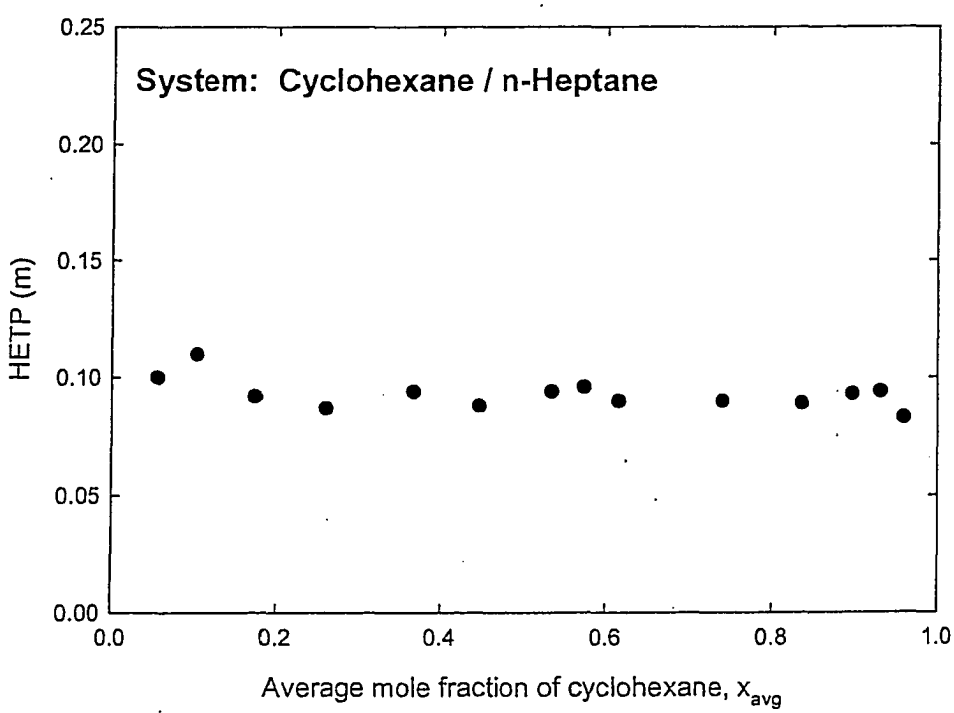

Figure 3.8 HETP as a function of average cyclohexane concentration for the surface tension neutral cyclohexane/n-heptane system.

In distillation, it is common practice to model tray and packed column efficiencies using the two-film theory, which is defined as the following:

$$\frac{1}{N_{OG}} = \frac{1}{N_G} + \frac{\lambda}{N_L} \tag{5}$$

where N_{OG}, N_G and N_L are the number of overall gas transfer units, number of gas phase transfer units and number of liquid phase transfer units, respectively, and λ represents the ratio of the slope of the equilibrium line to the slope of the operating line. Under total reflux conditions (V = L), λ is equal to the slope of the equilibrium line, m. The two-film theory assumes that the liquid and vapor phases present the only resistance to mass transfer near a vapor-liquid interface. It can be seen from Figures 3.1 through 3.8 that the HETP data obtained for the surface tension positive and negative systems behaves quite differently compared to those obtained for the surface tension neutral systems. In an attempt to explain the measured efficiency trends shown in Figures 3.1 through 3.8, $1/N_{OG}$ as a function of the slope of the equilibrium line, m, has been plotted in Figures 3.9 through 3.16 for the surface tension positive, negative and neutral systems. The N_{OG} values were determined at each measured concentration using the following equation (Kister, 1992):

$$N_{OG} = \int_{yb}^{yt} \frac{dy}{y^* - y} \tag{6}$$

where

$$y^* = \frac{\alpha x}{1 + (\alpha - 1)x} \tag{7}$$

Under total reflux conditions, y = x and dy = dx. Substitution of Equation (7) into Equation (6) followed by numerical integration results in the equation given below, which was used to calculated the number of overall gas transfer units (Moens, 1972):

$$N_{OG} = \frac{1}{\alpha - 1}\left[\alpha \ln \frac{1 - x_{bottom}}{1 - x_{top}} + \ln \frac{x_{top}}{x_{bottom}}\right] \tag{8}$$

where α is the average relative volatility, and x_{top} and x_{bottom} correspond to the liquid composition of the mixture above and below the packed bed, respectively. The slope of the equilibrium line was calculated using the following equation:

$$m = \frac{\alpha}{[1 + (\alpha - 1)x]^2} \tag{9}$$

If the two-film theory holds for the binary systems studied a positive slope should be equal to $1/N_L$ and the y-intercept equal to $1/N_G$. This is definitely not the case for the surface tension positive, negative or neutral systems. It can be seen from Figures 3.9 through 3.16 that a minimum of two distinct slopes exist for each system studied. According to the two-film theory, only one slope should be expected. For the surface tension positive systems, $1/N_L$ changes sign when the slope of the equilibrium line values are between 0.5 and 0.95, for the negative systems, when slope of the equilibrium line values are between 0.8 and 1.1 and for the neutral systems when slope of the equilibrium line values are near 0.7. Based on the data presented above, it can be concluded that the two-film theory does not hold for the large majority of systems studied and therefore, additional factors must be affecting HETP. According to the mass transfer efficiency correlations developed by Onda et al. (1968) and Billet (1993), the liquid side mass transfer coefficient and effective interfacial area are functions of liquid viscosity, density, diffusivity and surface tension. Furthermore, research suggests that the surface tension gradient (Zuiderweg and Harmens, 1958; Danckwerts et al., 1960; Moens, 1972; King, 1980) and thermal distillation (Sawistowski and Smith, 1959; Danckwerts et al., 1960; Liang and Smith, 1962) influence packing efficiency.

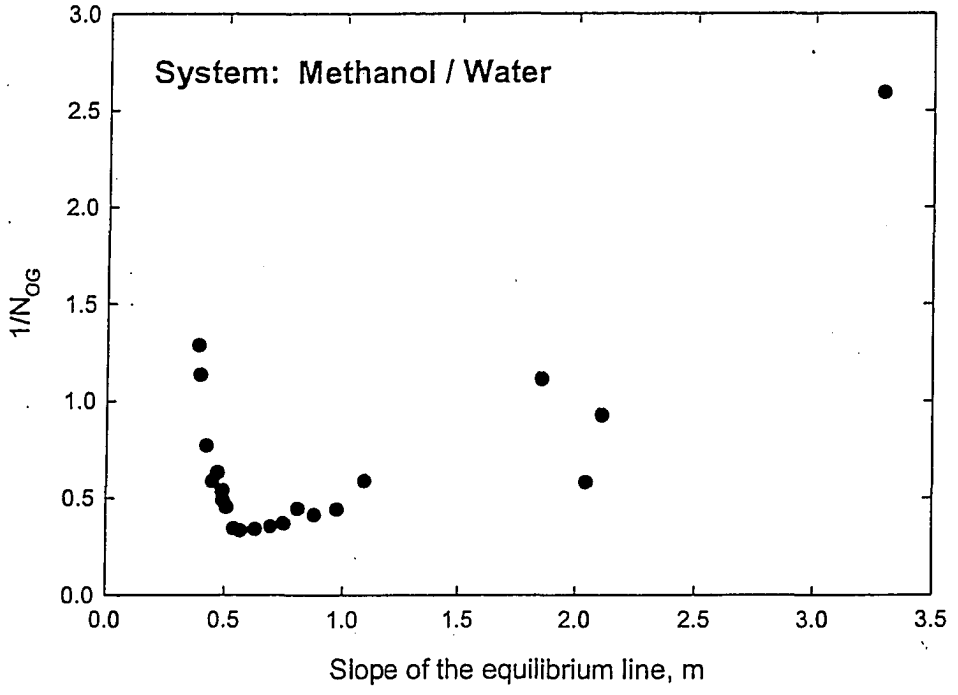

Figure 3.9 $1/N_{OG}$ as a function of the slope of the equilibrium line for the surface tension positive methanol/water system.

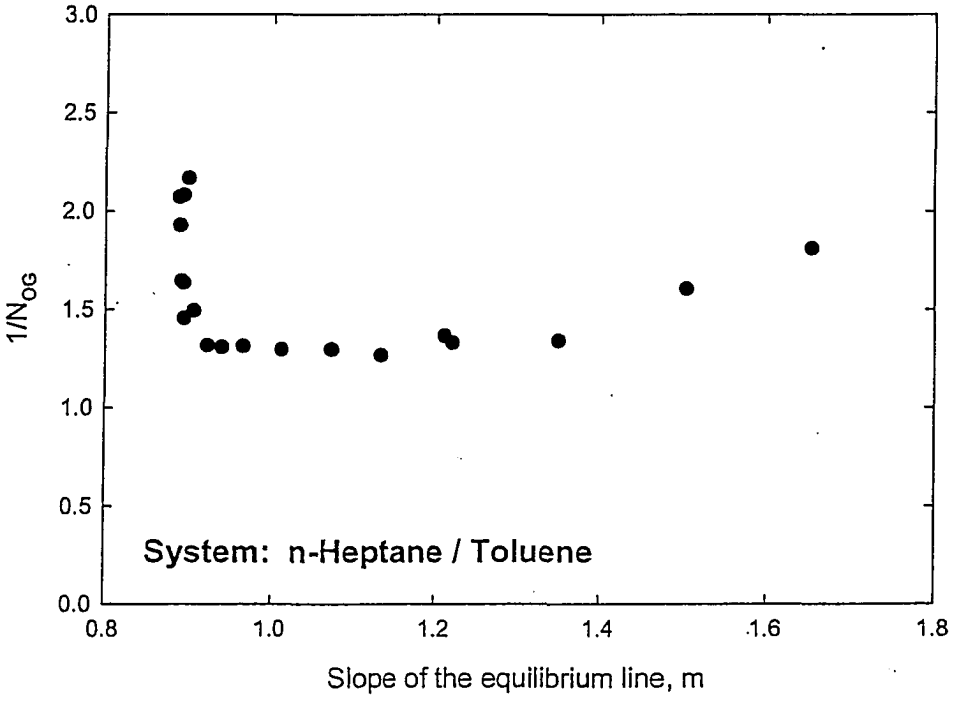

Figure 3.10 $1/N_{OG}$ as a function of the slope of the equilibrium line for the surface tension positive n-heptane/toluene system.

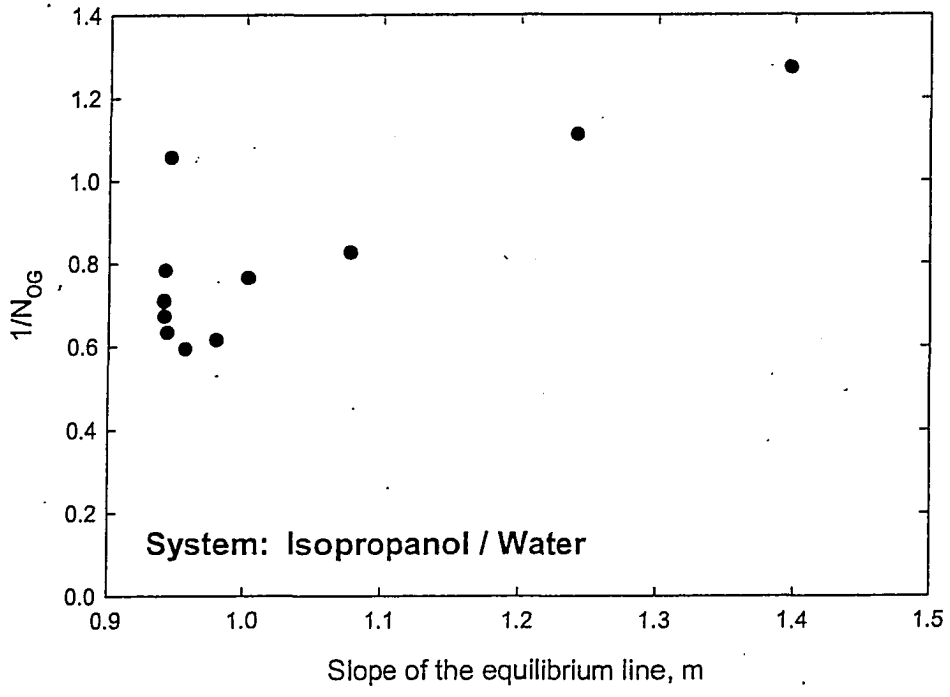

Figure 3.11 $1/N_{OG}$ as a function of the slope of the equilibrium line for the surface tension positive isopropanol/water system.

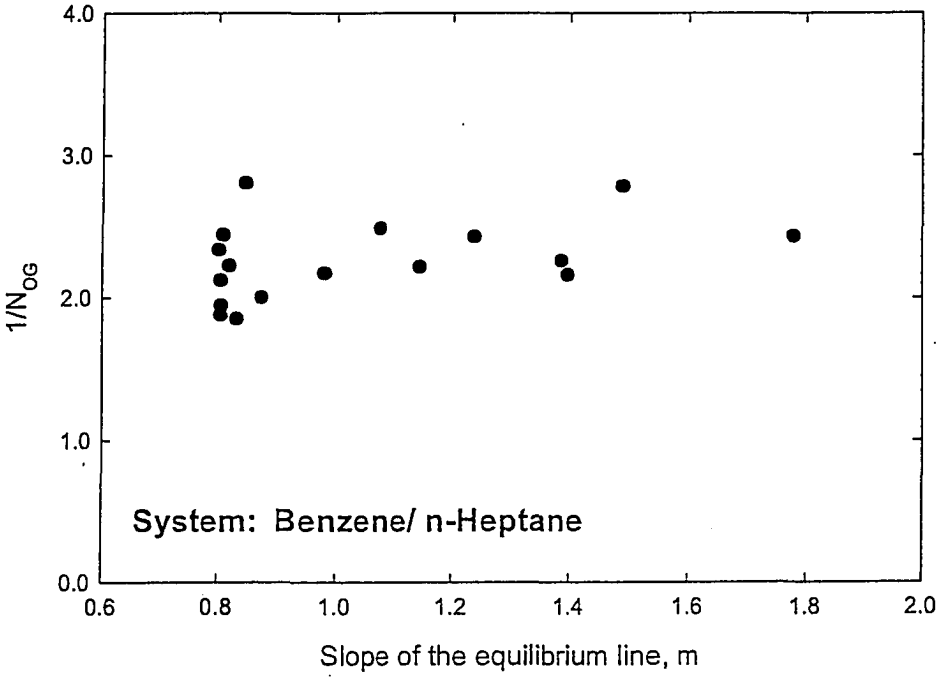

Figure 3.12 $1/N_{OG}$ as a function of the slope of the equilibrium line for the surface tension negative benzene/n-heptane system.

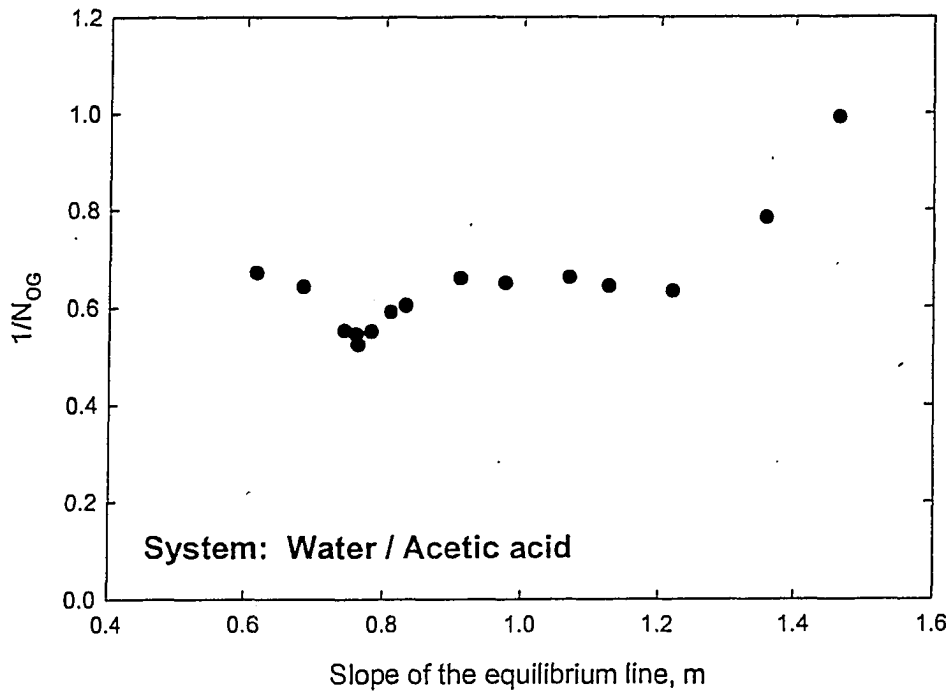

Figure 3.13 $1/N_{OG}$ as a function of the slope of the equilibrium line for the surface tension negative water/acetic acid system.

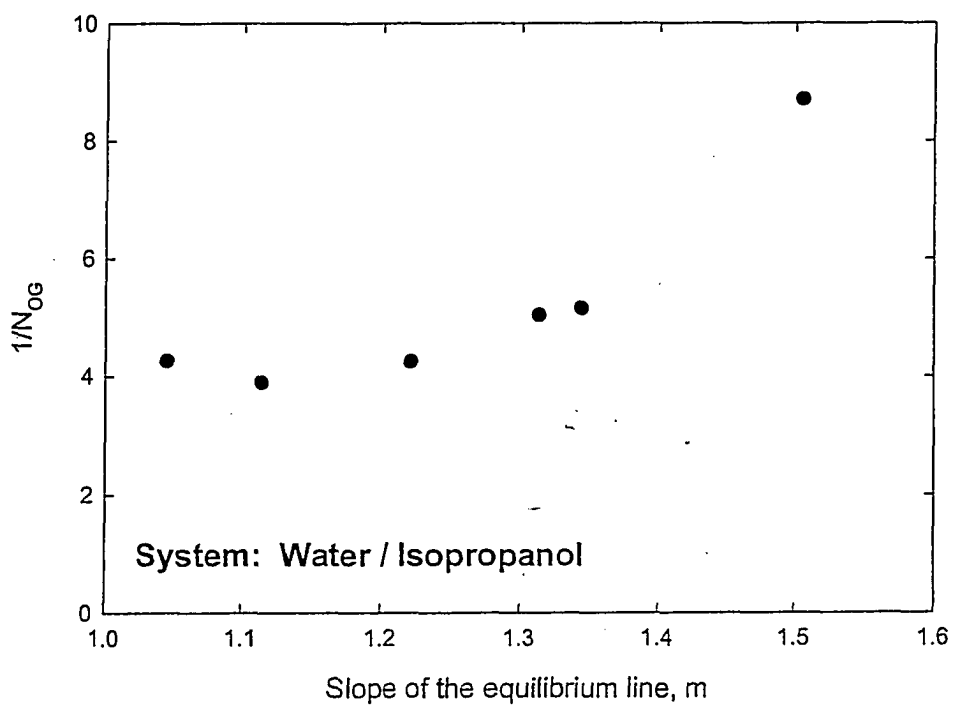

Figure 3.14 $1/N_{OG}$ as a function of the slope of the equilibrium line for the surface tension negative water/isopropanol system.

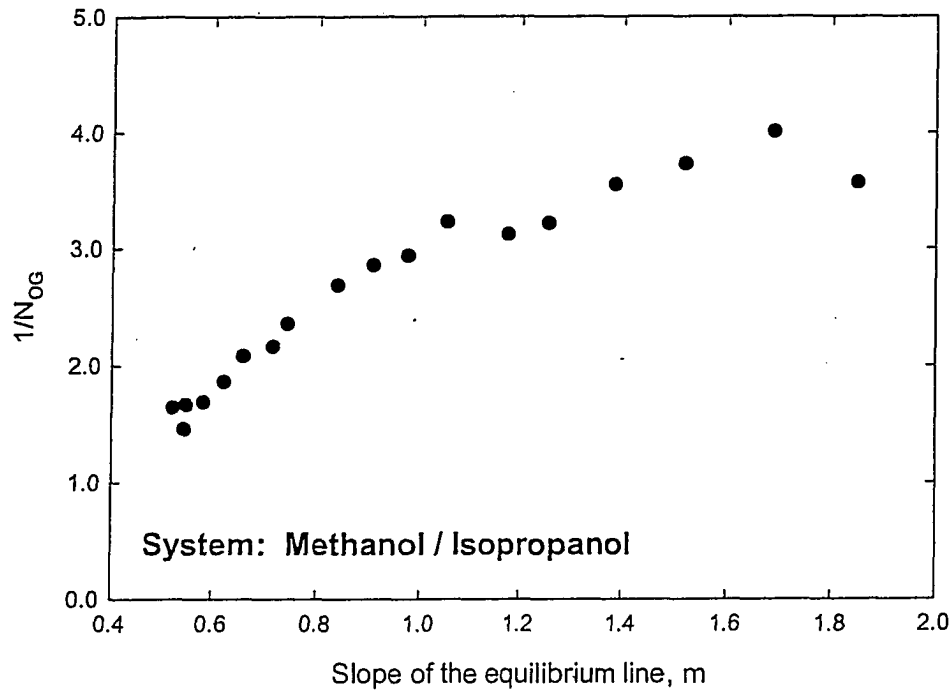

Figure 3.15 $1/N_{OG}$ as a function of the slope of the equilibrium line for the surface tension neutral methanol/isopropanol system.

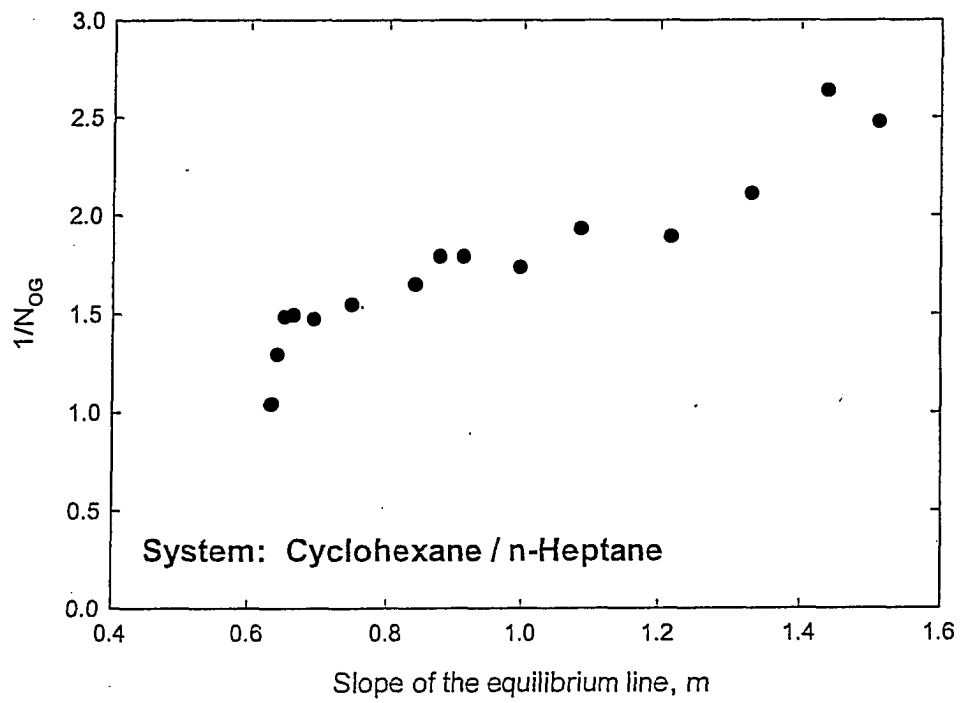

Figure 3.16 $1/N_{OG}$ as a function of the slope of the equilibrium line for the surface tension neutral cyclohexane/n-heptane system.

In order to determine if packing and trays are affected in a similar manner by the liquid properties a comparison must be made between packing efficiency data and tray efficiency data. Syeda (2002) measured the separation of methanol/water, n-heptane/toluene, benzene/n-heptane, water/acetic acid, methanol/isopropanol and cyclohexane/n-heptane mixtures using a sieve tray column. Her tray efficiency data, given in Appendix D, have been converted to HETP using the tray spacing. Figures 3.17 through 3.22 show HETP (tray) as a function of average concentration of the more volatile component for the surface tension positive, negative and neutral systems. It is important to note that it is the trends of the HETP (tray) data, which are significant and not the absolute values of HETP (tray), since tray efficiency is a function of tray spacing. The HETP data obtained from the present study, referred to as HETP (packing), have also been included in these Figures so that comparisons can be made between the two efficiency trends. The Murphree tray efficiency data were converted to HETP using the following equation (Kister, 1992):

$$HETP\,(tray) = 100 \cdot \frac{S}{E_{MV}} \tag{9}$$

where S is tray spacing in meters and E_{MV} is the Murphree tray efficiency in percent. For the surface tension positive and negative systems, both HETP (packing) and HETP (tray) trends show lower HETP values over the middle concentration range and increasing HETP near the pure component concentrations. For the neutral systems, the HETP trends are similar. For the methanol/isopropanol system, HETP values decrease with increasing methanol concentration. HETP values remain relatively constant over then entire concentration range investigated for the cyclohexane/n-heptane system.

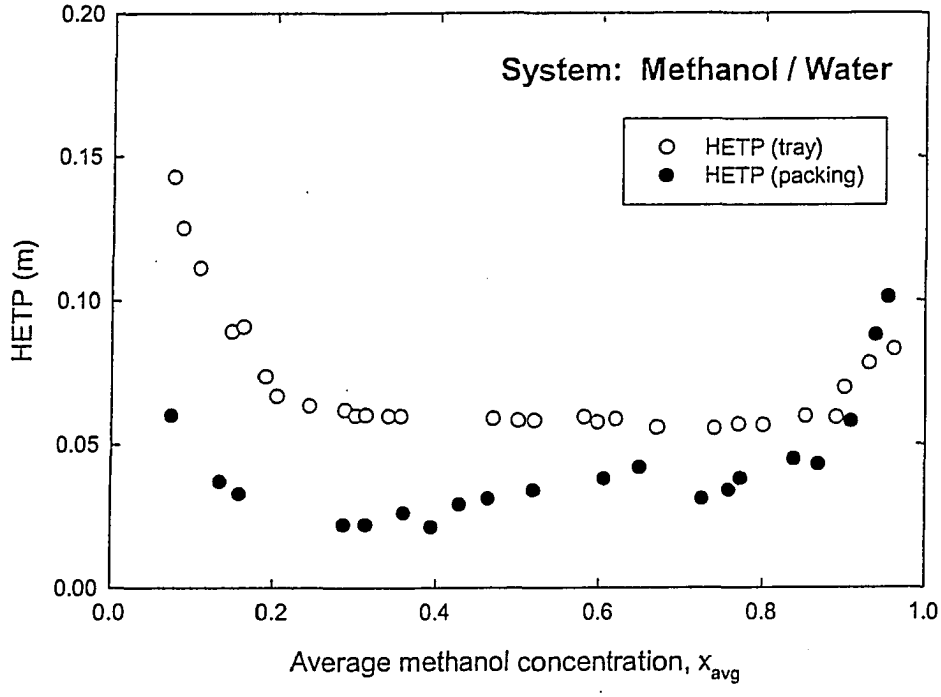

Figure 3.17 Comparison of HETP trends for the surface tension positive methanol/water system.

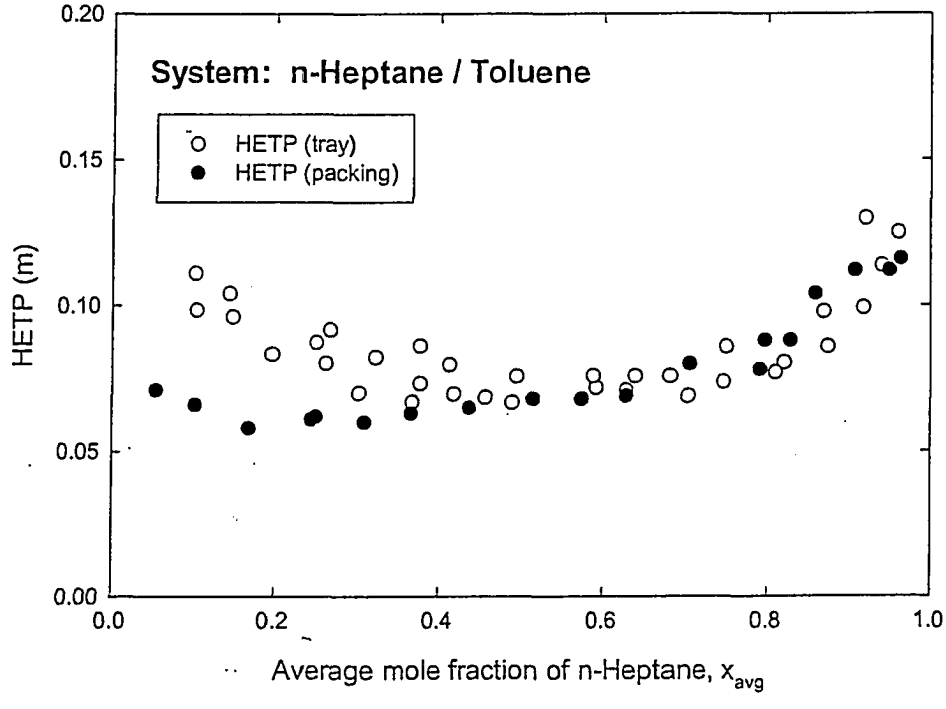

Figure 3.18 Comparison of HETP trends for the surface tension positive n-heptane/toluene system.

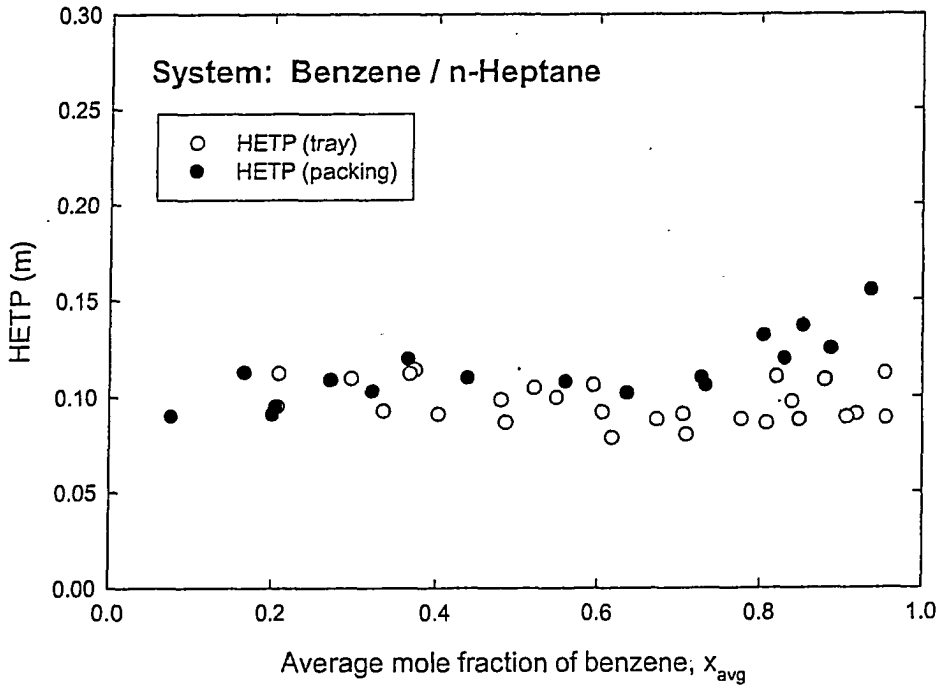

Figure 3.19 Comparison of HETP trends for the surface tension negative benzene/n-heptane system.

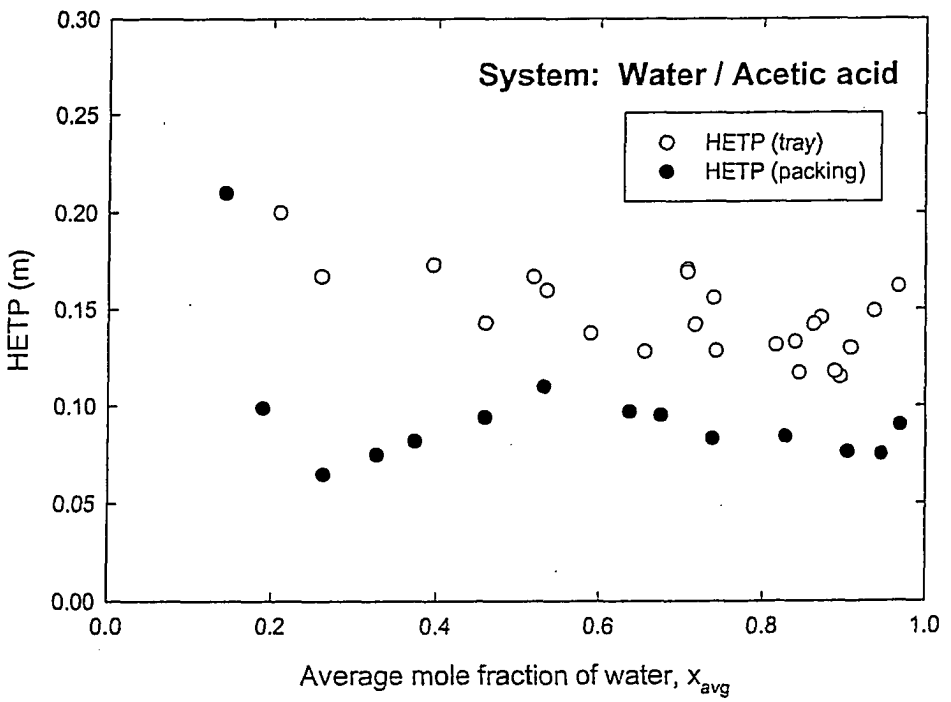

Figure 3.20 Comparison of HETP trends for the surface tension negative water/acetic acid system.

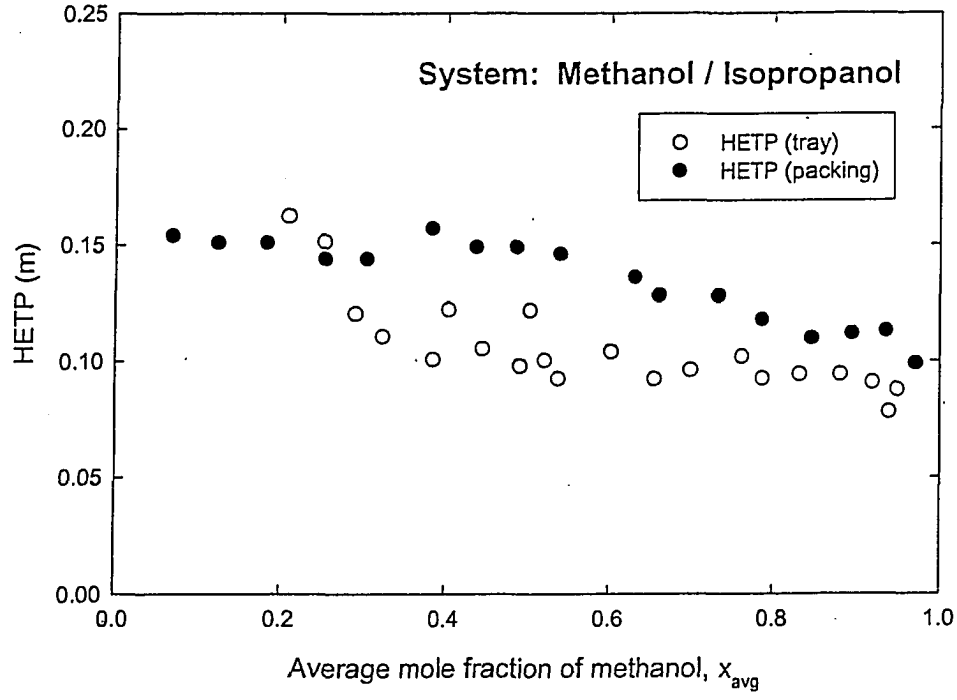

Figure 3.21 Comparison of HETP trends for the surface tension neutral methanol/isopropanol system.

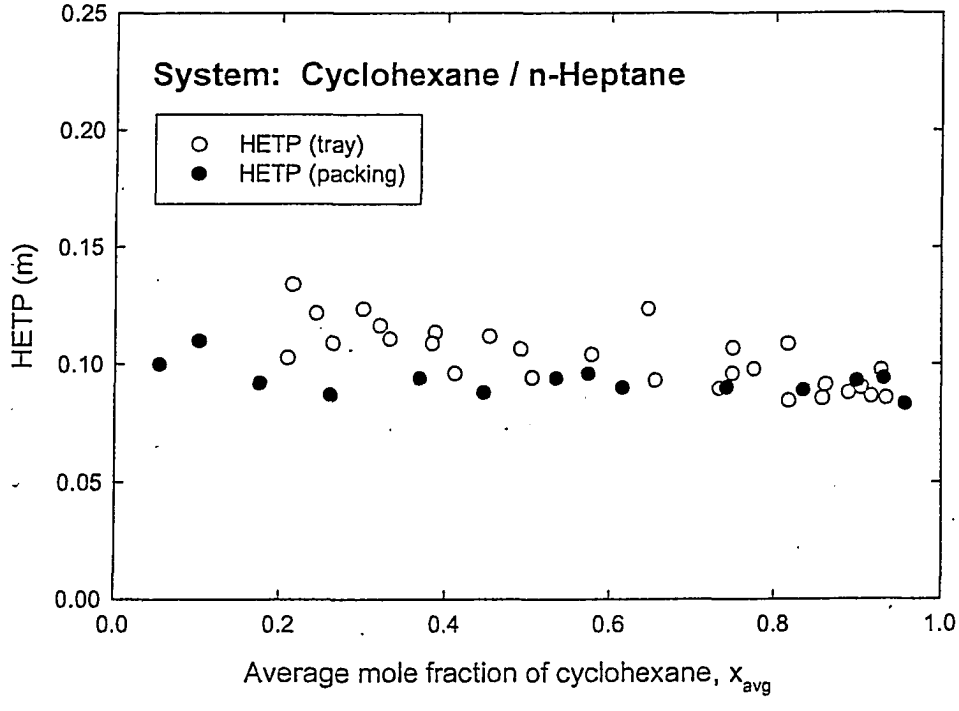

Figure 3.22 Comparison of HETP trends for the surface tension neutral cyclohexane/n-heptane system.

Chapter 4

DISCUSSION

The HETP data obtained for the surface tension positive and negative systems behaved quite differently compared to that obtained for the surface tension neutral systems. For the positive and negative test systems, shown in Figures 3.1 through 3.6, HETP remained lower over the middle concentration range of the more volatile component and increased as the system concentration approached that of the pure components. The increase in HETP was most prominent for the aqueous methanol/water, isopropanol/water and water/acetic acid systems. For the surface tension neutral test systems, no increase in HETP was observed near the pure component concentrations. HETP decreased with increasing methanol concentration for the methanol/isopropanol system, as shown in Figure 3.7. For the cyclohexane/n-heptane system, shown in Figure 3.8, HETP remained relatively constant over the entire concentration range investigated. The two-film theory was used to model the experimental data in an attempt to explain the observed HETP trends and differences in the absolute values of HETP. At total reflux (V = L), the relationship between $1/N_{OG}$ and m should be linear, with the slope equal to $1/N_L$ and intercept equal to $1/N_G$. It was obvious by looking at Figures 3.9 through 3.16 that this was not the case. The negative values of $1/N_L$, shown in Figures 3.9 though 3.14, indicated that the two-film theory does not hold for surface tension positive and negative systems. These results support the findings of Sawistowski and Smith (1959). The two-film theory most closely represented the surface tension neutral systems. However, it was still found to be invalid since multiple slopes were observed on the plots. Clearly, the two-film theory does not hold for the systems included in this study, since the film coefficients were found to be indirect functions of the slope of the equilibrium line, m. Additional factors must be influencing the number of overall gas transfer units. It has been reported in literature (Zuiderweg and Harmens, 1958; Sawistowski and Smith, 1959; Danckwerts et al., 1960; Liang and Smith, 1962; Onda et al., 1968; Moens, 1972; Onda et al., 1973; King, 1980) that possible factors include static

surface tension, driving force, the surface tension gradient, heat transfer effects or thermal distillation, liquid viscosity, density and diffusivity. A process of elimination was used to determine which properties or combinations thereof, had the greatest affect on packing efficiency.

Ceramic Intalox® saddles were selected as the packing material in an attempt to eliminate the wetting characteristics of the liquid mixtures studied, specifically the effect of static surface tension. HETP variation as a function of surface tension was plotted for all positive, negative and neutral systems studied. According to Kister (1992), the wettability of a packing surface increases with decreasing surface tension. If the absolute values of surface tension were affecting HETP, then lower HETP values would be expected when the surface tension of the mixture was lower. Under saturation conditions, the surface tension and HETP values for the methanol/water mixture at 14 mole %, 50 mole % and 95 mole % methanol correspond to 21 mN/m, 41 mN/m and 55 mN/m and 0.060 m, 0.030 m and 0.100 m, respectively. The results suggest that the absolute value of surface tension does not affect HETP since higher HETP values were observed at lower surface tensions. The next step was to determine if the driving force of the system was causing an increase in HETP near the pure component concentrations. It is known that packing efficiency increases with increasing driving force; therefore, one would expect to see lower HETP values over the middle concentration range, where the driving force is largest, and increasing HETP values near the pure component concentrations, where the driving force diminishes. This statement agrees with the efficiency trends obtained for the surface tension positive and negative systems. However, there was no increase in HETP observed for either of the surface tension neutral systems. It was concluded that it is not the driving force itself that caused the differences in the efficiency trends observed for the surface tension positive, negative and neutral systems. Studies by Ruckenstein and Smigelschi (1967) and Moens (1972) suggested that it was a quantity related to driving force, such as surface tension gradients and/or thermal effects that likely caused the observed maximum in efficiency over the middle concentration range of the more volatile component.

Numerous studies, including those by Zuiderweg and Harmens (1958) and King (1980), have concluded that the surface tension gradient effect is significant in surface tension positive systems. The strength of the Marangoni forces present in the liquid film act to strengthen or weaken the film. A stabilized film provides the maximum interfacial area available for mass transfer, which results in lower observed HETP values. Rivulet flow, which results from breakage of an unstable film, reduces the interfacial area available for mass transfer and consequently higher HETP values result. Figure 4.1 illustrates film stabilization that occurs in surface tension positive systems. As mass transfer takes place on the non-uniform packing surface, portions of the film become thinner in comparison to the surrounding film, as shown in Figure 4.1(a). The thinner portions are saturated with the less volatile component of higher surface tension and consequently, a surface tension gradient develops between the thinner portions of the film and the surrounding liquid, as illustrated in Figure 4.1(b). Liquid flows up the surface tension gradient, from the surrounding film into the thinner portions. This locally thickens and reinforces the weakened areas, which stabilizes the liquid film, as shown in Figure 4.1(c). Across the middle concentration range, Marangoni forces are much stronger due to the larger surface tension gradient that exists within the liquid film. The stabilized film provides the maximum interfacial area available for mass transfer. As the system approaches the pure component concentrations, the surface tension gradient diminishes, and as a result, portions of the liquid film become unstable. Instability of the liquid film results in the formation of rivulets, which reduces the interfacial area available for mass transfer. The efficiency trends obtained for the surface tension positive systems were in agreement with the theory presented, however, rivulet flow could not be visually confirmed near the pure component concentrations for all of the surface tension positive systems studied. Surface tension neutral systems do not exhibit film stabilization. In the absence of a surface tension gradient, one would assume the film should be of uniform thickness throughout the entire concentration range investigated because the static surface tension values of the pure components are quite close in magnitude. The HETP trend obtained for the cyclohexane/n-heptane system validated the preceding statement, however, a decreasing HETP trend was observed

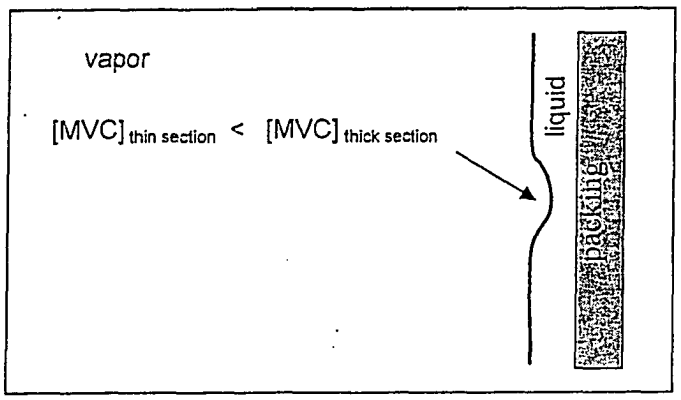

(a) MVC = More Volatile Component

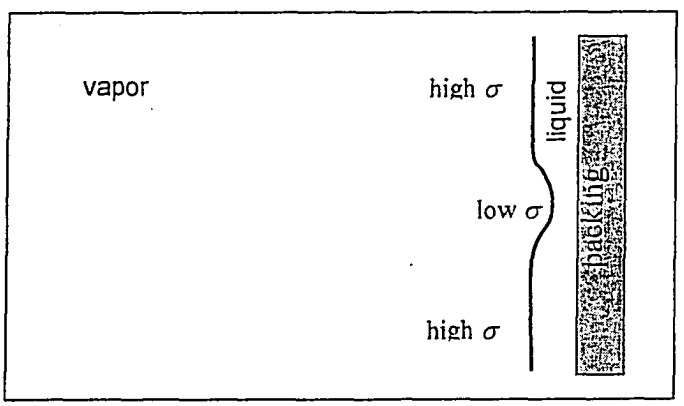

(b)

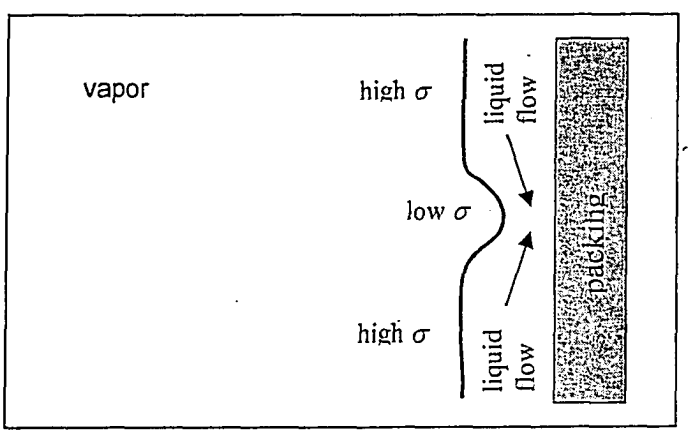

(c)

Figure 4.1 Film stabilization that occurs in surface tension positive systems.

for the methanol/isopropanol system. In surface tension negative systems, there are also no stabilizing effects present. In fact, Zuiderweg and Harmens (1958) reported that negative systems exhibit film destabilization. They explained the reversal of the surface tension gradient effect acts to destabilize the liquid film across the entire concentration range of the more volatile component. Since similar efficiency trends were obtained for the surface tension positive and negative systems, it was concluded that additional factors were affecting HETP. According to Zuiderweg and Harmens (1958), the effects of channeling caused by destabilization of the liquid film in negative systems, may be reduced due to liquid retention in the packing by capillary forces in the interstices between the packing elements. The occurrence of such an event would likely influence HETP values. Perhaps this has something to do with the measured trends observed for the negative systems. At the onset of the study, it was thought that only the surface tension gradient played a significant role in influencing HETP values, however, the experimental results suggest that this is not the case.

Thus far, the effects of static surface tension, driving force and the surface tension gradient have been discussed as possible factors contributing to the efficiency trends obtained for the surface tension positive, negative and neutral systems. Several authors, including Sawistowski and Smith (1959), Danckwerts et al (1960), Liang and Smith (1962), Ruckenstein and Smigelschi (1967) and King (1980) suggest that heat transfer effects are also partially responsible for the observed efficiency trends. They explain that in addition to diffusional mass transfer resulting from contact distillation, mass transfer also occurs as a result of thermal distillation due to the differences between the latent heats of vaporization of the individual components that constitute a binary mixture. According to Sawistowski and Smith (1959), under conditions when the differences between the heats of vaporization are large, sufficient heat is removed from the bulk vapor to maintain the bulk vapor at its condensation point and sufficient heat is added to the bulk liquid to keep the bulk liquid at its boiling point. Mass transfer results from the partial condensation and partial evaporation of the vapor and liquid phases, respectively. Conversely, when the rate of heat transfer is small, or the heats of vaporization of the system components are similar, the vapor phase remains superheated and the liquid phase remains subcooled, consequently, there is

insufficient heat transfer to promote mass transfer. Danckwerts et al. (1960) suggest the contribution of thermal distillation towards the total mass transferred (the combination of mass transferred by contact distillation and mass transferred by thermal distillation) likely varies directly with the temperature difference between the bulk vapor and liquid phases. They concluded that thermal distillation should be the most significant when relative volatilities are high or when large boiling point differences exist between the pure components. Thermal distillation should therefore be least significant when separating components with similar boiling points or when separating mixtures near pure component concentrations, when the saturated vapor and liquid temperatures are quite similar. The pure component heats of vaporization were calculated using ASPENTech simulation software, at the boiling point temperature and 94 kPa. The heat of vaporization values for the surface tension positive, negative and neutral test systems are compared in Table 4.1.

Table 4.1 Heats of vaporization at boiling point temperature and 94 kPa.

System classification	Mixture	ΔH_{Vap} (kJ/kg)
Surface tension positive	Methanol / Water	1101 / 2270
	n-Heptane / Toluene	320 / 364
	Isopropanol / Water	658 / 2270
Surface tension negative	Benzene / n-Heptane	396 / 320
	Water / Acetic acid	2270 / 632
	Water / Isopropanol	2270 / 658
Surface tension neutral	Methanol / Isopropanol	1101 / 658
	Cyclohexane / n-Heptane	357 / 320

It can be seen, from Table 4.1, that the largest differences exist between the latent heats of vaporization for the methanol/water, isopropanol/water, water/acetic acid and methanol/isopropanol systems. According to the theory presented above, lower HETP values should be expected over the middle concentration range, where the rate of heat transfer is the largest. Near the pure component concentrations, the rate of heat transfer between the phases is reduced; therefore, higher HETP values should be

observed. The efficiency trends obtained for the aqueous systems, shown in Figures 3.1, 3.3, 3.5 and 3.6, agree with the theoretical efficiency trend suggested. Similar efficiency trends were also obtained for the n-heptane/toluene and benzene/n-heptane systems, Figures 3.2 and 3.4, respectively. However, the increase in HETP near the pure component concentrations was less dramatic. According to the theory, the increase in HETP should be less significant because the heats of vaporization of the components are much closer in magnitude. Based on the experimental results obtained for the surface tension positive systems, it was concluded that in addition to the surface tension gradient, thermal distillation was also a dominant factor affecting HETP. The individual effects of these factors could not be quantified. For the surface tension negative systems, thermal distillation was found to be the most significant factor affecting HETP. Entirely different efficiency trends were obtained for the neutral hydrocarbon systems shown in Figure 3.7 and 3.8. According to the theory behind thermal distillation, trends similar to those obtained for the surface tension positive and negative systems should have been observed for the neutral systems. Also, lower HETP values should have been obtained for the methanol/isopropanol system because the rate of heat transfer between the phases is higher for this system. Comparisons were made between the relative volatilities and boiling point differences between the components of each system. Relative volatility values were slightly higher for the methanol/isopropanol system ($\alpha = 2.02$) compared to the cyclohexane/n-heptane system ($\alpha = 1.65$). Also, the boiling point differences between the individual components were identical, 18 °C, for both systems. Since packing efficiency increases with increasing relative volatility, lower HETP values should be expected for the methanol/isopropanol system. Figures 3.7 and 3.8 reveal the opposite is in fact true. The measured efficiency trends obtained for the surface tension neutral systems could not be explained by the thermal distillation theory. Therefore, the effect of thermal distillation on HETP was concluded to be negligible for the neutral systems.

The remaining factors to be examined included the effects of liquid viscosity, density and diffusivity. These properties likely influence HETP values in all of the systems studied, but to what extent? The surface tension neutral systems were

selected for analysis because there is no surface tension gradient present to influence mass transfer. It can be seen in Figures 3.7 and 3.8 that slightly lower HETP values were obtained for the cyclohexane/n-heptane system, remaining near 0.090 m over the entire concentration range. For the methanol/isopropanol system, HETP values decreased with increasing methanol concentration, from 0.150 m down to 0.100 m. The differences in the magnitude of the HETP values obtained are partially attributed to the differences in liquid viscosity and liquid diffusivity values, as shown in Table 4.2.

Table 4.2 System property ranges calculated over the entire concentration range of the more volatile component for the surface tension neutral systems.

Properties	Methanol / Isopropanol	Cyclohexane / n-Heptane
x (mole fraction)	0.070 – 0.972	0.055 – 0.958
ρ_L (kg/m^3)	698 – 643	620 – 753
μ_L (N m/s^2)	(4.85 – 3.13) x 10^{-4}	(2.05 – 2.42) x 10^{-4}
σ (mN/m)	16.7 – 19.0	13.1 – 18.1
D_L (m^2/s)	(4.30 – 2.90) x 10^{-9}	(7.10 – 6.14) x 10^{-9}

The methanol/isopropanol system exhibits nearly twice the viscosity and roughly half of the diffusivity of the cyclohexane/n-heptane system. In theory, increasing viscosity causes a reduction in the liquid spread on the packing surface. This reduces the interfacial area available for mass transfer and results in higher HETP values. In addition, increasing viscosity has been thought to reduce liquid diffusivity. The experimental data obtained for the surface tension neutral systems support both of these claims. The decreasing efficiency trend observed for the methanol/isopropanol system verifies that HETP does in fact decrease with decreasing viscosity. From the experimental data, it was concluded that liquid viscosity had the most significant affect on packing efficiency for the surface tension neutral systems. This statement was verified by analyzing the liquid-side mass transfer correlation developed by Onda et al. (1968). Examination of the exponents on the liquid properties in the correlation revealed that viscosity was the most important property. It should be noted the model does not take into account surface tension gradient or thermal distillation effects. The liquid property ranges for the surface tension positive and tension negative systems

were also investigated. However, no direct conclusions were drawn because the effects of the surface tension gradient and thermal distillation could not be separated from the effects of viscosity, density and diffusivity.

Due to the lack of calculated data available, it was not possible to say with confidence the exact effects of the factors mentioned throughout this discussion. It was, however, concluded that the surface tension gradient, thermal distillation and liquid viscosity had the greatest influence on the separating power of a randomly packed distillation column and the extent to which these factors influenced separation efficiency varied from system to system.

In order to determine if packing and trays were affected in a similar manner by the system properties a comparison was made between packing efficiency data and tray efficiency data. The Murphree tray efficiency data, obtained by Syeda (2002), was converted to HETP using the tray spacing and was present along side the measured HETP data. Both HETP (packing) and HETP (tray) trends showed lower HETP values over the middle concentration range and increasing HETP near the pure component concentrations for the surface tension positive and negative systems. For the methanol/isopropanol system, HETP values decreased with increasing methanol concentration. HETP values remained relatively constant over then entire concentration range investigated for the cyclohexane/n-heptane system. The experimental results suggested that packing and tray efficiencies are affected in a similar manner by the liquid properties.

Chapter 5

CONCLUSIONS

A randomly packed distillation column, operated under total reflux and at atmospheric pressure, was used to investigate the effects of the liquid properties on packing efficiency for surface tension positive, negative and neutral systems. Furthermore, HETP values obtained from the packed column were compared to Murphree tray efficiency data to determine if trays and packing are affected in a similar manner by the liquid properties.

The experimental results suggested the surface tension gradient and thermal distillation had the most significant affect on HETP for the surface tension positive systems and that thermal distillation was the dominant factor affecting HETP for the negative systems. For the surface tension neutral systems, it was believed that liquid viscosity had the greatest influence on HETP. Due to the limited number of test mixtures used, it was not possible to quantify the individual effects of the surface tension gradient, thermal distillation and viscosity on HETP. Overall, lower HETP values were obtained over the middle concentration range of the more volatile component for the surface tension positive systems. This result is likely attributed to a combination of relative volatility, surface tension gradient and thermal distillation effects.

The measured HETP values were also compared to experimental tray efficiency data (Syeda, 2002) to determine if packing and trays are influenced in a similar manner by the liquid properties. Both HETP (packing) and HETP (tray) trends showed lower HETP values over the middle concentration range and increasing HETP near the pure component concentrations for the surface tension positive and negative systems. Both HETP trends decreased with increasing methanol concentration for the methanol/isopropanol system and remained relatively constant over then entire concentration range investigated for the cyclohexane/n-heptane system. The experimental results suggested that packing and tray efficiencies are affected in a similar manner by the liquid properties.

In industry, packing efficiency is thought to be largely packing-dependent. The experimental results suggest that packing efficiency is in fact largely system-dependent. It is therefore important to pilot test packings with the systems of interest before making any recommendations so that wasteful over-design or under-design does not occur.

RECOMMENDATIONS:

The conclusions drawn from this study are largely speculative. The measured efficiency data supports the statements made. However, additional research must be carried out to quantify the individual effects of the surface tension gradient, thermal distillation and viscosity. It would also be of interest to examine, under distillation conditions, how the stability of the liquid film on ceramic, stainless steel and plastic surfaces, changes with concentration for each of the systems studied.

Chapter 6

REFERENCES

Billet, R., "Evaluation of random packings and the extent of their development", Chem.-Ing.-Tech., **65**, 157 (1993).

Chen, G. X. and K. T. Chuang, "Prediction of point efficiency for sieve trays in distillation", Ind. Eng. Chem. Res., **32**, No. 4, 701-707 (1993).

Coker, A. K. "Understand the basics of packed-column design", Chem. Eng. Prog., Nov., 93-99 (1991).

Danckwerts, P. V., H. Sawistowski and W. Smith, "The effects of heat transfer and interfacial tension in distillation", International symposium on distillation, 7-12 (1960).

Fenske, M. R., "Fractionation of straight-run Pennsylvania gasoline", Ind. Eng. Chem., **24**, 482 (1932).

Furnas, C. C. and M. L. Taylor, "Distillation in packed columns", AICHE J., 135-171 (1939).

Ghmeling, J., U. Onken and W. Arlt, "Vapor-liquid equilibrium data collection", Vol. 1 part 1a, 6a, 6b, DECHEMA, Frankfurt (1980, 1981).

King, C., "Separation processes", 2nd Edition, McGraw-Hill, New York (1980).

Kister, H. Z., "Distillation design", McGraw-Hill, New York (1992).

Liang, S. Y. and W. Smith, "The effect of heat transfer between the phases on the performance of countercurrent distillation columns", Chem. Eng. Sci., **17**, 11-21 (1962).

Moens, F. P., "The effect of composition and driving force on the performance of packed distillation columns – I", Chem. Eng. Sci., **27**, 275-283 (1972).

Nicolaiewsky, E. M. A, F. W. Tavares, K. Rajogopal and J. Fair, "Liquid film flow and area generation in structured packed columns", Powder Technology, **104**, 84-94 (1999).

Norman, W. S. and D. T. Binns, "The effect of surface tension changes on the minimum wetting rates in a wetted-rod distillation column", Trans. Instn. Chem. Engrs., **38**, 294-300 (1960).

Norman, W. S., T. Cakalor, A. Z. Fresco, D. H. Sutcliffe, "The two film theory of distillation in packed towers", Trans. Instn. Chem. Engrs., **41**, 61-71 (1963).

Onda, K., H Takeuchi, Y. Maeda and N. Takeuchi, "Liquid distribution in a packed column", Chem. Eng. Sci., **28**, 1677-1683 (1973).

Onda, K., H. Takeuchi and Y. Okumoto, "Mass transfer coefficiencts between gas and liquid phases in packed columns", J. of Chem. Eng. of Japan, 1, No. 1, 56-62 (1968)

Ponter, A. B., G. A. Davis, W. Beaton and T. K. Ross, "Wetting of packings in distillation: the influence of contact angle", Trans. Instn. Chem. Engrs., **45**, T345-352 (1967).

Ruckenstein, E., and O. Smigelschi, "The thermal theory and the plate efficiency", Can. J. of Chem. Eng., **45**, Dec., 334-340 (1967).

Sawistowski, H, "The performance of packed distillation columns", Final report and proceedings of the symposium held in London, 231-255 (1964).

Sawistowski, H. and W. Smith, "Performance of packed distillation columns", Ind. Eng. Chem., **51**, No. 8, 915-918 (1959).

Sharp, D, "Simulation of a 2-dimensional bubble column", M.Sc. Thesis, University of Alberta (2000).

Shi, M. G. and A. Mersmann, "Effective interfacial area in packed columns", Ger. Chem. Eng, **8**, 87-96 (1985).

Syeda, S., "Froth structure and mass transfer on distillation trays", Ph.D. Thesis, University of Alberta (2002).

van Wijk, W. R. and H. A. C. Thijssen, "Concentration and plate efficiency in distillation columns", Chem. Eng. Sci., **3**, 153-160 (1954).

Wong, A., "New correlations for predicting sieve tray efficiencies", M.Sc. Thesis, University of Alberta (1993).

Yang, L. and K. T. Chuang, "Efficiency considerations for choice between trays and packing", Chem. Eng. Comm., **137**, 161-175 (1995).

Yoshida, F., T. Koyanagi, T. Katayama and H. Sasai, "Distillation in packed columns", Ind. Eng. Chem., **46**, No. 9, 1756-1762 (1954).

Zuiderweg, F. J. and A. Harmens, "The influence of surface phenomena on the performance of distillation columns", Chem. Eng. Sci, **9**, 89-108 (1958).

Appendix A

EXPERIMENTAL DATA

A1 Experimental data for the METHANOL / WATER system

All experimental data was obtained at atmospheric pressure (94 kPa).

Table A1.1 Concentration data for the methanol/water system.

	Area % Methanol		Weight % Methanol		Mole % Methanol	
Run	Top	Bottom	Top	Bottom	x_{Top}	x_{Bottom}
1	98.770	97.449	97.974	96.670	96.454	94.228
2	98.198	96.210	97.410	95.447	95.486	92.181
3	97.442	93.183	96.663	92.459	94.217	87.335
4	96.693	88.863	95.924	88.194	92.976	80.774
5	95.363	86.164	94.611	85.530	90.804	76.875
6	94.728	54.757	93.984	54.525	89.786	40.275
7	94.256	45.789	93.518	45.671	89.028	32.102
8	94.170	75.662	93.433	75.162	88.892	62.990
9	93.969	78.157	93.235	77.625	88.573	66.121
10	93.778	70.333	93.046	69.901	88.271	56.643
11	92.343	27.977	92.629	28.087	86.027	18.010
12	89.958	17.123	89.275	17.372	82.400	10.574
13	87.440	11.557	86.789	11.878	78.700	7.046
14	80.715	4.233	80.150	4.647	69.430	2.668
15	74.808	0.846	74.319	1.303	61.947	0.737
16	39.731	0.150	39.691	0.617	27.020	0.348

Table A1.2 Cooling water, reflux and duty data for the methanol/water system.

	Cooling Water						
	Temperature		Flow rate	Vapor Rate	Duty		
Run	$(T_{CW})_{in}$ ° C	$(T_{CW})_{out}$ ° C	$m_{cooling}$ % RR	m_{reflux} % RR	$Q_{reboiler}$ kW	$Q_{condensor}$ kW	Heat Loss %
1	13.95	60.25	23.50	52.50	2.080	1.775	14.64
2	9.80	60.75	21.75	56.75	2.180	1.809	17.04
3	11.40	61.15	22.50	57.00	2.270	1.827	19.53
4	9.25	61.40	22.00	57.00	2.320	1.872	19.30
5	9.70	61.80	25.00	60.00	2.400	2.125	11.44
6	22.00	63.00	22.00	50.00	2.160	1.472	31.85
7	21.50	62.10	23.00	48.00	2.160	1.524	29.45
8	15.10	62.10	22.00	47.00	2.260	1.687	25.34
9	11.80	62.10	24.75	59.00	2.520	2.032	19.37
10	17.25	62.40	22.50	46.00	2.160	1.658	23.26
11	21.95	63.05	24.00	49.25	2.160	1.610	25.47
12	26.20	54.10	35.00	50.00	2.200	1.594	27.56
13	26.10	56.60	31.00	47.00	2.200	1.543	29.86
14	21.95	60.65	24.50	42.25	2.200	1.548	29.64
15	20.80	62.80	23.50	39.50	2.200	1.611	26.78
16	21.00	72.00	15.00	30.00	2.000	1.248	37.58

Table A1.3 Reflux flow rate data for the methanol/water system.

Run	m_{H2O} (kg/s)	m_{Mix} (kg/s)	L (kmol/s)	U_g (m/s)	f-Factor $(m/s)(kg/m^3)^{0.5}$
1	$1.21x10^{-3}$	$1.13x10^{-3}$	$1.51x10^{-6}$	0.25	0.25
2	$1.32x10^{-3}$	$1.23x10^{-3}$	$1.64x10^{-6}$	0.27	0.28
3	$1.32x10^{-3}$	$1.23x10^{-3}$	$1.64x10^{-6}$	0.27	0.28
4	$1.32x10^{-3}$	$1.23x10^{-3}$	$1.64x10^{-6}$	0.28	0.28
5	$1.40x10^{-3}$	$1.30x10^{-3}$	$1.73x10^{-6}$	0.29	0.30
6	$1.15x10^{-3}$	$1.07x10^{-3}$	$1.42x10^{-6}$	0.24	0.25
7	$1.10x10^{-3}$	$1.02x10^{-3}$	$1.36x10^{-6}$	0.23	0.23
8	$1.07x10^{-3}$	$1.00x10^{-3}$	$1.33x10^{-6}$	0.23	0.23
9	$1.37x10^{-3}$	$1.28x10^{-3}$	$1.70x10^{-6}$	0.29	0.29
10	$1.05x10^{-3}$	$9.78x10^{-4}$	$1.30x10^{-6}$	0.22	0.22
11	$1.13x10^{-3}$	$1.05x10^{-3}$	$1.40x10^{-6}$	0.24	0.24
12	$1.15x10^{-3}$	$1.07x10^{-3}$	$1.42x10^{-6}$	0.25	0.25
13	$1.07x10^{-3}$	$1.00x10^{-3}$	$1.32x10^{-6}$	0.24	0.24
14	$9.54x10^{-4}$	$8.97x10^{-4}$	$1.16x10^{-6}$	0.23	0.22
15	$8.85x10^{-4}$	$8.35x10^{-4}$	$1.07x10^{-6}$	0.22	0.21
16	$6.48x10^{-4}$	$6.24x10^{-4}$	$7.43x10^{-7}$	0.21	0.17

Table A1.4 Efficiency data for the methanol/water system

Run	Mole fraction Methanol x_{Avg}	Number of theoretical stages N_T	Height equivalent to a theoretical plate HETP (m)
1	0.953	0.503	0.101
2	0.938	0.575	0.088
3	0.908	0.874	0.058
4	0.869	1.177	0.043
5	0.838	1.119	0.045
6	0.650	1.196	0.042
7	0.606	1.330	0.038
8	0.759	1.476	0.034
9	0.773	1.343	0.038
10	0.725	1.620	0.031
11	0.520	1.486	0.034
12	0.465	1.635	0.031
13	0.429	1.731	0.029
14	0.360	1.942	0.026
15	0.313	2.298	0.022
16	0.137	1.384	0.037

A2 Experimental data for the n-HEPTANE / TOLUENE system

All experimental data was obtained at atmospheric pressure (94 kPa).

Table A2.1 Concentration data for the n-heptane/toluene system.

	Area % n-Heptane		Weight % n-Heptane		Mole % n-Heptane	
Run	Top	Bottom	Top	Bottom	x_{Top}	x_{Bottom}
1	97.284	97.135	96.690	96.527	96.411	96.235
2	96.146	95.915	95.450	95.198	95.071	94.800
3	92.630	92.157	91.633	91.122	90.967	90.420
4	88.703	87.887	87.401	86.524	86.448	85.516
5	86.067	84.841	84.576	83.267	83.450	82.066
6	83.497	81.993	81.837	80.240	80.557	78.876
7	83.081	81.327	81.395	79.534	80.091	78.135
8	75.570	72.887	73.471	70.668	71.804	68.900
9	69.266	65.149	66.908	62.665	65.025	60.684
10	64.468	59.492	61.967	56.891	59.971	54.823
11	59.278	53.434	56.674	50.779	54.604	48.683
12	52.058	45.002	49.402	42.396	47.308	40.362
13	44.977	37.088	42.372	34.659	40.339	32.785
14	39.309	30.853	36.818	28.653	34.890	26.969
15	32.633	24.757	30.360	22.856	28.616	21.411
16	32.039	23.991	29.789	22.133	28.065	20.721
17	23.375	16.192	21.552	14.837	20.168	13.809
18	14.438	9.875	13.214	9.019	12.282	8.354
19	7.456	4.995	6.813	4.579	6.299	4.226

Table A2.2 Cooling water, reflux and duty data for the n-heptane/toluene system.

	Cooling Water						
	Temperature		Flow rate	Vapor Rate	Duty		
Run	$(T_{CW})_{in}$ ° C	$(T_{CW})_{out}$ ° C	$m_{cooling}$ % RR	m_{reflux} % RR	$Q_{reboiler}$ kW	$Q_{condensor}$ kW	Heat Loss %
1	22.00	44.90	12.50	68.50	1.250	0.467	62.64
2	23.00	54.15	10.50	65.50	1.210	0.535	55.76
3	23.45	63.10	7.50	67.25	1.240	0.486	60.84
4	24.05	77.60	6.00	66.75	1.210	0.525	56.64
5	24.95	83.45	7.50	68.25	1.210	0.717	40.74
6	24.90	85.00	6.50	68.75	1.210	0.638	47.29
7	21.35	26.20	58.50	62.00	1.220	0.463	62.05
8	19.35	26.25	51.50	76.50	1.340	0.580	56.73
9	19.80	25.00	66.50	69.50	1.340	0.564	57.92
10	18.55	26.25	45.00	65.50	1.350	0.566	58.11
11	17.20	25.05	45.50	67.25	1.380	0.583	57.75
12	17.70	28.60	32.25	66.50	1.380	0.574	58.41
13	18.60	33.35	23.25	61.50	1.360	0.560	58.84
14	18.15	23.25	61.25	62.75	1.360	0.520	61.79
15	16.05	25.00	41.75	71.25	1.490	0.610	59.06
16	23.05	27.55	68.50	64.50	1.360	0.503	63.01
17	23.00	30.35	42.25	59.50	1.360	0.507	62.73
18	21.50	31.35	39.50	74.00	1.400	0.635	54.65
19	19.20	33.95	23.75	64.50	1.400	0.572	59.16

Table A2.3 Reflux flow rate data for the n-heptane/toluene system.

Run	m_{H2O} (kg/s)	m_{Mix} (kg/s)	L (kmol/s)	U_g (m/s)	f-Factor $(m/s)(kg/m^3)^{0.5}$
1	$1.61x10^{-3}$	$1.33x10^{-3}$	$2.52x10^{-6}$	0.10	0.18
2	$1.53x10^{-3}$	$1.27x10^{-3}$	$2.39x10^{-6}$	0.10	0.17
3	$1.58x10^{-3}$	$1.32x10^{-3}$	$2.42x10^{-6}$	0.10	0.17
4	$1.56x10^{-3}$	$1.32x10^{-3}$	$2.37x10^{-6}$	0.10	0.17
5	$1.60x10^{-3}$	$1.36x10^{-3}$	$2.40x10^{-6}$	0.10	0.18
6	$1.61x10^{-3}$	$1.68x10^{-3}$	$2.39x10^{-6}$	0.11	0.18
7	$1.45x10^{-3}$	$1.24x10^{-3}$	$2.14x10^{-6}$	0.09	0.16
8	$1.81x10^{-3}$	$1.57x10^{-3}$	$2.61x10^{-6}$	0.12	0.21
9	$1.63x10^{-3}$	$1.43x10^{-3}$	$2.31x10^{-6}$	0.11	0.19
10	$1.53x10^{-3}$	$1.36x10^{-3}$	$2.13x10^{-6}$	0.11	0.18
11	$1.58x10^{-3}$	$1.40x10^{-3}$	$2.16x10^{-6}$	0.11	0.19
12	$1.56x10^{-3}$	$1.40x10^{-3}$	$2.09x10^{-6}$	0.11	0.18
13	$1.43x10^{-3}$	$1.30x10^{-3}$	$1.89x10^{-6}$	0.10	0.19
14	$1.47x10^{-3}$	$1.34x10^{-3}$	$1.91x10^{-6}$	0.11	0.18
15	$1.68x10^{-3}$	$1.54x10^{-3}$	$2.15x10^{-6}$	0.13	0.21
16	$1.51x10^{-3}$	$1.39x10^{-3}$	$1.93x10^{-6}$	0.11	0.19
17	$1.38x10^{-3}$	$1.28x10^{-3}$	$1.74x10^{-6}$	0.11	0.18
18	$1.75x10^{-3}$	$1.63x10^{-3}$	$2.16x10^{-6}$	0.14	0.23
19	$1.51x10^{-3}$	$1.42x10^{-3}$	$1.84x10^{-6}$	0.12	0.20

Table A2.4 Efficiency data for the n-heptane/toluene system.

Run	Mole fraction n-Heptane x_{Avg}	Number of theoretical stages N_T	Height equivalent to a theoretical plate HETP (m)
1	0.963	0.437	0.116
2	0.949	0.455	0.112
3	0.907	0.455	0.112
4	0.859	0.489	0.104
5	0.828	0.574	0.088
6	0.797	0.578	0.088
7	0.791	0.650	0.078
8	0.704	0.638	0.080
9	0.629	0.731	0.069
10	0.574	0.743	0.068
11	0.516	0.751	0.068
12	0.438	0.780	0.065
13	0.366	0.804	0.063
14	0.309	0.846	0.060
15	0.250	0.814	0.062
16	0.244	0.838	0.061
17	0.170	0.878	0.058
18	0.103	0.744	0.066
19	0.053	0.720	0.071

A3 Experimental data for the BENZENE / n-HEPTANE system

All experimental data was obtained at atmospheric pressure (94 kPa).

Table A3.1 Concentration data for the benzene/n-heptane system.

	Area % Benzene		Weight % Benzene		Mole % Benzene	
Run	Top	Bottom	Top	Bottom	x_{Top}	x_{Bottom}
1	87.671	86.750	92.063	91.591	93.702	93.321
2	85.202	84.118	86.606	85.376	89.240	88.219
3	81.202	79.507	82.683	81.108	85.963	84.632
4	78.629	76.311	80.291	78.122	83.936	82.079
5	75.445	72.946	77.310	74.955	81.379	79.333
6	67.891	63.499	70.149	65.928	75.088	71.280
7	67.256	62.928	69.542	65.376	74.545	70.776
8	58.051	52.055	60.633	54.730	66.393	60.795
9	50.204	43.774	52.892	46.448	59.019	52.662
10	38.606	32.025	41.202	34.438	47.335	40.253
11	31.527	25.816	33.922	27.968	39.703	33.245
12	27.964	21.768	30.216	23.704	35.707	28.495
13	23.314	18.018	25.337	19.723	30.327	23.961
14	17.634	12.773	19.313	14.101	23.490	17.394
15	17.345	12.337	19.005	13.631	23.134	16.836
16	13.754	10.336	15.157	11.469	18.643	14.249
17	6.375	4.271	7.163	4.861	9.005	6.150

Table A3.2 Cooling water, reflux and duty data for the benzene/n-heptane system.

Run	Cooling Water			Vapor Rate	Duty		
	Temperature		Flow rate				
	$(T_{CW})_{in}$ ° C	$(T_{CW})_{out}$ ° C	$m_{cooling}$ % RR	m_{reflux} % RR	$Q_{reboiler}$ kW	$Q_{condensor}$ kW	Heat Loss %
1	17.98	28.45	39.75	73.25	1.250	0.672	46.26
2	24.80	34.30	45.00	75.00	1.220	0.698	42.82
3	24.80	32.40	55.00	74.00	1.220	0.682	44.09
4	18.70	29.00	41.25	77.50	1.243	0.684	44.94
5	25.70	34.40	45.00	78.00	1.230	0.639	48.06
6	20.30	24.60	92.00	74.00	1.250	0.646	48.34
7	233.50	30.30	58.00	70.00	1.230	0.644	47.67
8	25.30	45.30	22.00	76.50	1.290	0.718	44.34
9	25.00	42.50	25.00	77.50	1.290	0.714	44.66
10	22.90	39.40	25.00	70.00	1.230	0.673	45.27
11	22.00	38.20	25.00	70.00	1.300	0.661	49.16
12	24.80	32.50	48.50	66.00	1.300	0.609	53.12
13	19.00	34.50	27.00	73.50	1.310	0.683	47.87
14	17.50	30.80	28.50	73.00	1.310	0.619	52.78
15	17.50	31.70	27.00	74.00	1.310	0.626	52.23
16	24.40	31.50	57.00	77.00	1.400	0.660	52.83
17	19.40	29.00	39.00	78.00	1.350	0.611	54.74

Table A3.3 Reflux flow rate data for the benzene/n-heptane system.

Run	m_{H2O} (kg/s)	m_{Mix} (kg/s)	L (kmol/s)	U_g (m/s)	f-Factor $(m/s)(kg/m^3)^{0.5}$
1	$1.75x10^{-3}$	$1.66x10^{-3}$	$2.09x10^{-6}$	0.14	0.23
2	$1.77x10^{-3}$	$1.67x10^{-3}$	$2.14x10^{-6}$	0.15	0.24
3	$1.75x10^{-3}$	$1.64x10^{-3}$	$2.12x10^{-6}$	0.15	0.23
4	$1.83x10^{-3}$	$1.72x10^{-3}$	$2.24x10^{-6}$	0.15	0.25
5	$1.85x10^{-3}$	$1.73x10^{-3}$	$2.27x10^{-6}$	0.15	0.25
6	$1.75x10^{-3}$	$1.62x10^{-3}$	$2.18x10^{-6}$	0.14	0.23
7	$1.65x10^{-3}$	$1.53x10^{-3}$	$2.06x10^{-6}$	0.13	0.22
8	$1.81x10^{-3}$	$1.67x10^{-3}$	$2.30x10^{-6}$	0.14	0.23
9	$1.83x10^{-3}$	$1.68x10^{-3}$	$2.37x10^{-6}$	0.14	0.23
10	$1.65x10^{-3}$	$1.49x10^{-3}$	$2.17x10^{-6}$	0.12	0.20
11	$1.65x10^{-3}$	$1.48x10^{-3}$	$2.20x10^{-6}$	0.12	0.20
12	$1.55x10^{-3}$	$1.39x10^{-3}$	$2.08x10^{-6}$	0.11	0.19
13	$1.73x10^{-3}$	$1.55x10^{-3}$	$2.35x10^{-6}$	0.12	0.21
14	$1.72x10^{-3}$	$1.53x10^{-3}$	$2.36x10^{-6}$	0.12	0.21
15	$1.75x10^{-3}$	$1.55x10^{-3}$	$2.40x10^{-6}$	0.12	0.21
16	$1.82x10^{-3}$	$1.61x10^{-3}$	$2.51x10^{-6}$	0.13	0.22
17	$1.85x10^{-3}$	$1.63x10^{-3}$	$2.58x10^{-6}$	0.12	0.22

Table A3.4 Efficiency data for the benzene/n-heptane system.

Run	Mole fraction Benzene x_{Avg}	Number of theoretical stages N_T	Height equivalent to a theoretical plate HETP (m)
1	0.935	0.328	0.155
2	0.887	0.407	0.125
3	0.853	0.370	0.137
4	0.830	0.424	0.120
5	0.804	0.385	0.132
6	0.732	0.480	0.106
7	0.727	0.464	0.110
8	0.636	0.497	0.102
9	0.558	0.472	0.108
10	0.438	0.463	0.110
11	0.365	0.425	0.120
12	0.321	0.492	0.103
13	0.271	0.468	0.109
14	0.204	0.533	0.095
15	0.200	0.559	0.091
16	0.165	0.449	0.113
17	0.0758	0.562	0.090

A4 Experimental data for the WATER / ACETIC ACID system

All experimental data was obtained at atmospheric pressure (94 kPa).

Table A4.1 Concentration data for the water/acetic acid system.

	Area % Water		Weight % Water		Mole % Water	
Run	Top	Bottom	Top	Bottom	x_{Top}	x_{Bottom}
1	98.382	96.787	97.055	94.833	99.098	98.391
2	97.397	95.465	95.678	93.018	98.663	97.797
3	95.028	91.844	92.424	88.172	97.599	96.130
4	91.074	85.781	87.165	80.446	95.768	93.202
5	84.817	75.981	79.260	68.895	92.719	88.068
6	74.353	59.961	67.079	52.125	87.163	78.394
7	63.386	44.484	55.515	37.831	80.615	66.973
8	55.492	36.287	47.835	30.795	75.344	59.724
9	51.064	31.875	43.721	27.117	72.136	55.354
10	38.918	21.917	33.022	18.999	62.164	43.871
11	32.268	16.340	27.442	14.515	55.759	36.136
12	24.471	11.000	21.063	10.227	47.068	27.518
13	20.929	8.448	18.203	8.173	42.581	22.875
14	16.151	5.523	14.363	5.808	35.853	17.046
15	9.846	3.350	9.299	4.042	25.465	12.310
16	6.377	2.279	6.499	3.168	18.808	9.832

Table A4.2 Cooling water, reflux and duty data for the water/acetic acid system.

Run	Cooling Water			Vapor Rate	Duty		
	Temperature		Flow rate				
	$(T_{CW})_{in}$ °C	$(T_{CW})_{out}$ °C	$m_{cooling}$ % RR	m_{reflux} % RR	$Q_{reboiler}$ kW	$Q_{condensor}$ kW	Heat Loss %
1	24.40	91.00	14.00	26.00	2.400	1.523	36.53
2	23.80	91.10	16.00	31.00	2.700	1.759	34.85
3	23.80	90.60	18.00	31.00	2.700	1.964	27.25
4	23.00	89.80	15.00	32.00	2.750	1.637	40.48
5	22.50	90.00	16.00	31.50	2.800	1.764	36.99
6	22.20	88.30	20.00	56.00	3.160	2.159	31.67
7	22.50	82.50	22.00	49.00	2.780	2.156	22.46
8	23.10	96.80	11.00	44.00	2.200	1.325	39.78
9	24.30	86.40	14.00	50.00	2.480	1.420	42.74
10	24.70	96.30	6.00	42.00	1.680	0.702	58.21
11	27.30	92.80	10.00	42.00	1.680	1.070	36.29
12	24.80	87.50	10.00	50.00	1.760	1.024	41.81
13	25.20	77.20	10.00	42.00	1.620	0.849	47.59
14	17.95	26.35	69.00	60.00	1.910	0.937	50.94
15	18.70	30.00	40.00	50.00	1.580	0.738	53.31
16	18.30	28.80	39.00	54.00	1.520	0.668	56.03

Table A4.3 Reflux flow rate data for the water/acetic acid system.

Run	m_{H2O} (kg/s)	m_{Mix} (kg/s)	L (kmol/s)	U_g (m/s)	f-Factor $(m/s)(kg/m^3)^{0.5}$
1	$5.49x10^{-4}$	$5.40x10^{-4}$	$5.89x10^{-7}$	0.22	0.17
2	$6.73x10^{-4}$	$6.63x10^{-4}$	$7.23x10^{-7}$	0.27	0.20
3	$6.73x10^{-4}$	$6.63x10^{-4}$	$7.25x10^{-7}$	0.26	0.20
4	$6.98x10^{-4}$	$6.86x10^{-4}$	$7.54x10^{-7}$	0.26	0.20
5	$6.86x10^{-4}$	$6.73x10^{-4}$	$7.43x10^{-7}$	0.24	0.19
6	$1.30x10^{-3}$	$1.27x10^{-3}$	$1.42x10^{-6}$	0.41	0.35
7	$1.12x10^{-3}$	$1.10x10^{-3}$	$1.23x10^{-6}$	0.32	0.29
8	$9.97x10^{-4}$	$9.77x10^{-4}$	$1.09x10^{-6}$	0.26	0.24
9	$1.15x10^{-3}$	$1.12x10^{-3}$	$1.25x10^{-6}$	0.29	0.27
10	$9.48x10^{-4}$	$9.29x10^{-4}$	$1.03x10^{-6}$	0.21	0.21
11	$9.48x10^{-4}$	$9.30x10^{-4}$	$1.03x10^{-6}$	0.20	0.21
12	$1.15x10^{-3}$	$1.13x10^{-3}$	$1.24x10^{-6}$	0.22	0.24
13	$9.48x10^{-4}$	$9.32x10^{-4}$	$1.02x10^{-6}$	0.17	0.19
14	$1.40x10^{-3}$	$1.38x10^{-3}$	$1.50x10^{-6}$	0.24	0.28
15	$1.15x10^{-3}$	$1.13x10^{-3}$	$1.22x10^{-6}$	0.18	0.22
16	$1.25x10^{-3}$	$1.23x10^{-3}$	$1.32x10^{-6}$	0.19	0.23

Table A4.4 Efficiency data for the water/acetic acid system.

Run	Mole fraction Water x_{Avg}	Number of theoretical stages N_T	Height equivalent to a theoretical plate HETP (m)
1	0.987	0.182	0.279
2	0.982	0.297	0.171
3	0.969	0.565	0.090
4	0.945	0.673	0.075
5	0.904	0.669	0.076
6	0.828	0.606	0.084
7	0.738	0.615	0.083
8	0.675	0.535	0.095
9	0.637	0.524	0.097
10	0.530	0.464	0.110
11	0.459	0.541	0.094
12	0.373	0.619	0.082
13	0.327	0.679	0.075
14	0.264	0.779	0.065
15	0.189	0.515	0.099
16	0.143	0.242	0.210

A5 Experimental data for the ISOPROPANOL / WATER system

All experimental data was obtained at atmospheric pressure (94 kPa).

Table A5.1 Concentration data for the isopropanol/water system.

	Area % Isopropanol		Weight % Isopropanol		Mole % Isopropanol	
Run	Top	Bottom	Top	Bottom	x_{Top}	x_{Bottom}
1	99.012	99.252	97.377	97.558	91.757	92.294
2	97.061	97.527	95.899	96.254	87.518	88.512
3	96.599	97.082	95.547	95.916	86.548	87.564
4	94.933	95.495	94.268	94.701	83.146	84.280
5	92.343	92.831	92.254	92.636	78.125	79.044
6	90.022	90.274	90.424	90.623	73.900	74.345
7	82.844	79.329	84.606	81.670	62.233	57.195
8	82.427	76.274	82.260	79.073	61.618	53.117
9	81.868	73.470	83.796	76.651	60.797	49.605
10	81.651	71.809	83.615	75.200	60.480	47.623
11	81.232	68.685	83.266	72.435	59.874	44.073
12	80.201	59.347	82.403	63.906	58.410	34.681
13	78.934	50.569	81.334	55.516	56.673	27.258
14	75.863	50.867	78.718	55.813	52.601	27.471
15	72.748	39.106	76.021	44.044	48.745	19.094
16	64.968	29.745	69.088	34.206	40.128	13.523
17	60.088	23.174	64.592	27.076	35.387	10.040

Table A5.2 Cooling water, reflux and duty data for the isopropanol/water system.

Run	Cooling Water						
	Temperature		Flow rate	Vapor Rate	Duty		
	$(T_{CW})_{in}$ °C	$(T_{CW})_{out}$ °C	$m_{cooling}$ % RR	m_{reflux} % RR	$Q_{reboiler}$ kW	$Q_{condensor}$ kW	Heat Loss %
1	16.95	61.55	11.50	53.00	1.290	0.838	35.04
2	19.05	73.65	12.00	56.75	1.400	1.070	23.58
3	18.85	75.05	10.00	63.25	1.490	0.917	38.43
4	20.60	76.08	9.75	54.38	1.390	0.882	36.51
5	19.78	73.33	10.00	53.50	1.395	0.875	37.22
6	20.70	72.95	10.75	50.50	1.400	0.917	34.51
7	16.60	74.50	12.50	64.00	1.720	1.182	31.29
8	17.15	73.85	10.50	53.25	1.540	0.972	36.90
9	17.40	73.65	12.00	51.50	1.500	1.102	26.53
10	17.75	73.75	13.00	53.00	1.550	1.188	23.33
11	16.25	74.05	13.00	53.00	1.680	1.226	27.00
12	13.80	73.20	14.50	55.75	1.760	1.406	20.12
13	14.50	71.65	14.50	54.00	1.760	1.352	23.18
14	17.10	63.55	15.00	46.00	1.620	1.137	29.81
15	14.80	60.65	15.00	54.00	1.940	1.122	42.15
16	13.00	53.25	17.00	46.50	1.940	1.116	42.45
17	12.50	50.80	24.50	46.25	1.940	1.533	20.99

Table A5.3 Reflux flow rate data for the isopropanol/water system.

Run	m_{H2O} (kg/s)	m_{Mix} (kg/s)	L (kmol/s)	U_g (m/s)	f-Factor $(m/s)(kg/m^3)^{0.5}$
1	$1.22x10^{-3}$	$1.13x10^{-3}$	$1.55x10^{-6}$	0.14	0.19
2	$1.32x10^{-3}$	$1.22x10^{-3}$	$1.66x10^{-6}$	0.16	0.21
3	$1.48x10^{-3}$	$1.37x10^{-3}$	$1.86x10^{-6}$	0.18	0.24
4	$1.26x10^{-3}$	$1.17x10^{-3}$	$1.58x10^{-6}$	0.16	0.21
5	$1.23x10^{-3}$	$1.15x10^{-3}$	$1.55x10^{-6}$	0.16	0.21
6	$1.16x10^{-3}$	$1.08x10^{-3}$	$1.45x10^{-6}$	0.16	0.20
7	$1.50x10^{-3}$	$1.40x10^{-3}$	$1.85x10^{-6}$	0.23	0.27
8	$1.23x10^{-3}$	$1.15x10^{-3}$	$1.52x10^{-6}$	0.19	0.22
9	$1.18x10^{-3}$	$1.11x10^{-3}$	$1.46x10^{-6}$	0.18	0.22
10	$1.22x10^{-3}$	$1.14x10^{-3}$	$1.51x10^{-6}$	0.19	0.22
11	$1.22x10^{-3}$	$1.14x10^{-3}$	$1.51x10^{-6}$	0.19	0.22
12	$1.29x10^{-3}$	$1.21x10^{-3}$	$1.59x10^{-6}$	0.21	0.24
13	$1.25x10^{-3}$	$1.17x10^{-3}$	$1.53x10^{-6}$	0.20	0.23
14	$1.05x10^{-3}$	$9.84x10^{-4}$	$1.28x10^{-6}$	0.18	0.20
15	$1.25x10^{-3}$	$1.17x10^{-3}$	$1.52x10^{-6}$	0.22	0.24
16	$1.06x10^{-3}$	$1.00x10^{-3}$	$1.27x10^{-6}$	0.21	0.22
17	$1.05x10^{-3}$	$1.00x10^{-3}$	$1.26x10^{-6}$	0.22	0.23

Table A5.4 Efficiency data for the isopropanol/water system.

Run	Mole fraction Isopropanol x_{Avg}	Number of theoretical stages N_T	Height equivalent to a theoretical plate HETP (m)
1	0.920	0.143	0.357
2	0.880	0.226	0.224
3	0.871	0.229	0.222
4	0.837	0.261	0.195
5	0.786	0.271	0.187
6	0.741	0.240	0.212
7	0.597	0.922	0.055
8	0.574	1.244	0.041
9	0.552	1.374	0.037
10	0.541	1.449	0.035
11	0.520	1.543	0.033
12	0.466	1.671	0.030
13	0.420	1.653	0.031
14	0.400	1.350	0.038
15	0.339	1.332	0.038
16	0.268	1.104	0.046
17	0.227	1.058	0.048

A6 Experimental data for the METHANOL / ISOPROPANOL system

All experimental data was obtained at atmospheric pressure (94 kPa).

Table A6.1 Concentration data for the methanol/isopropanol system.

	Area % Methanol		Weight % Methanol		Mole % Methanol	
Run	Top	Bottom	Top	Bottom	x_{Top}	x_{Bottom}
1	96.290	94.912	95.643	94.061	97.629	96.744
2	91.529	88.665	90.205	86.969	94.528	92.603
3	86.226	81.924	84.235	79.458	90.928	87.887
4	80.231	74.597	77.595	71.460	86.660	82.446
5	72.963	66.587	69.700	62.915	81.185	76.090
6	66.328	59.771	62.642	55.806	75.877	70.315
7	58.672	51.622	54.675	47.506	69.351	62.929
8	55.037	48.384	50.958	44.264	66.091	59.834
9	45.452	39.451	41.362	35.506	56.955	50.804
10	40.062	34.578	36.097	30.836	51.446	45.543
11	35.369	30.311	31.589	26.810	46.413	40.727
12	30.277	26.035	26.778	22.834	40.688	35.693
13	23.348	19.668	20.366	17.023	32.420	27.789
14	19.177	16.073	16.581	13.801	27.158	23.096
15	13.544	11.353	11.558	9.632	19.687	16.661
16	9.062	7.512	7.635	6.293	13.423	11.188
17	4.978	4.050	4.269	3.475	7.718	6.325
18	2.603	2.001	2.238	1.723	4.116	3.184

Table A6.2 Cooling water, reflux and duty data for the methanol/isopropanol system.

Run	Cooling Water						
	Temperature		Flow rate	Vapor Rate	Duty		
	$(T_{CW})_{in}$ ° C	$(T_{CW})_{out}$ ° C	$m_{cooling}$ % RR	m_{reflux} % RR	$Q_{reboiler}$ kW	$Q_{condensor}$ kW	Heat Loss %
1	9.60	31.85	47.75	59.50	2.120	1.734	18.23
2	13.70	60.60	22.25	59.50	2.080	1.703	18.13
3	14.70	60.70	23.00	60.50	2.120	1.727	18.56
4	10.95	60.90	21.50	66.25	2.140	1.752	18.11
5	12.40	60.85	22.50	68.75	2.180	1.779	18.40
6	12.50	60.80	22.50	68.50	2.180	1.773	18.65
7	13.65	56.65	22.75	66.00	2.000	1.596	20.19
8	15.00	62.53	19.50	68.25	2.020	1.513	25.09
9	12.10	61.35	18.00	72.00	1.960	1.447	26.18
10	14.30	60.90	17.50	65.50	1.800	1.331	26.06
11	14.00	60.60	16.50	62.75	1.720	1.255	27.05
12	15.80	61.00	16.50	65.50	1.720	1.216	29.28
13	14.95	66.85	14.75	74.00	1.800	1.249	30.59
14	15.30	67.53	13.75	67.13	1.680	1.172	30.25
15	15.23	69.58	14.33	70.33	1.730	1.272	26.47
16	12.70	35.60	30.50	71.75	1.700	1.140	32.94
17	16.19	74.41	12.21	72.79	1.730	1.164	32.74
18	15.53	74.10	14.50	73.00	1.730	1.384	20.00

Table A6.3 Reflux flow rate data for the methanol/isopropanol system.

Run	m_{H2O} (kg/s)	m_{Mix} (kg/s)	L (kmol/s)	U_g (m/s)	f-Factor $(m/s)(kg/m^3)^{0.5}$
1	$1.38x10^{-3}$	$1.23x10^{-3}$	$1.91x10^{-6}$	0.25	0.27
2	$1.38x10^{-3}$	$1.23x10^{-3}$	$1.91x10^{-6}$	0.25	0.26
3	$1.41x10^{-3}$	$1.25x10^{-3}$	$1.94x10^{-6}$	0.25	0.27
4	$1.55x10^{-3}$	$1.38x10^{-3}$	$2.13x10^{-6}$	0.26	0.29
5	$1.61x10^{-3}$	$1.44x10^{-3}$	$2.20x10^{-6}$	0.26	0.30
6	$1.61x10^{-3}$	$1.44x10^{-3}$	$2.19x10^{-6}$	0.25	0.29
7	$1.55x10^{-3}$	$1.39x10^{-3}$	$2.09x10^{-6}$	0.23	0.27
8	$1.60x10^{-3}$	$1.44x10^{-3}$	$2.16x10^{-6}$	0.24	0.28
9	$1.70x10^{-3}$	$1.53x10^{-3}$	$2.28x10^{-6}$	0.24	0.29
10	$1.53x10^{-3}$	$1.38x10^{-3}$	$2.05x10^{-6}$	0.21	0.26
11	$1.47x10^{-3}$	$1.32x10^{-3}$	$1.96x10^{-6}$	0.19	0.24
12	$1.53x10^{-3}$	$1.39x10^{-3}$	$2.04x10^{-6}$	0.20	0.25
13	$1.75x10^{-3}$	$1.58x10^{-3}$	$2.31x10^{-6}$	0.22	0.28
14	$1.57x10^{-3}$	$1.43x10^{-3}$	$2.08x10^{-6}$	0.19	0.25
15	$1.65x10^{-3}$	$1.50x10^{-3}$	$2.18x10^{-6}$	0.19	0.26
16	$1.69x10^{-3}$	$1.54x10^{-3}$	$2.22x10^{-6}$	0.19	0.26
17	$1.72x10^{-3}$	$1.56x10^{-3}$	$2.24x10^{-6}$	0.19	0.26
18	$1.72x10^{-3}$	$1.57x10^{-3}$	$2.25x10^{-6}$	0.19	0.26

Table A6.4 Efficiency data for the methanol/isopropanol system.

Run	Mole fraction Methanol x_{Avg}	Number of theoretical stages N_T	Height equivalent to a theoretical plate HETP (m)
1	0.972	0.515	0.099
2	0.936	0.440	0.113
3	0.894	0.453	0.112
4	0.846	0.461	0.110
5	0.786	0.432	0.118
6	0.731	0.398	0.128
7	0.661	0.399	0.128
8	0.630	0.372	0.136
9	0.539	0.349	0.146
10	0.485	0.340	0.149
11	0.436	0.342	0.149
12	0.382	0.323	0.157
13	0.301	0.352	0.144
14	0.251	0.354	0.144
15	0.182	0.336	0.151
16	0.123	0.335	0.151
17	0.070	0.330	0.154
18	0.037	0.389	0.131

A7 Experimental data for the CYCLOHEXANE / n-HEPTANE system

All experimental data was obtained at atmospheric pressure (94 kPa).

Table A7.1 Concentration data for the cyclohexane/n-heptane system.

	Area % Cyclohexane		Weight % Cyclohexane		Mole % Cyclohexane	
Run	Top	Bottom	Top	Bottom	x_{Top}	x_{Bottom}
1	95.885	94.993	98.329	97.423	98.593	97.827
2	93.420	91.940	95.825	94.321	96.470	95.186
3	90.529	88.500	92.887	90.826	93.957	92.180
4	87.199	84.357	89.504	86.617	91.034	88.513
5	80.970	76.656	83.176	78.792	85.478	81.561
6	71.437	65.634	73.491	67.595	76.747	71.293
7	58.875	52.060	60.728	53.803	64.802	58.100
8	54.504	47.985	56.287	49.663	60.522	54.016
9	50.683	44.015	52.405	45.630	56.727	49.980
10	42.296	35.400	43.884	36.878	48.215	41.023
11	34.327	28.442	35.787	29.808	39.887	33.581
12	23.981	18.955	25.276	20.170	28.710	23.125
13	15.731	12.294	16.894	13.402	19.486	15.559
14	8.602	6.817	9.651	7.838	11.283	9.194
15	4.220	3.113	5.199	4.075	6.130	4.814

Table A7.2 Cooling water, reflux and duty data for the cyclohexane/n-heptane system.

	Cooling Water						
	Temperature		Flow rate	Vapor Rate	Duty		
Run	$(T_{CW})_{in}$ ° C	$(T_{CW})_{out}$ ° C	$\dot{m}_{cooling}$ % RR	m_{reflux} % RR	$Q_{reboiler}$ kW	$Q_{condensor}$ kW	Heat Loss %
1	17.65	63.05	12.00	67.75	1.100	0.890	19.11
2	19.95	71.40	11.00	68.00	1.120	0.924	17.53
3	20.40	71.60	9.50	68.50	1.120	0.793	29.16
4	20.20	72.20	10.00	69.00	1.120	0.849	24.21
5	20.45	72.95	6.50	68.50	1.120	0.557	50.28
6	20.90	74.00	8.75	68.50	1.120	0.758	32.29
7	21.10	75.30	7.50	68.00	1.120	0.664	40.76
8	21.45	75.60	7.00	63.50	1.120	0.619	44.75
9	21.05	75.80	7.50	66.00	1.120	0.670	44.14
10	10.9	19.40	44.00	64.00	1.220	0.611	49.94
11	10.95	21.25	38.00	76.00	1.280	0.639	50.10
12	10.35	23.95	27.75	70.50	1.280	0.616	51.87
13	10.55	26.70	21.00	68.25	1.270	0.554	56.40
14	26.10	83.00	6.00	62.00	1.120	0.558	50.21
15	23.60	81.50	10.00	59.75	1.210	0.933	22.86

Table A7.3 Reflux flow rate data for the cyclohexane/n-heptane system.

Run	m_{H2O} (kg/s)	m_{Mix} (kg/s)	L (kmol/s)	U_g (m/s)	f-Factor $(m/s)(kg/m^3)^{0.5}$
1	$1.59x10^{-3}$	$1.49x10^{-3}$	$1.96x10^{-6}$	0.12	0.20
2	$1.60x10^{-3}$	$1.49x10^{-3}$	$1.98x10^{-6}$	0.12	0.21
3	$1.61x10^{-3}$	$1.50x10^{-3}$	$2.00x10^{-6}$	0.12	0.21
4	$1.60x10^{-3}$	$1.51x10^{-3}$	$2.03x10^{-6}$	0.12	0.21
5	$1.61x10^{-3}$	$1.49x10^{-3}$	$2.03x10^{-6}$	0.12	0.21
6	$1.61x10^{-3}$	$1.48x10^{-3}$	$2.06x10^{-6}$	0.12	0.20
7	$1.60x10^{-3}$	$1.45x10^{-3}$	$2.09x10^{-6}$	0.11	0.20
8	$1.48x10^{-3}$	$1.35x10^{-3}$	$1.95x10^{-6}$	0.11	0.18
9	$1.55x10^{-3}$	$1.40x10^{-3}$	$2.05x10^{-6}$	0.11	0.19
10	$1.50x10^{-3}$	$1.35x10^{-3}$	$2.00x10^{-6}$	0.10	0.18
11	$1.80x10^{-3}$	$1.61x10^{-3}$	$2.44x10^{-6}$	0.12	0.21
12	$1.66x10^{-3}$	$1.47x10^{-3}$	$2.28x10^{-6}$	0.11	0.19
13	$1.60x10^{-3}$	$1.42x10^{-3}$	$2.23x10^{-6}$	0.10	0.18
14	$1.45x10^{-3}$	$1.27x10^{-3}$	$2.03x10^{-6}$	0.09	0.16
15	$1.39x10^{-3}$	$1.22x10^{-3}$	$1.96x10^{-6}$	0.09	0.16

Table A7.4 Efficiency data for the cyclohexane/n-heptane system.

Run	Mole fraction Cyclohexane x_{Avg}	Number of theoretical stages N_T	Height equivalent to a theoretical plate HETP (m)
1	0.982	0.724	0.070
2	0.958	0.610	0.083
3	0.931	0.542	0.094
4	0.898	0.548	0.093
5	0.835	0.570	0.089
6	0.740	0.566	0.090
7	0.615	0.562	0.090
8	0.573	0.528	0.096
9	0.534	0.538	0.094
10	0.446	0.579	0.088
11	0.367	0.542	0.094
12	0.259	0.587	0.087
13	0.175	0.551	0.092
14	0.102	0.460	0.110
15	0.055	0.507	0.100

Appendix B

SYSTEM PROPERTY DATA

ASPENTech Simulation Software was used to obtain all system property data at 94 kPa. The vapor-liquid equilibrium data, taken from Gmehling (1980, 1981), was obtained at 101 kPa.

B1 Saturated system property data for the METHANOL / WATER system determined using the NRTL method

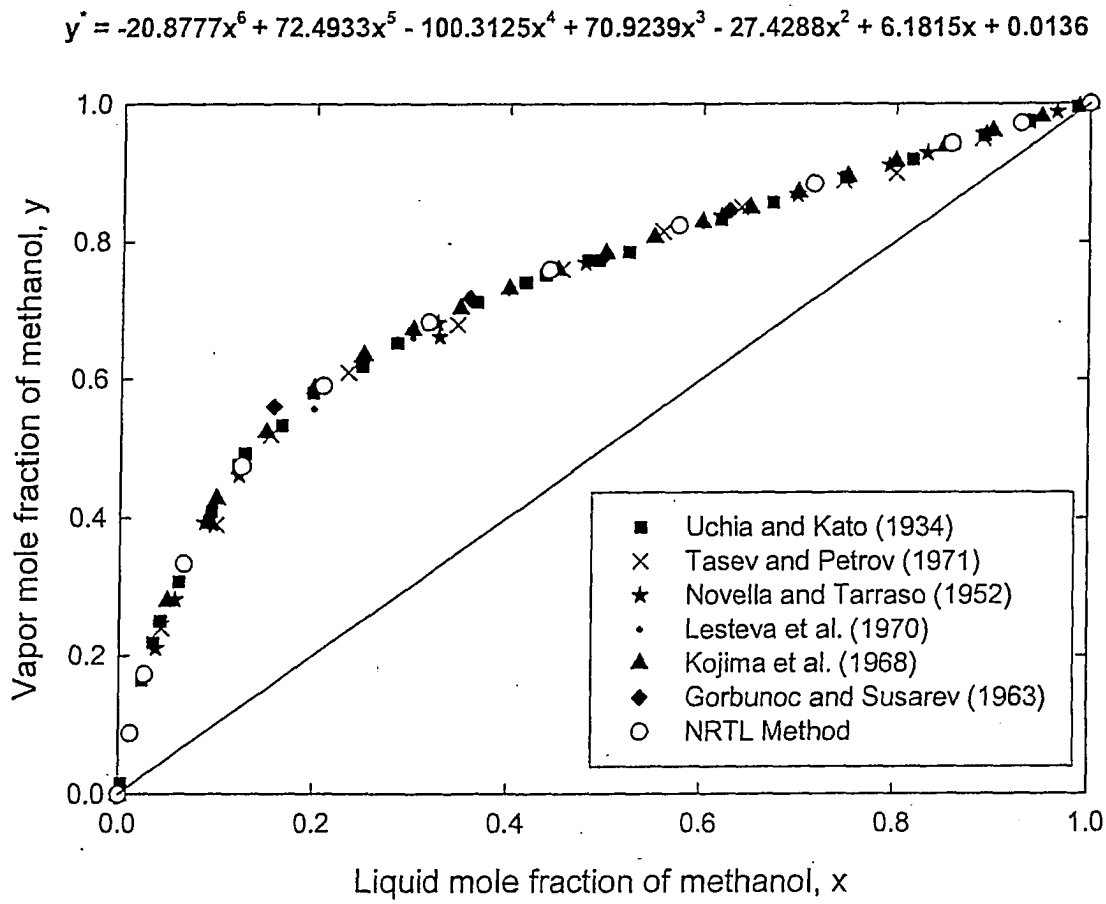

Figure B1.1 Vapor-liquid equilibrium data for the methanol/water system.

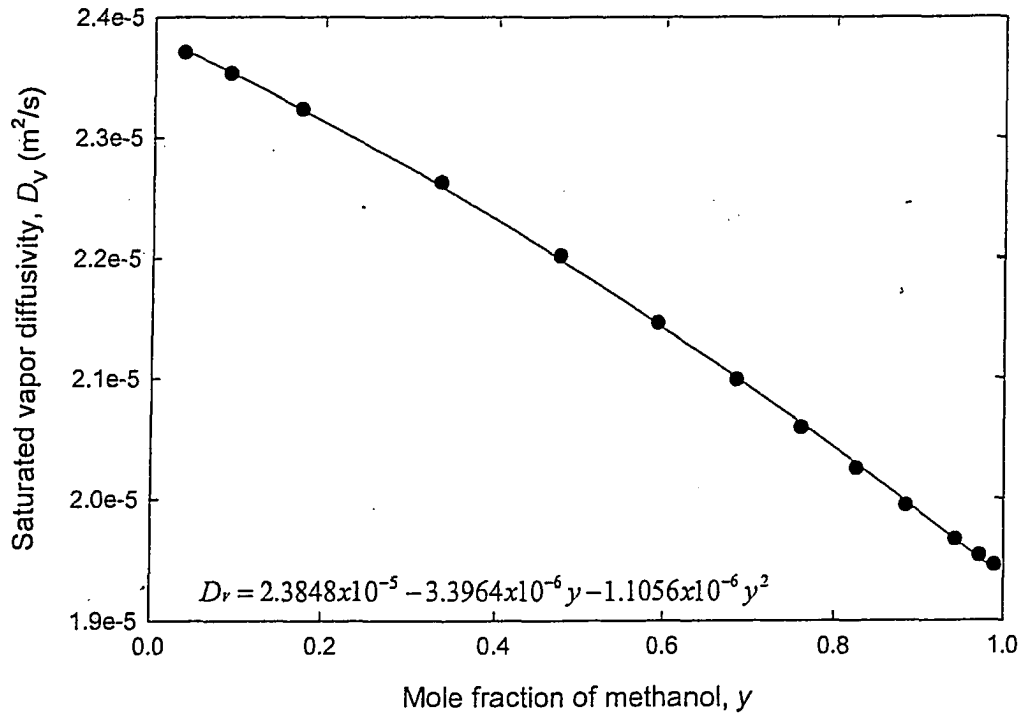

Figure B1.2 Saturated vapor diffusivity as a function of methanol concentration.

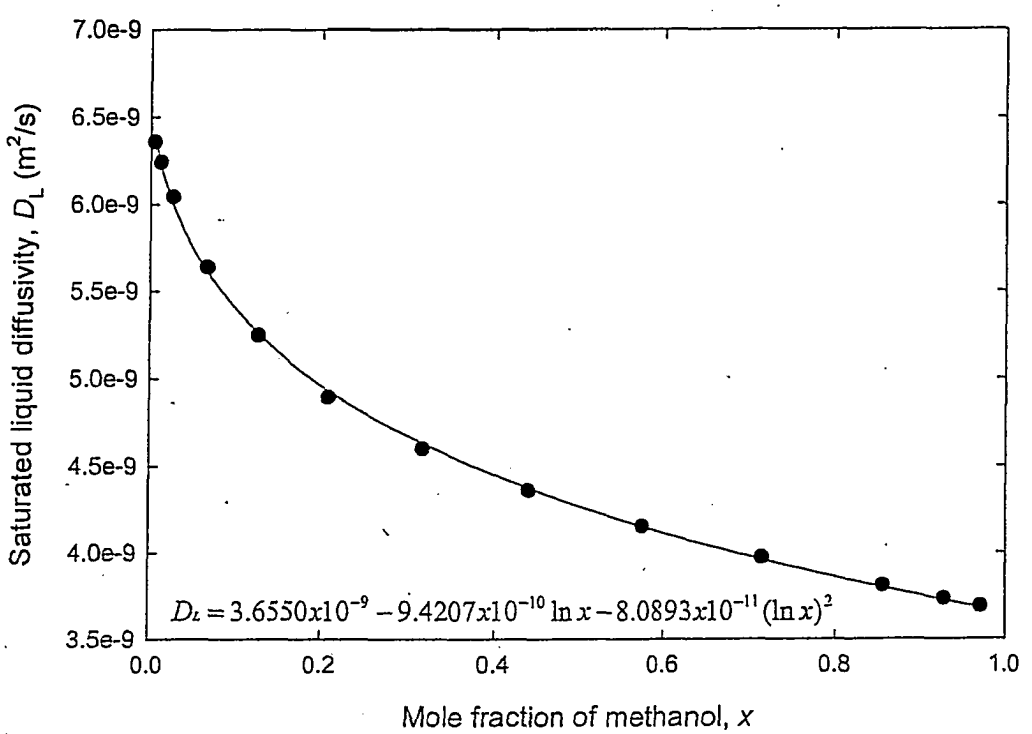

Figure B1.3 Saturated liquid diffusivity as a function of methanol concentration.

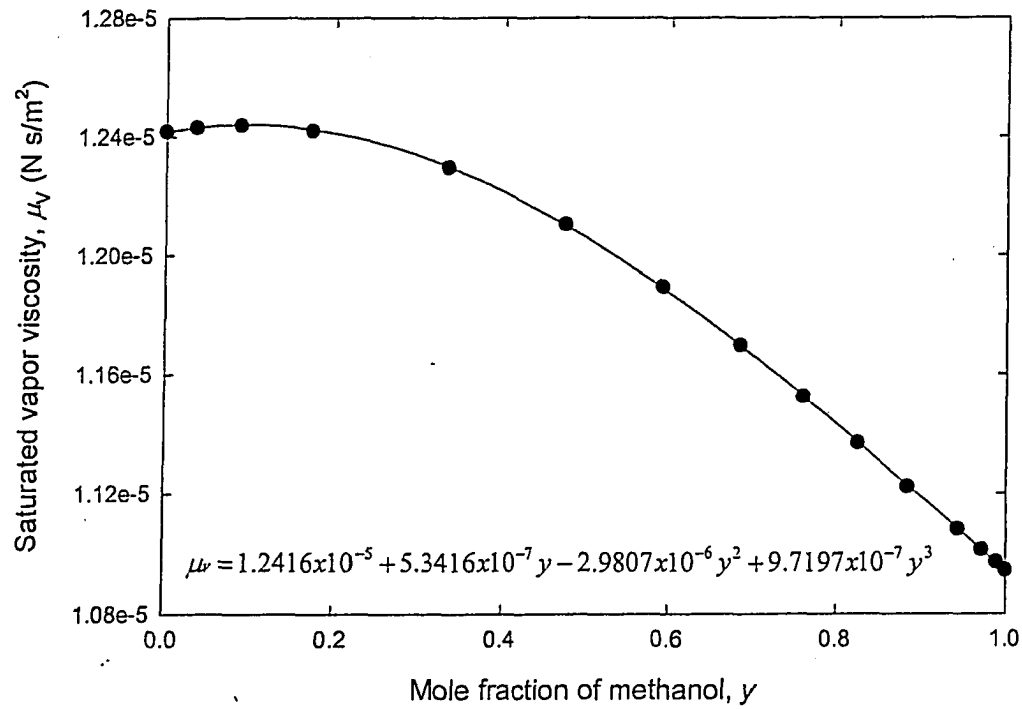

Figure B1.4 Saturated vapor viscosity as a function of methanol concentration.

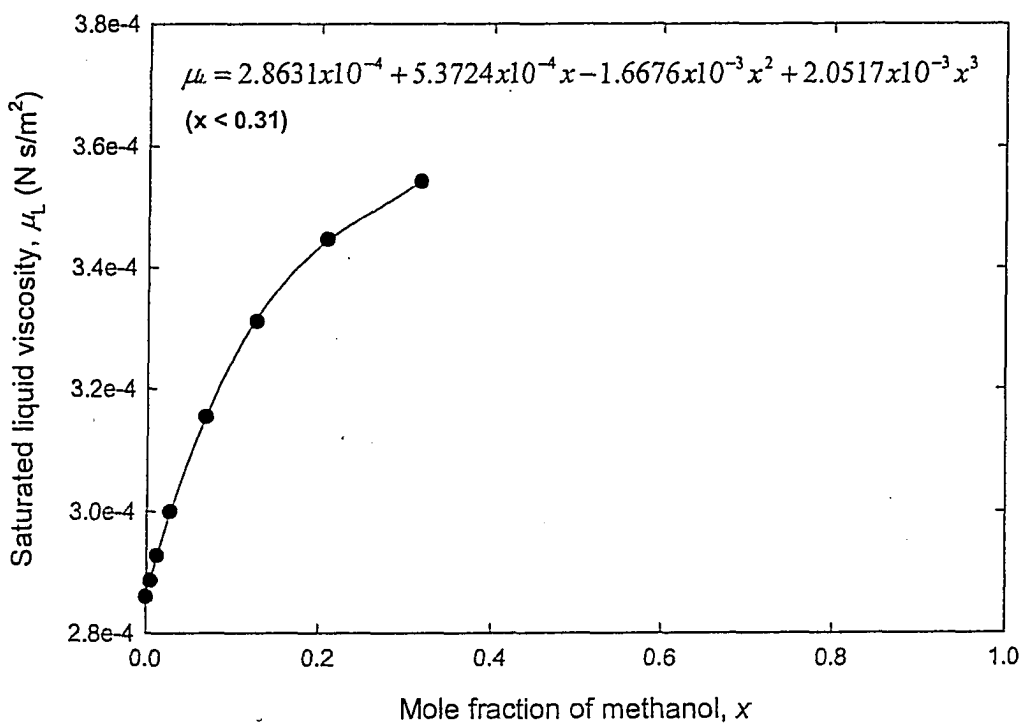

Figure B1.5 Saturated liquid viscosity as a function of methanol concentration (x < 0.31).

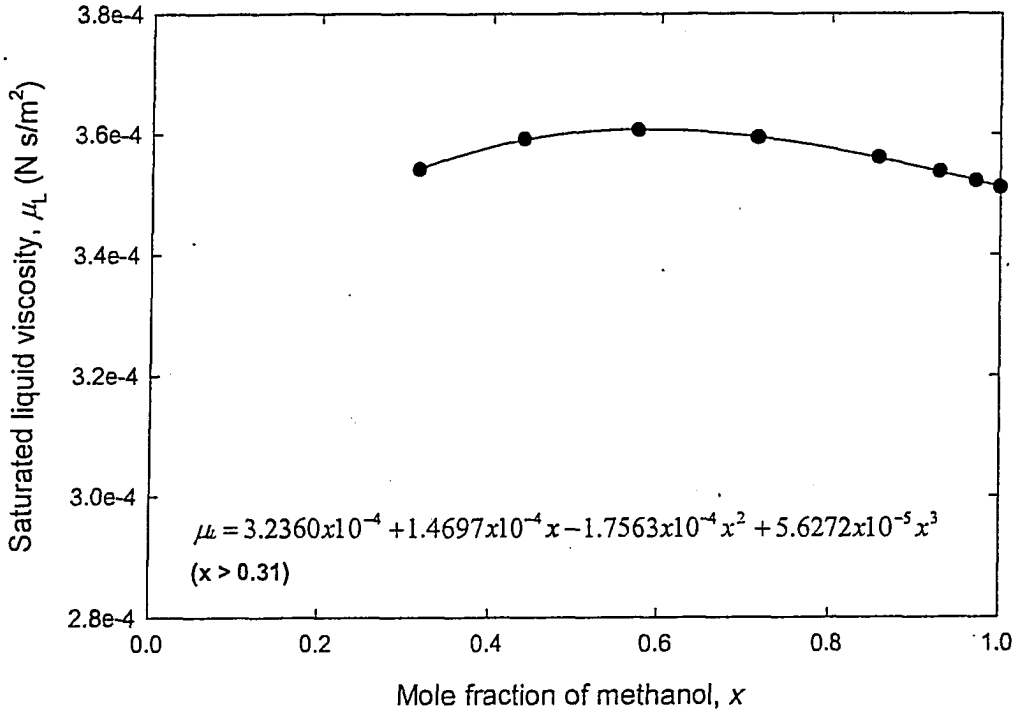

Figure B1.6 Saturated liquid viscosity as a function of methanol concentration (x > 0.31).

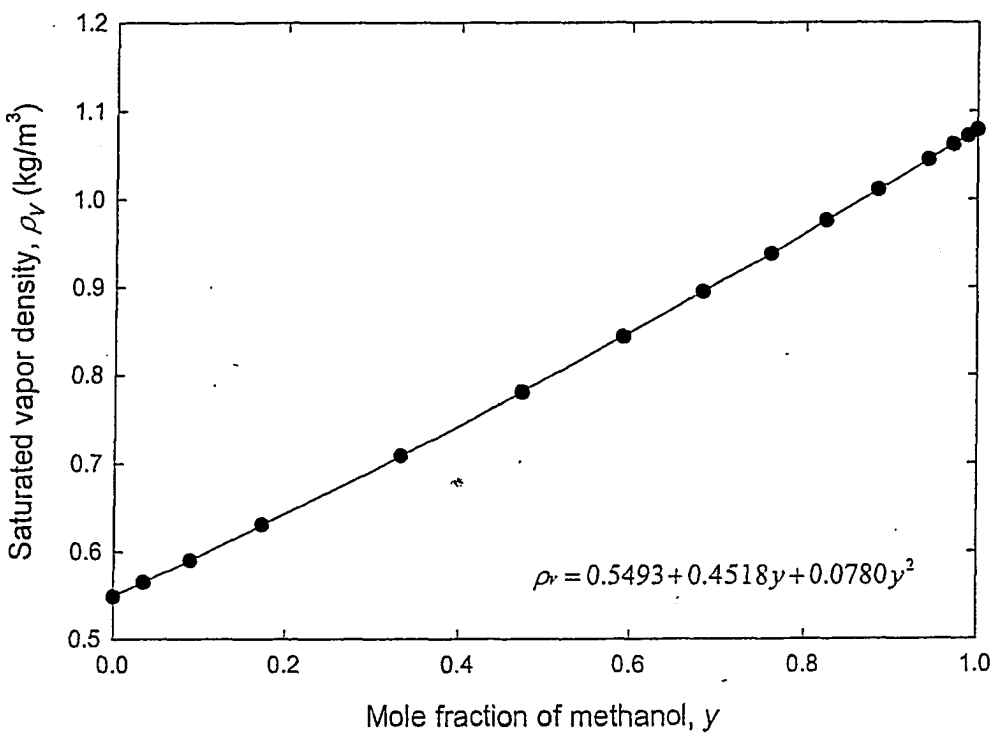

Figure B1.7 Saturated vapor density as a function of methanol concentration.

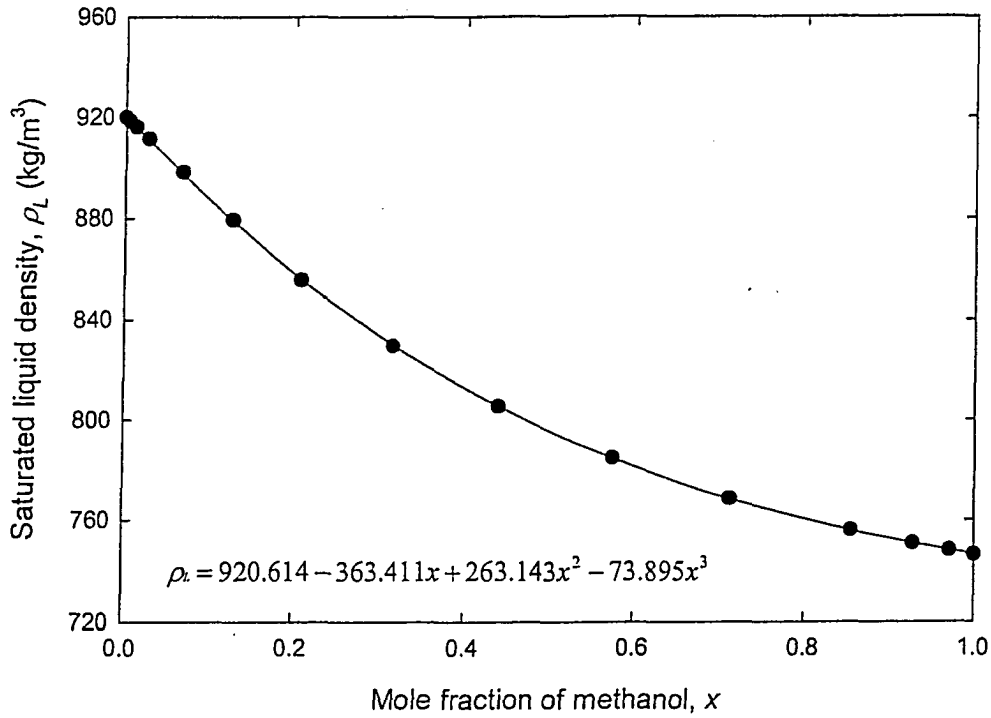

Figure B1.8 Saturated liquid density as a function of methanol concentration.

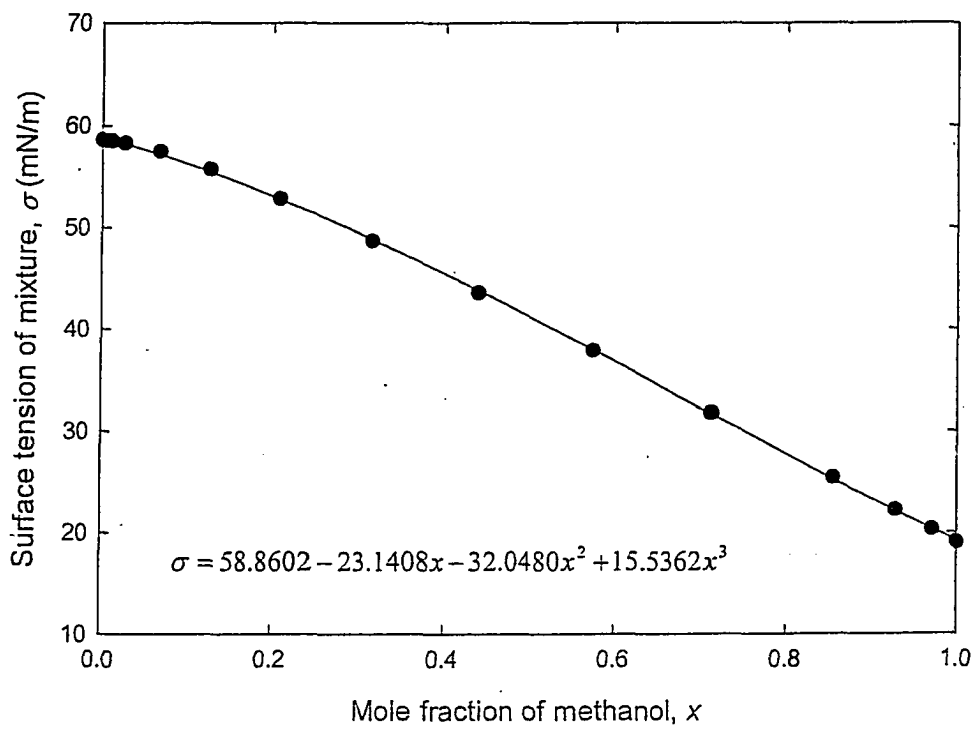

Figure B1.9 Surface tension of the mixture as a function of methanol concentration.

B2 Saturated system property data for the n-HEPTANE / TOLUENE system determined using the NRTL method

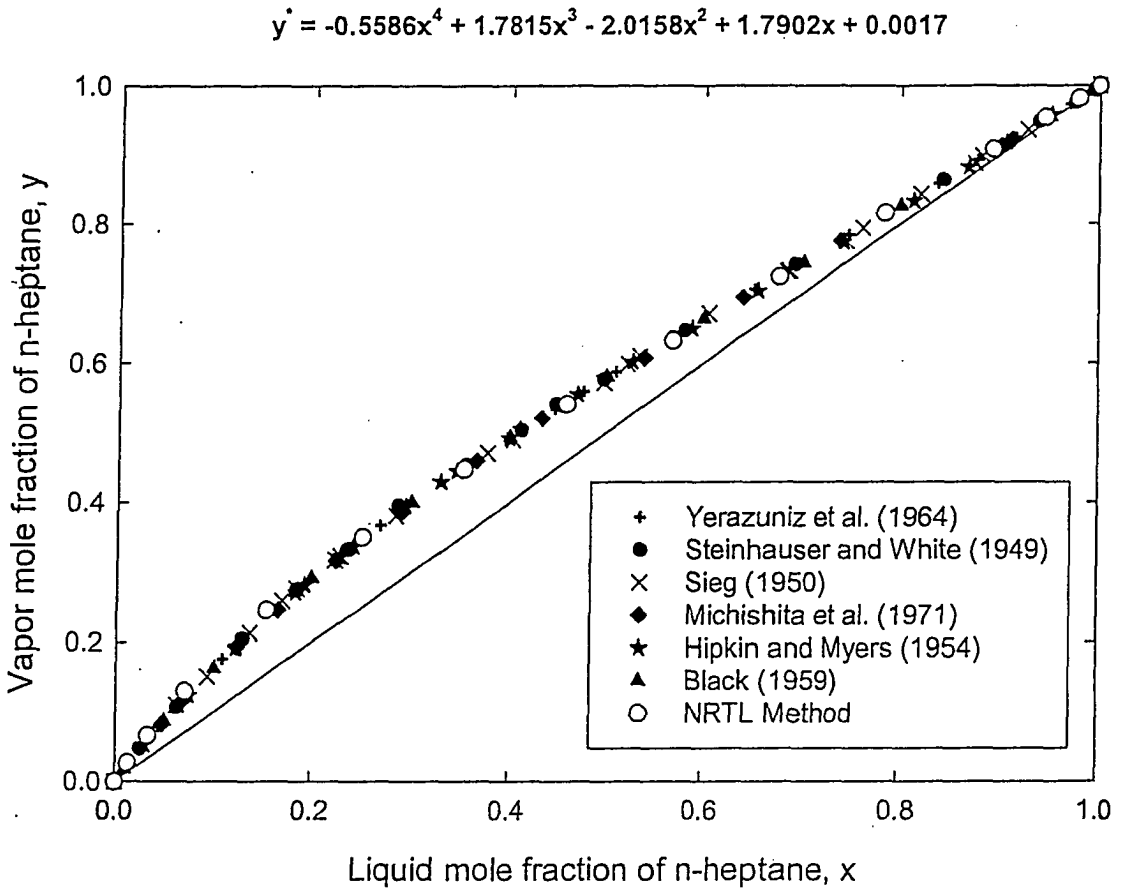

Figure B2.1 Vapor-liquid equilibrium data for the n-heptane/toluene system.

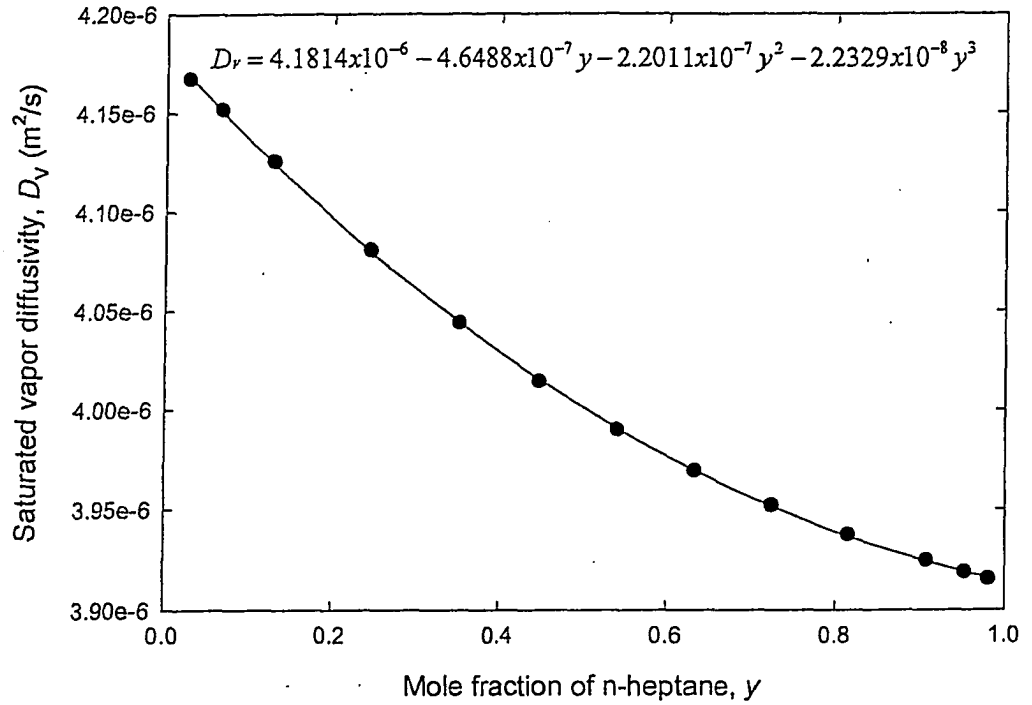

Figure B2.2 Saturated vapor diffusivity as a function of n-heptane concentration.

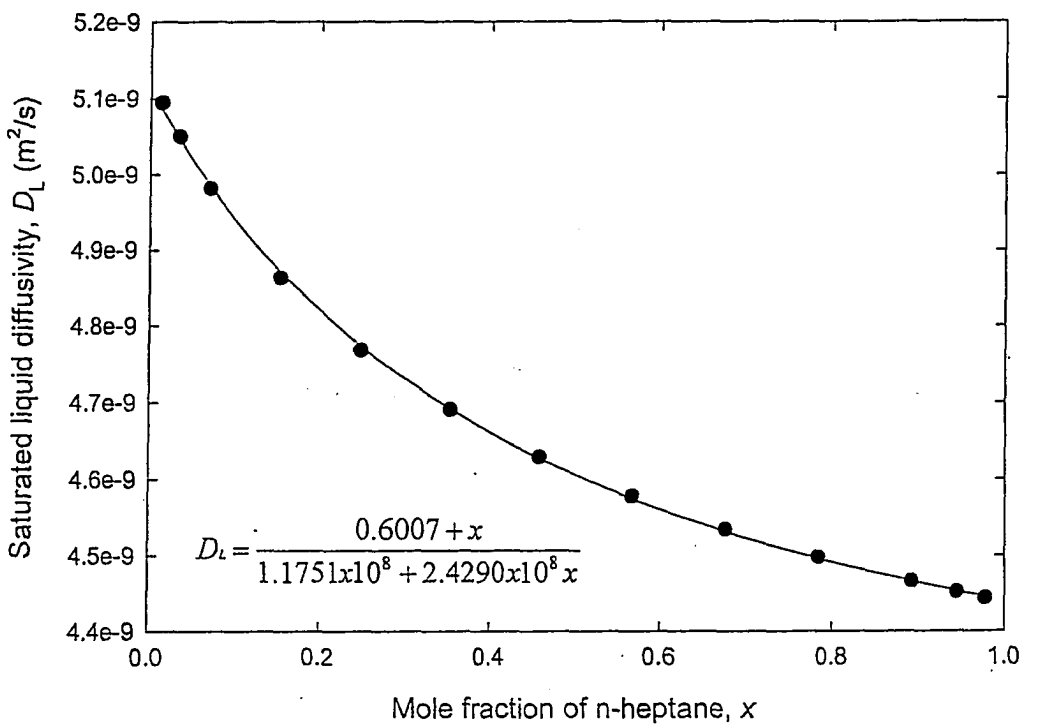

Figure B2.3 Saturated liquid diffusivity as a function of n-heptane concentration.

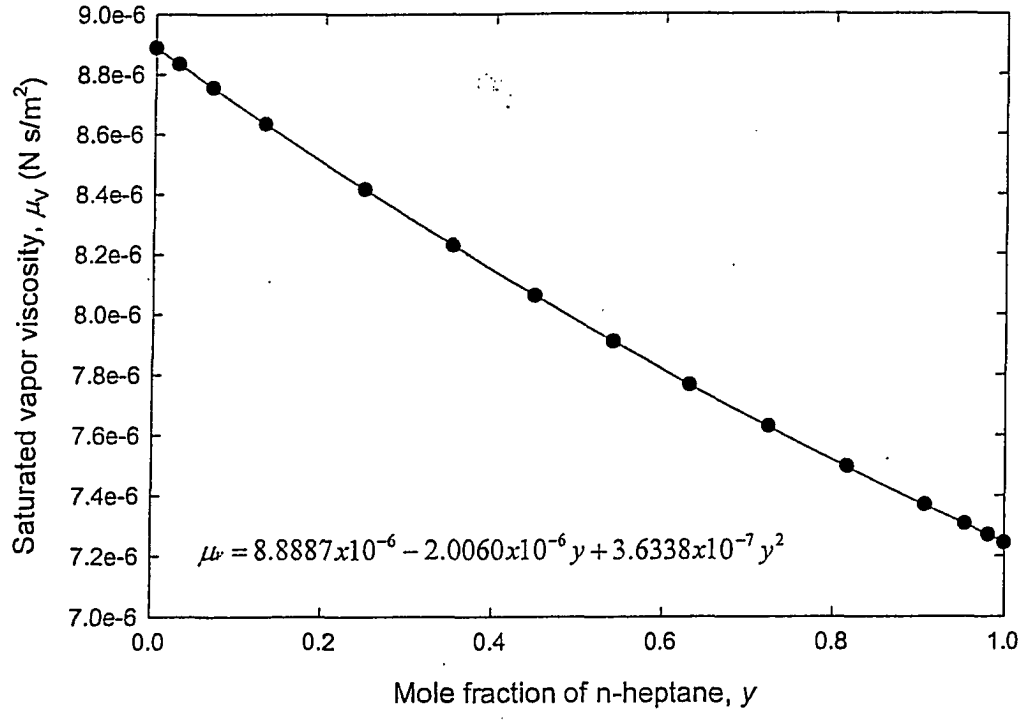

Figure B2.4 Saturated vapor viscosity as a function of n-heptane concentration.

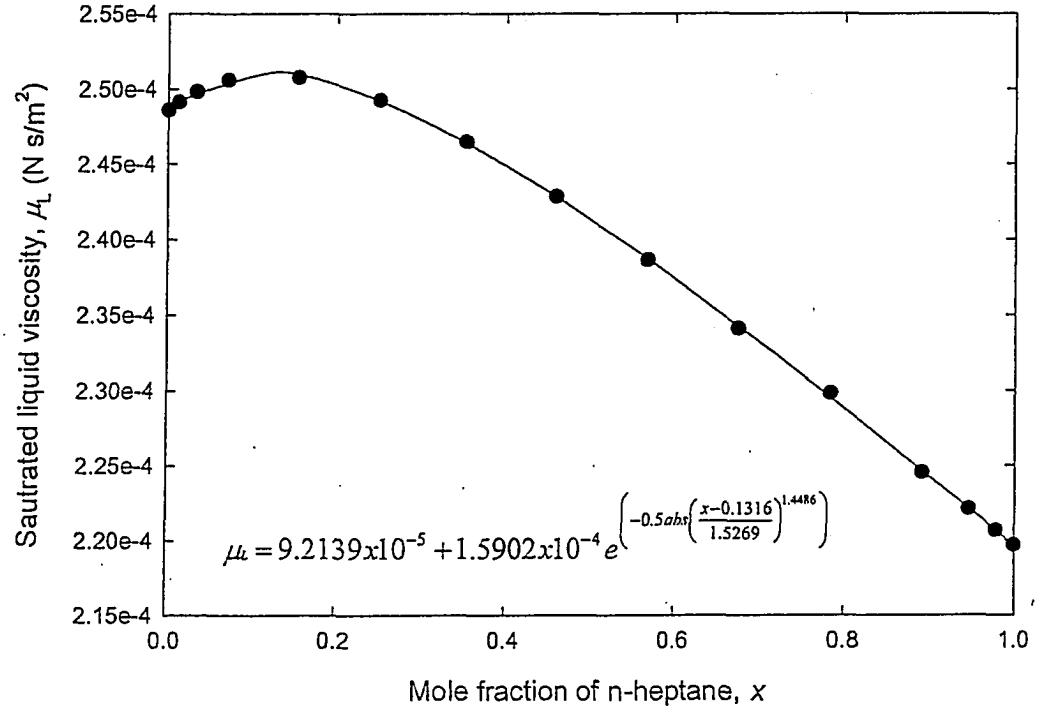

Figure B2.5 Saturated liquid viscosity as a function of n-heptane concentration.

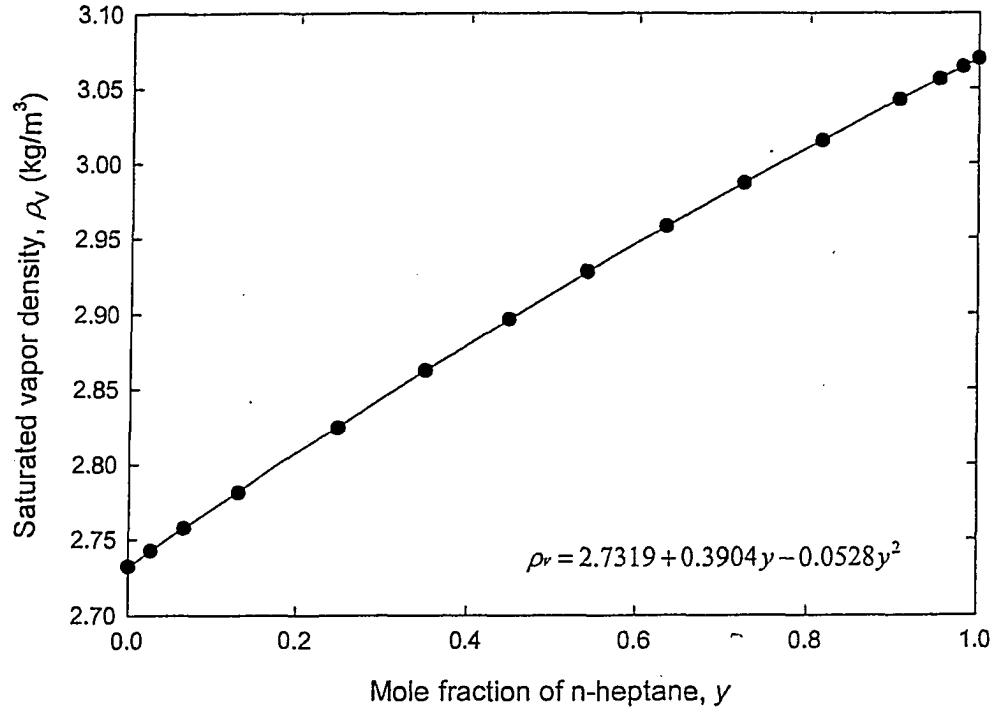

Figure B2.6 Saturated vapor density as a function of n-heptane concentration.

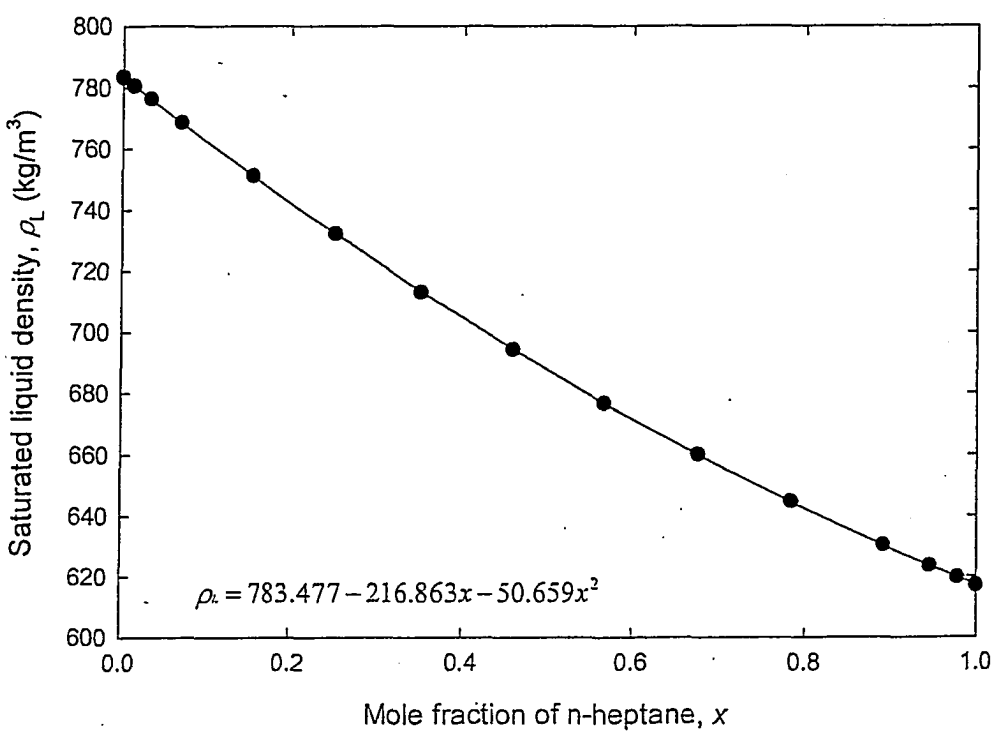

Figure B2.7 Saturated liquid density as a function of n-heptane concentration.

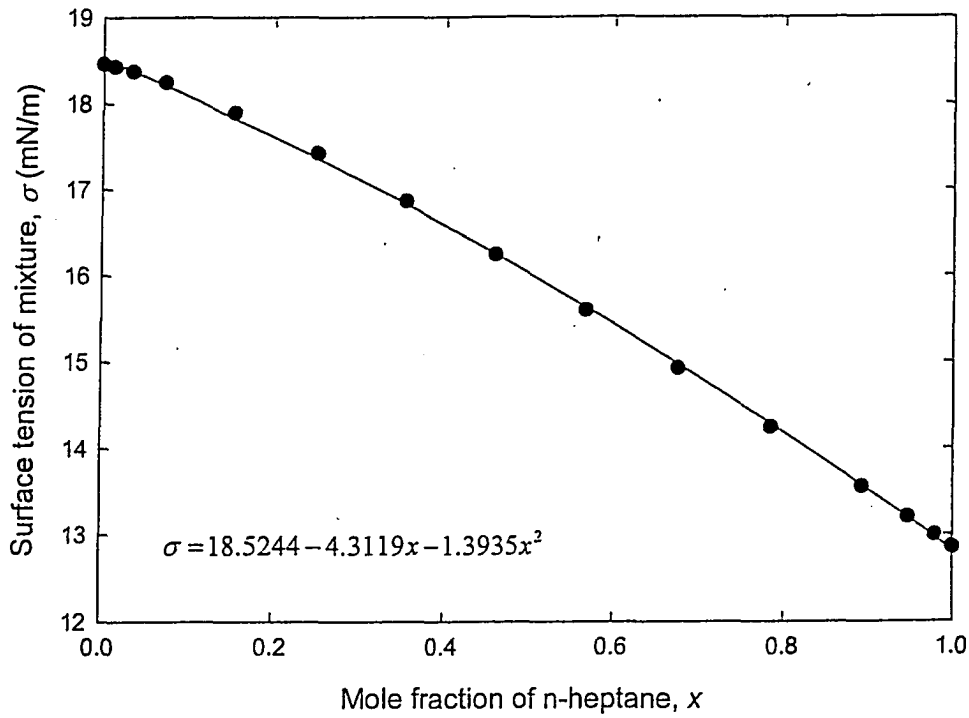

Figure B2.8 Surface tension of the mixture as a function of n-heptane concentration.

B3 Saturated system property data for the BENZENE / n-HEPTANE system determined using the NRTL method

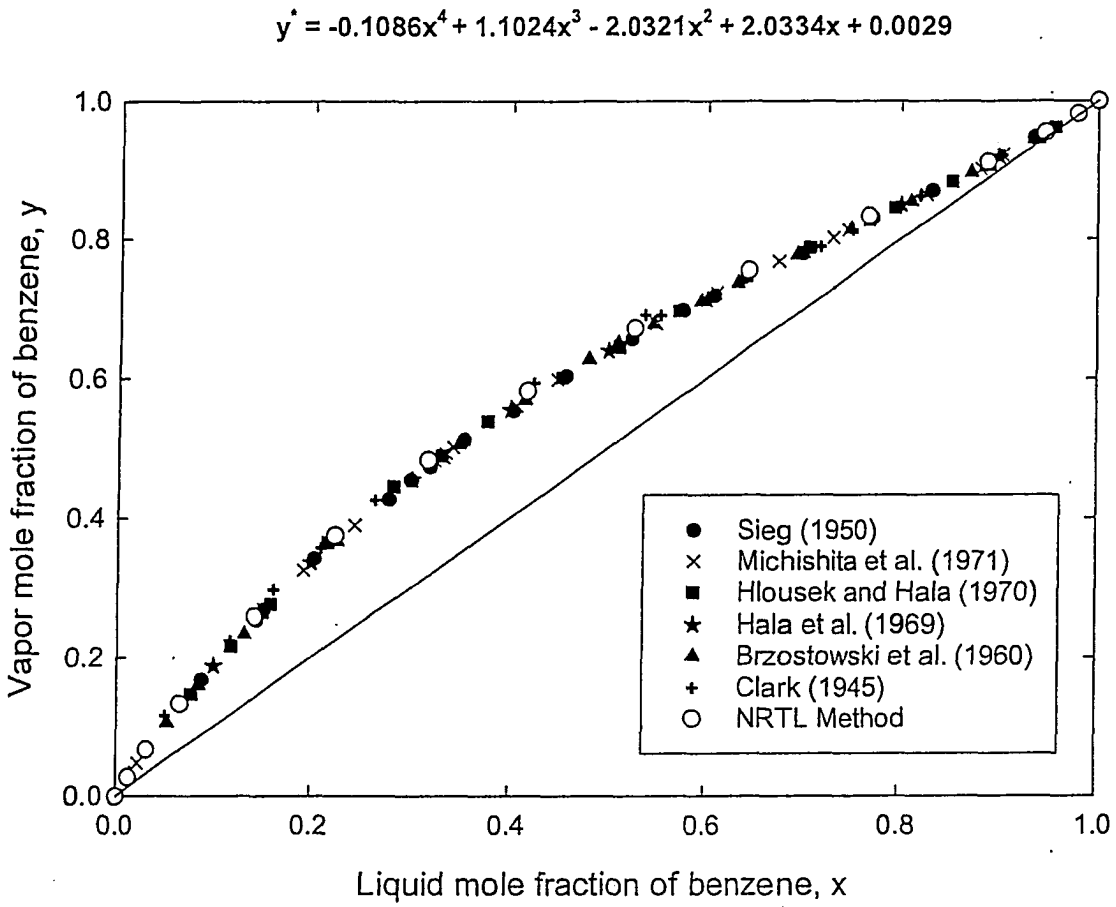

Figure B3.1 Vapor-liquid equilibrium data for the benzene/n-heptane system.

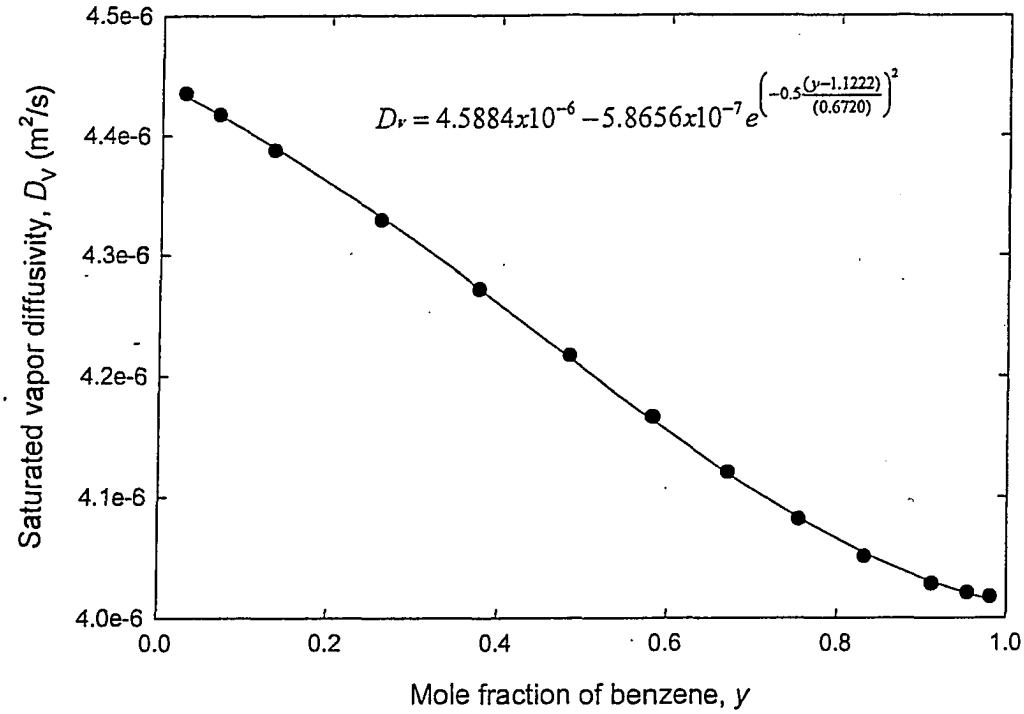

Figure B3.2 Saturated vapor diffusivity as a function of benzene concentration

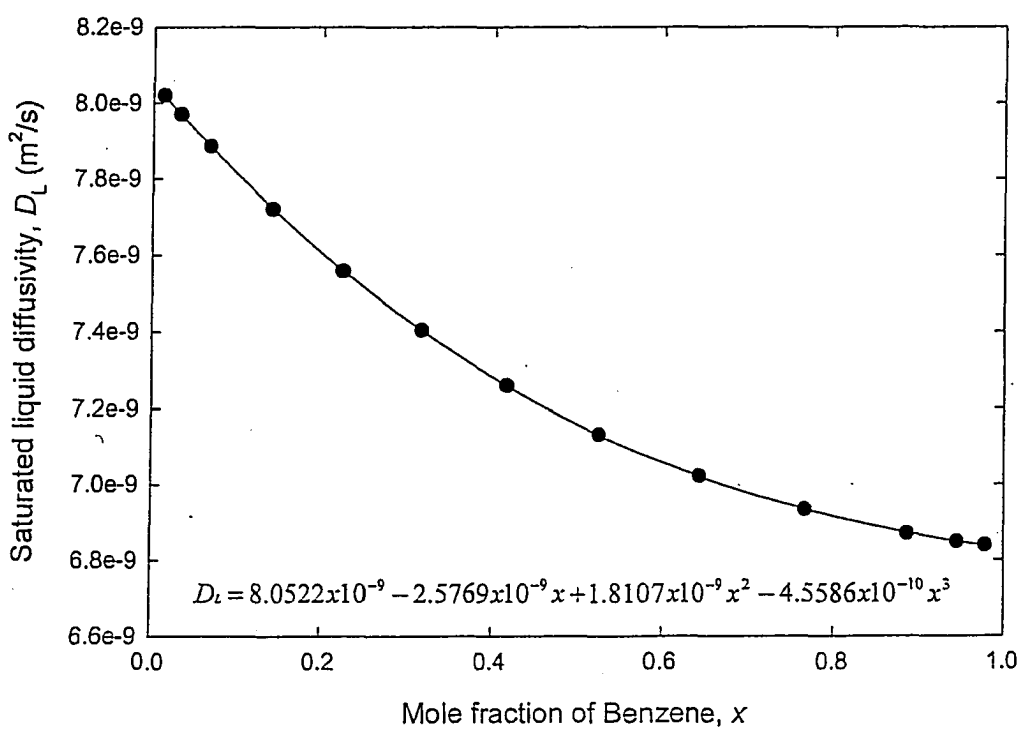

Figure B3.3 Saturated liquid diffusivity as a function of benzene concentration

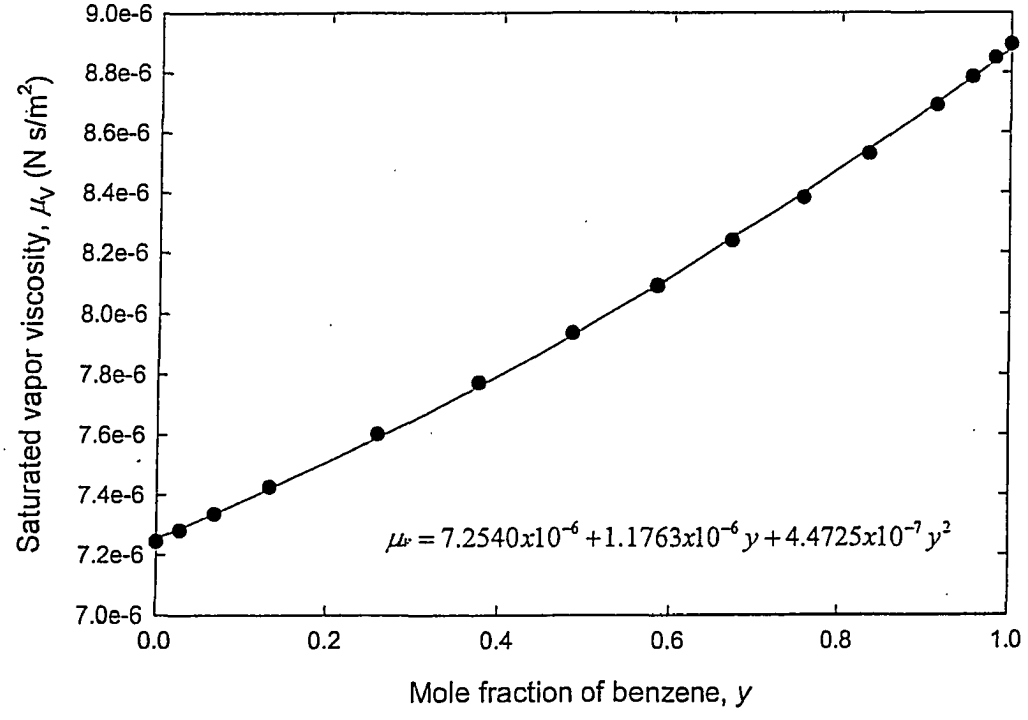

Figure B3.4 Saturated vapor viscosity as a function of benzene concentration.

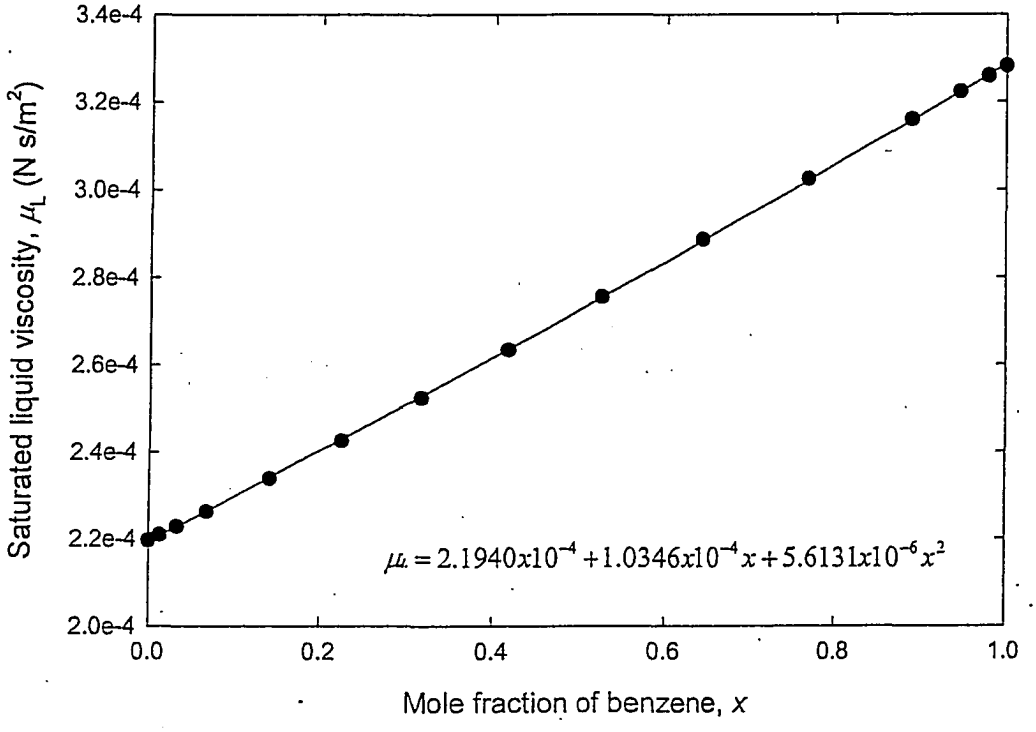

Figure B3.5 Saturated liquid viscosity as a function of benzene concentration.

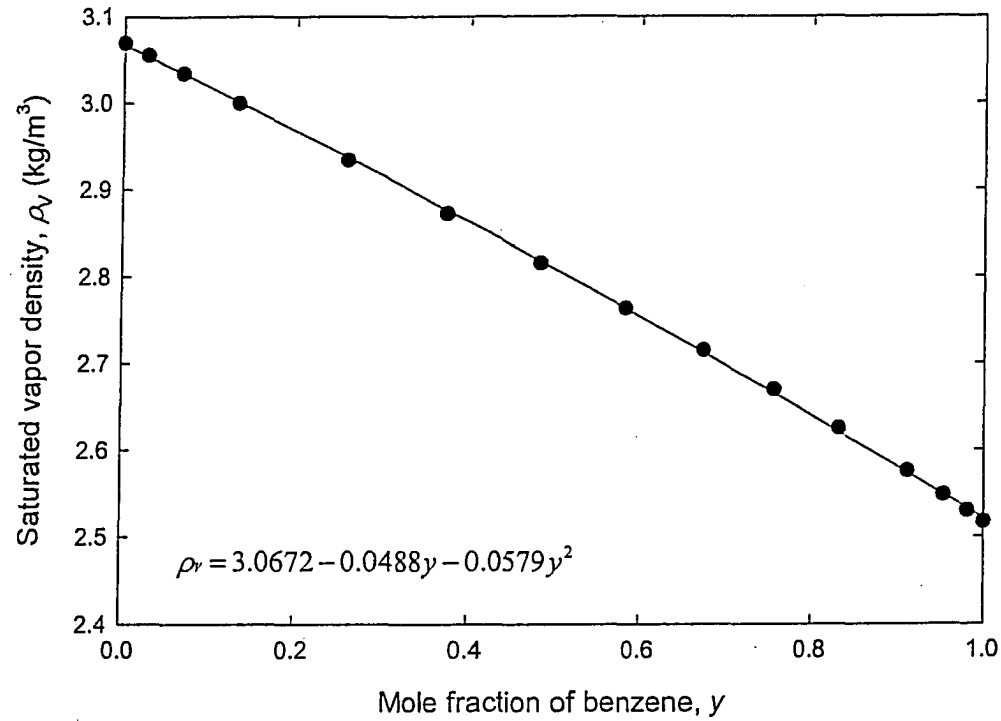

Figure B3.6 Saturated vapor density as a function of benzene concentration.

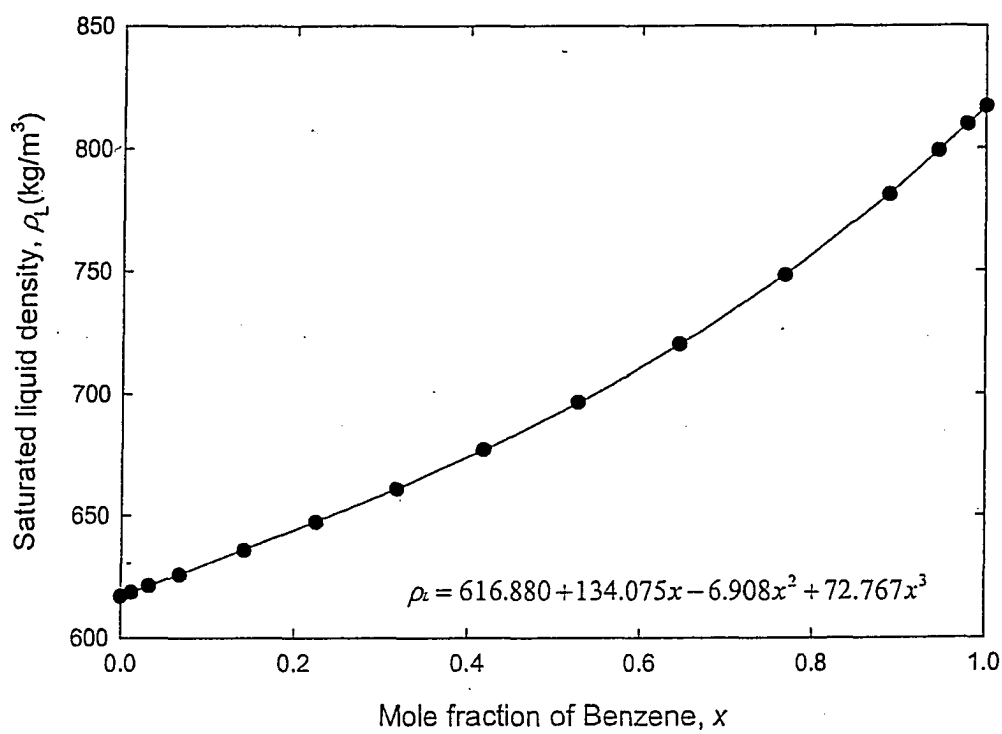

Figure B3.7 Saturated liquid density as a function of benzene concentration.

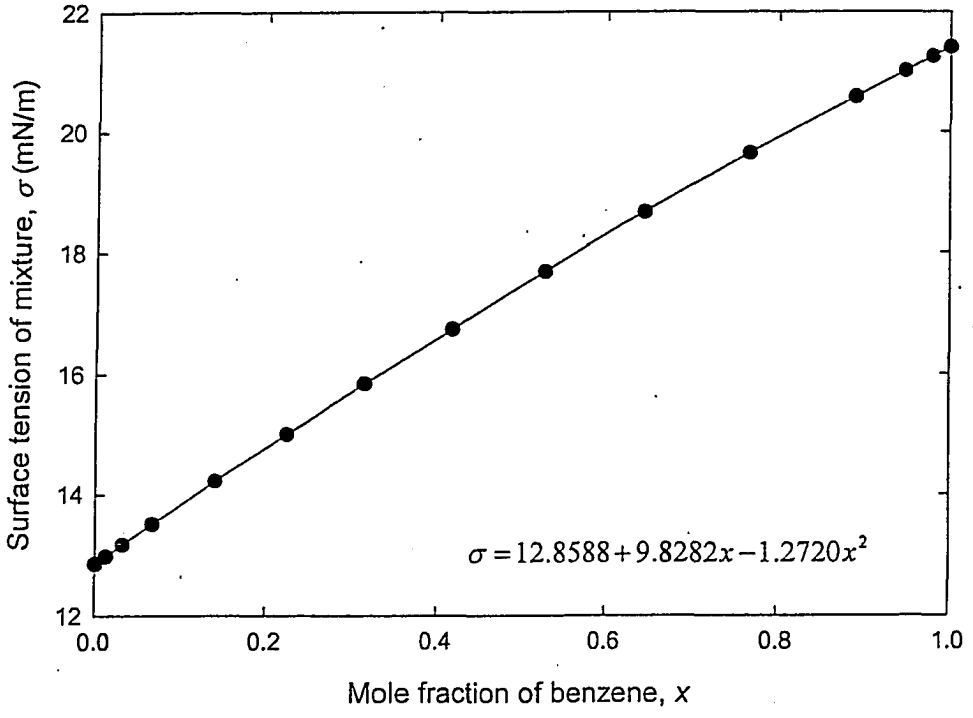

Figure B3.8 Surface tension of the mixture as a function of benzene concentration.

B4 Saturated system property data for the WATER / ACETIC ACID system determined using the Peng- Robinson Wong-Sandler method

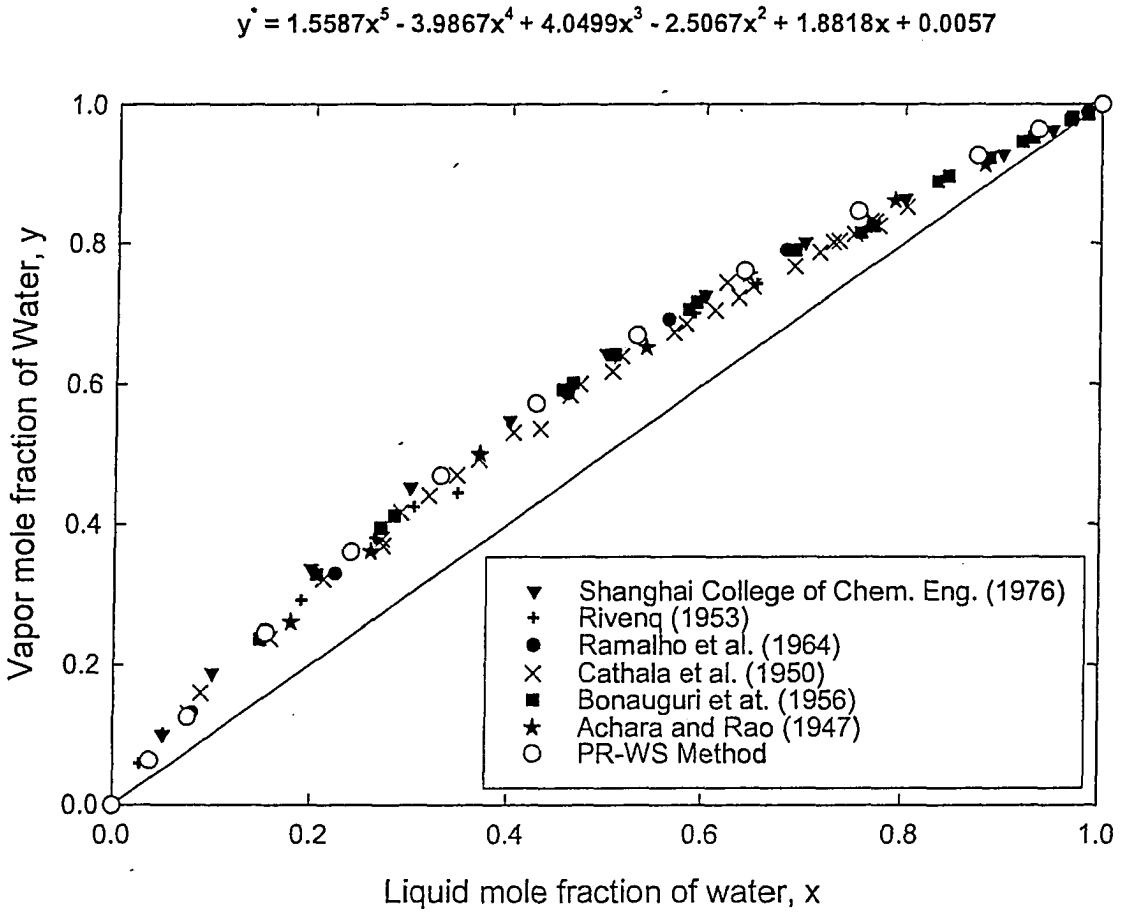

Figure B4.1 Vapor-liquid equilibrium data for the water/acetic acid system.

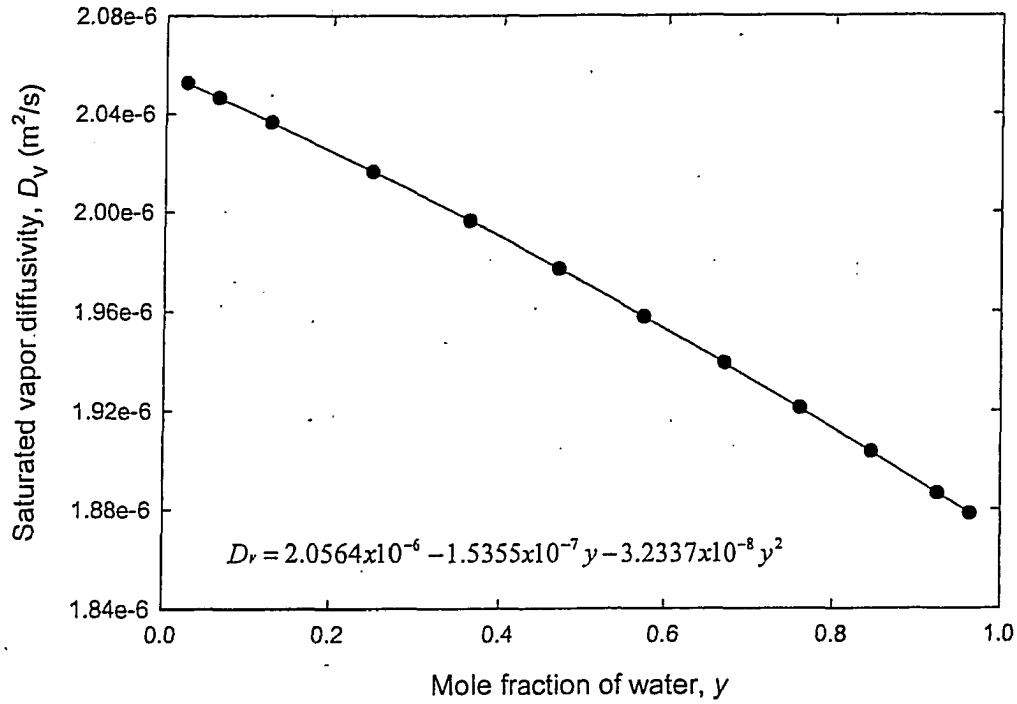

Figure B4.2 Saturated vapor diffusivity as a function of water concentration

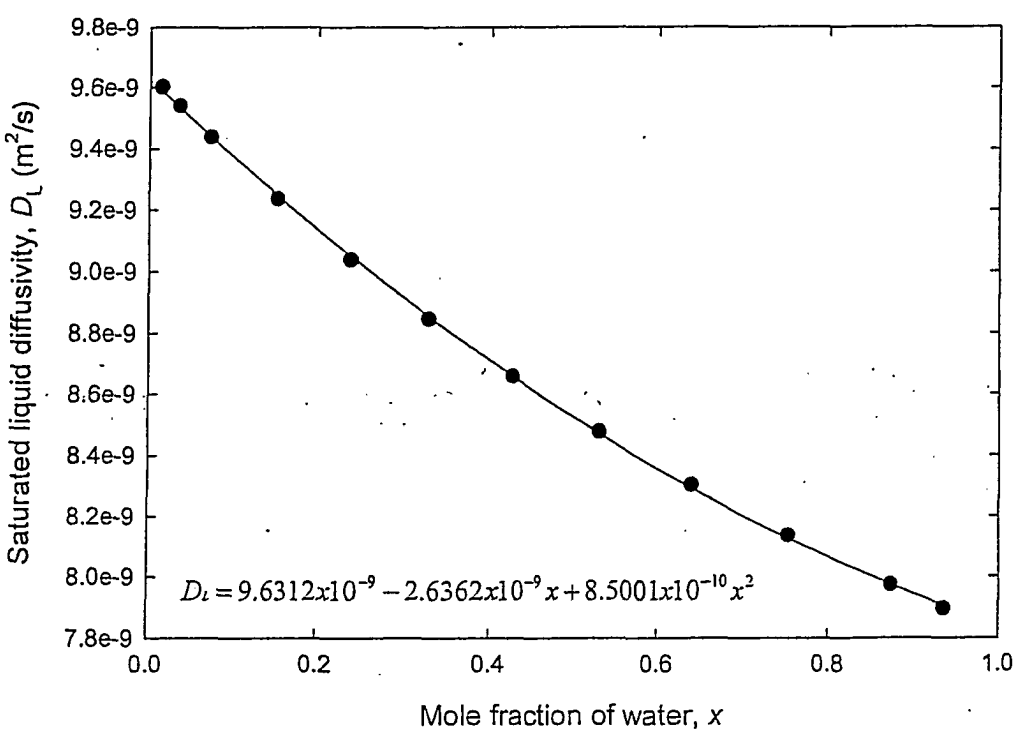

Figure B4.3 Saturated liquid diffusivity as a function of water concentration

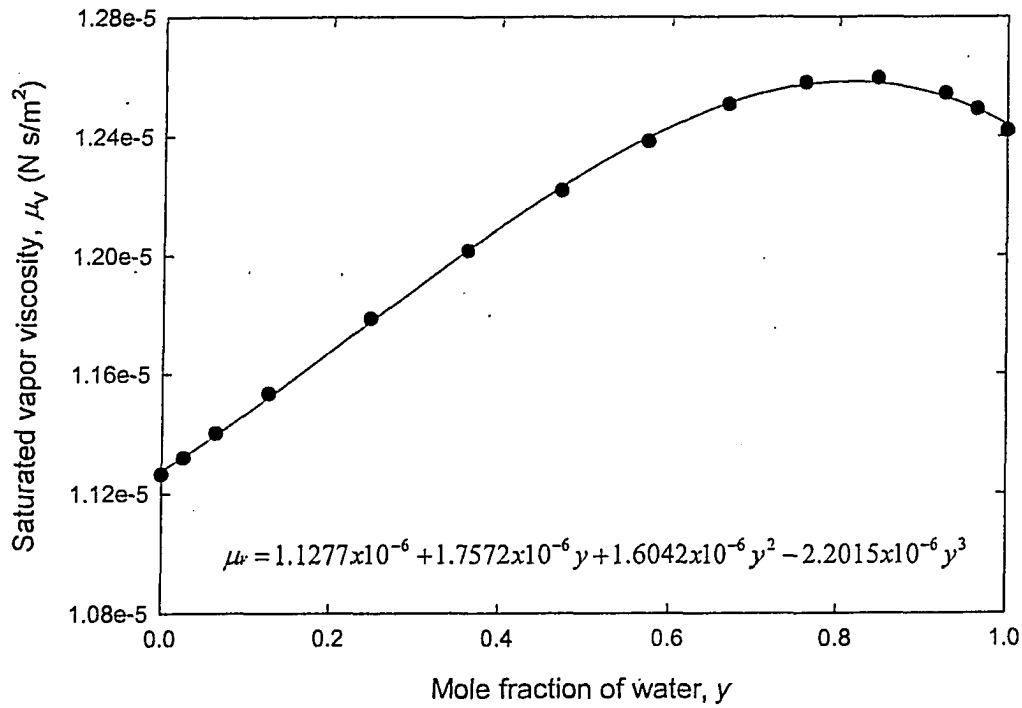

Figure B4.4 Saturated vapor viscosity as a function of water concentration.

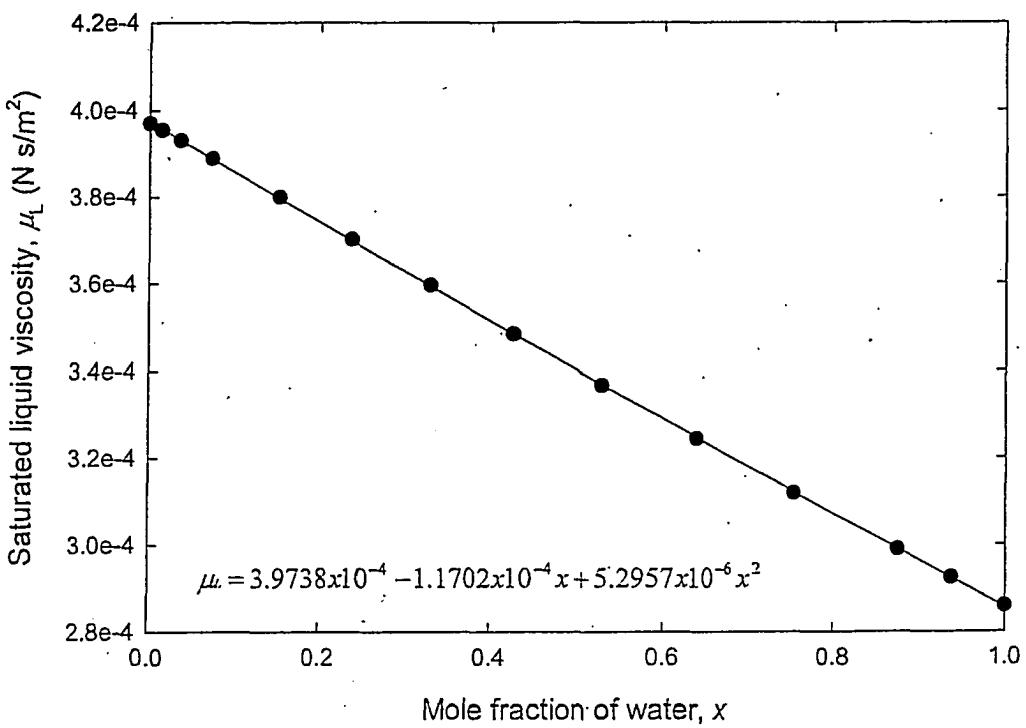

Figure B4.5 Saturated liquid viscosity as a function of water concentration.

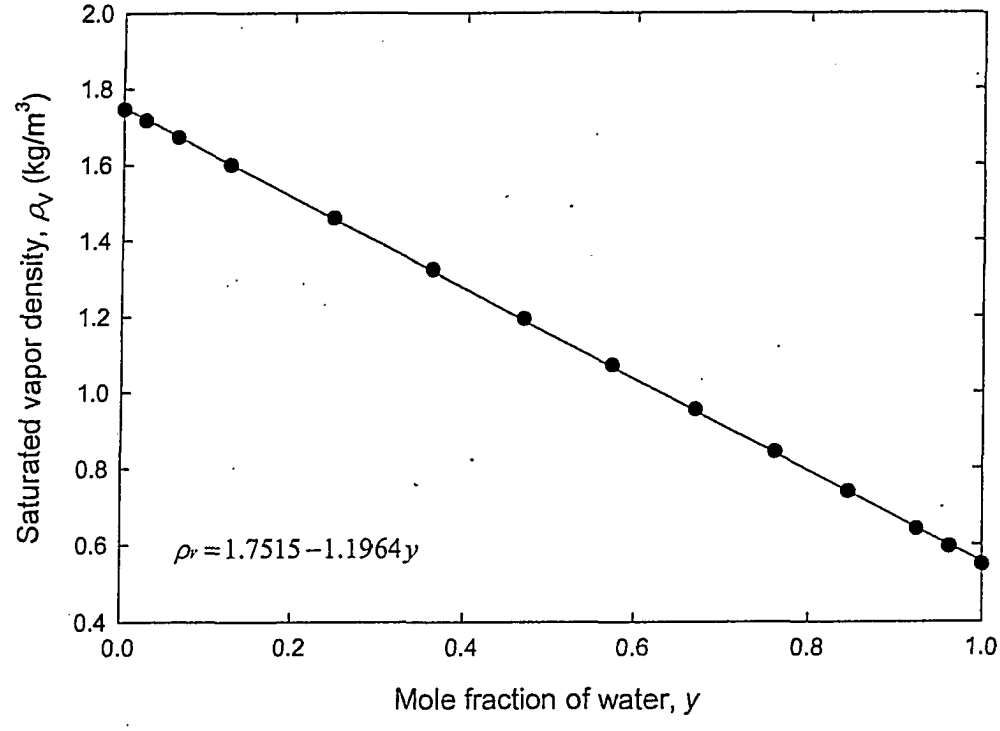

Figure B4.6 Saturated vapor density as a function of water concentration.

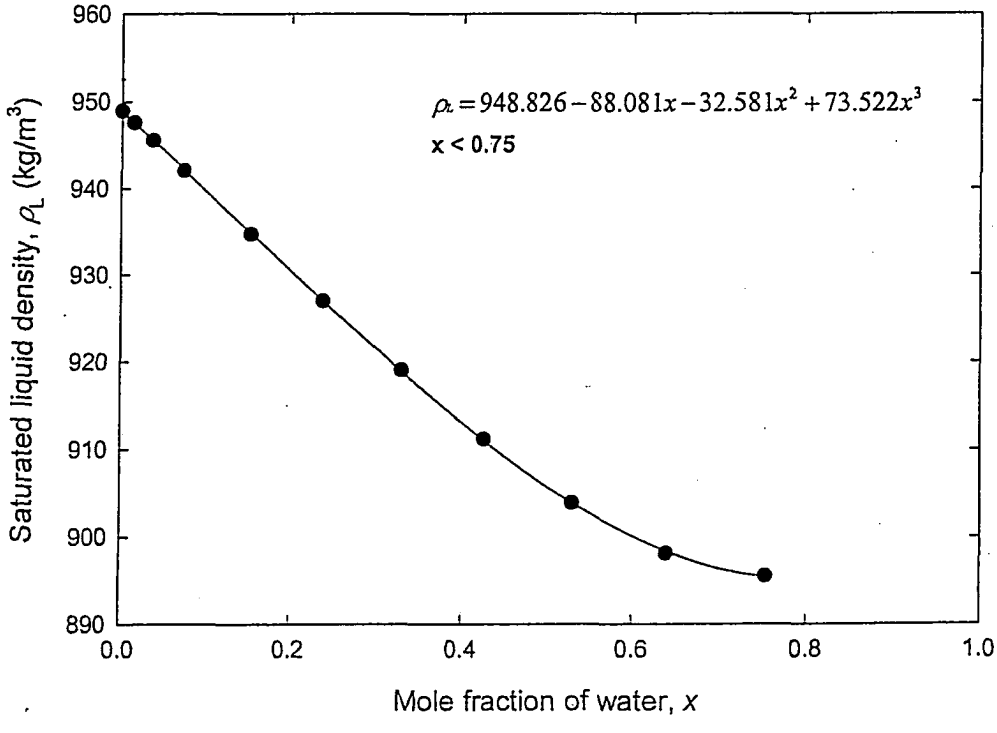

Figure B4.7 Saturated liquid density as a function of water concentration (x < 0.75).

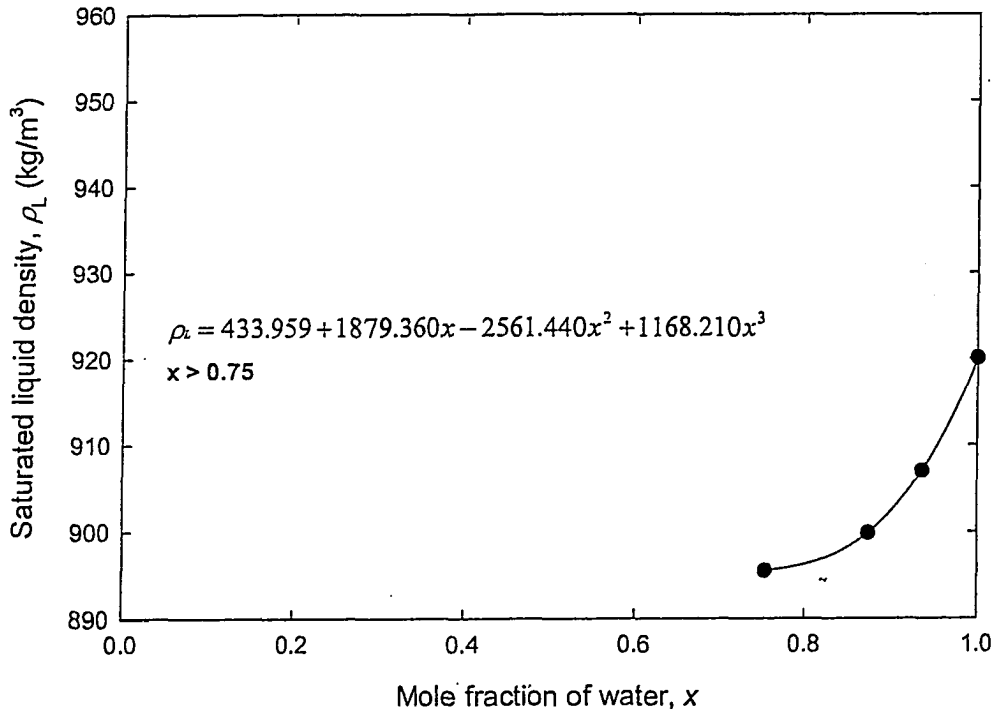

Figure B4.8 Saturated liquid density as a function of water concentration (x > 0.75).

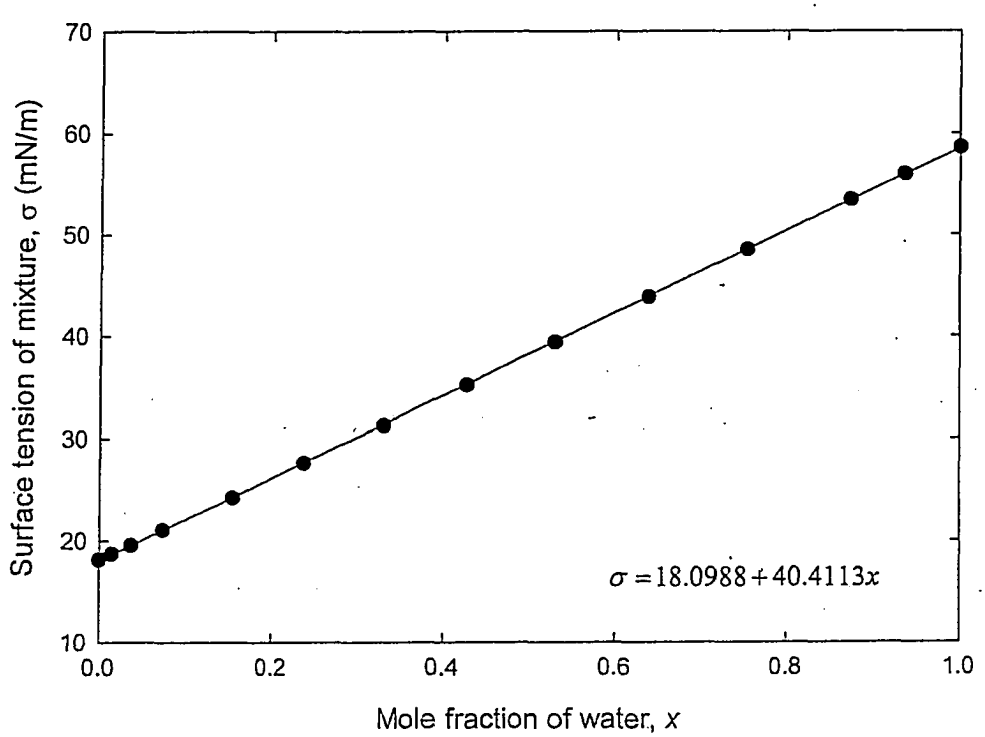

Figure B4.9 Surface tension of the mixture as a function of water concentration.

B5 Saturated system property data for the ISOPROPANOL / WATER system determined using the NRTL method

$$y^*(x_{isopropanol}) = -8.7072x^6 + 36.081x^5 - 57.216x^4 + 44.950x3 - 18.032x^2 + 3.6566x + 0.2558$$

x < 0.68

$$y^*(1 - x_{isopropanol}) = 2.9422(1 - x_{isopropanol})^3 - 3.2816(1 - x_{isopropanol})^2 + 1.6795(1 - x_{isopropanol}) + 0.0119$$

x > 0.68

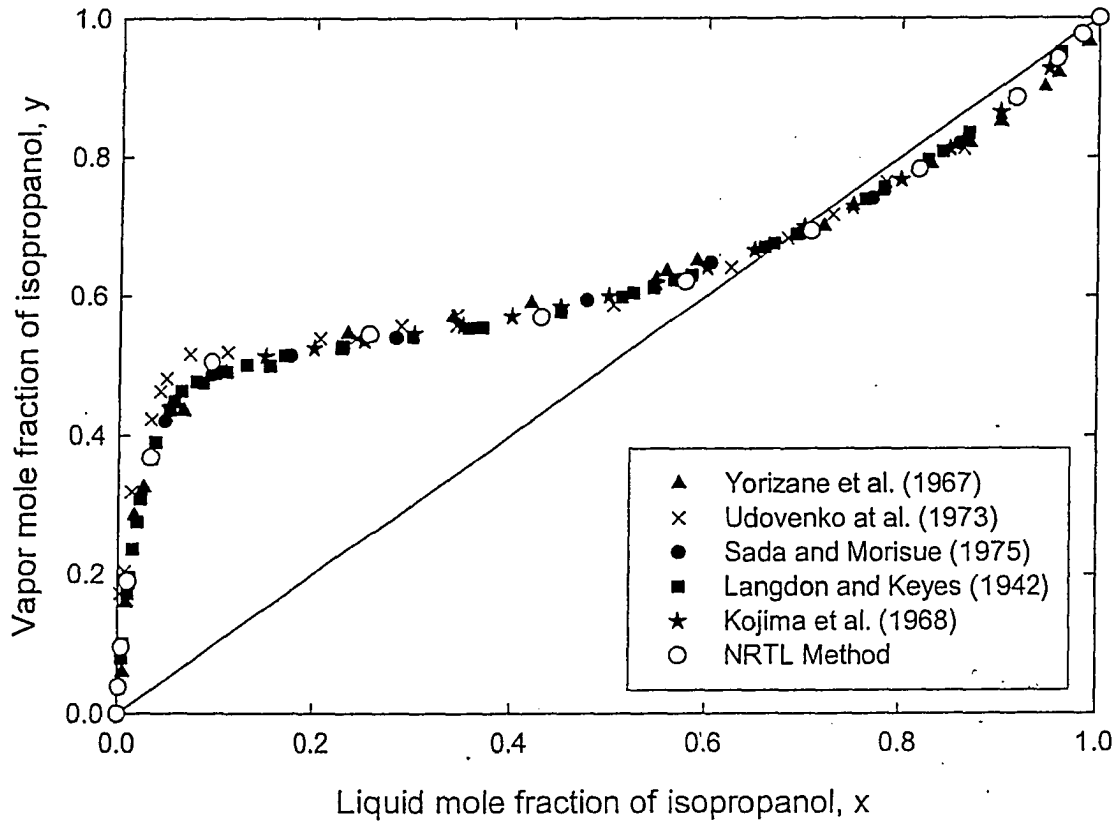

Figure B5.1 Vapor-liquid equilibrium data for the isopropanol/water system.

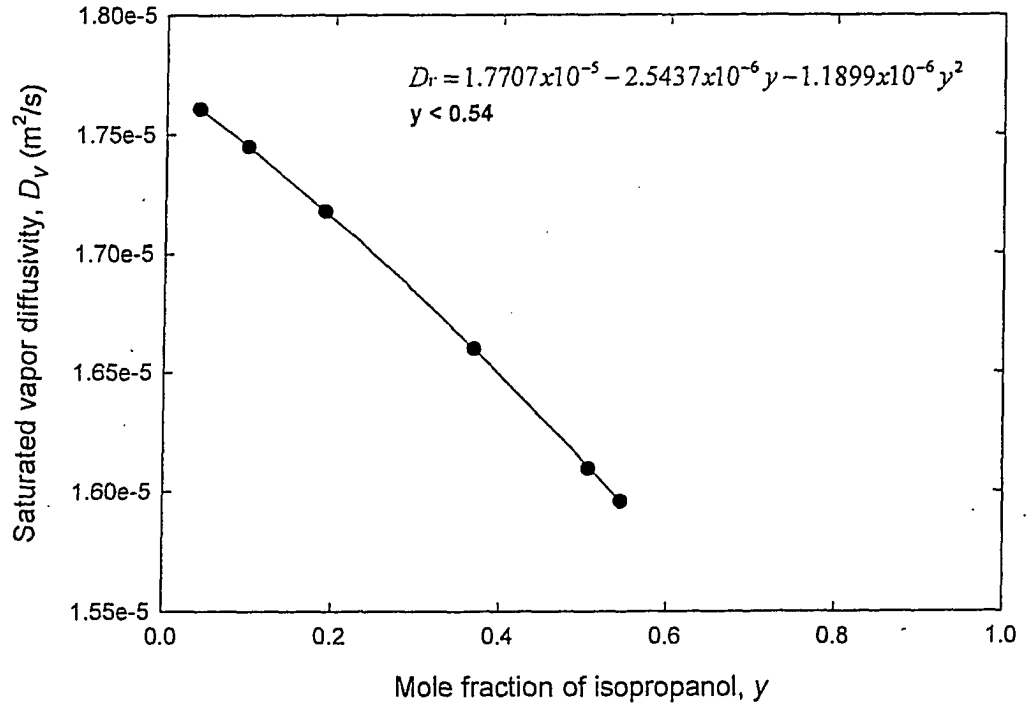

Figure B5.2 Saturated vapor diffusivity as a function of isopropanol concentration (x < 0.54).

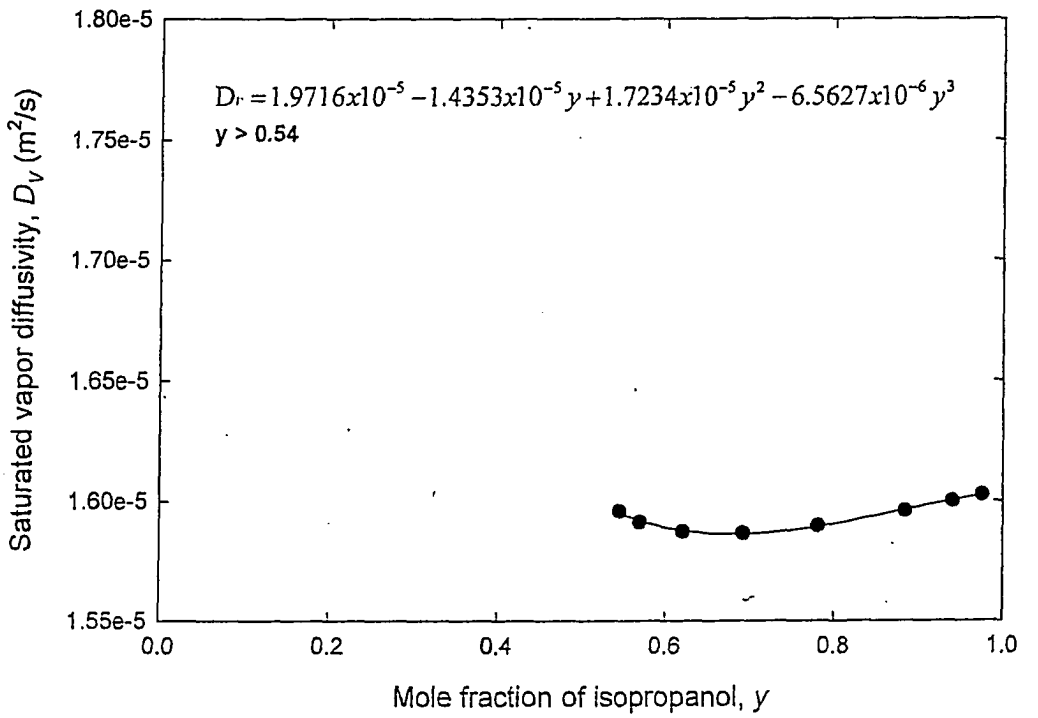

Figure B5.3 Saturated vapor diffusivity as a function of isopropanol concentration (x > 0.54).

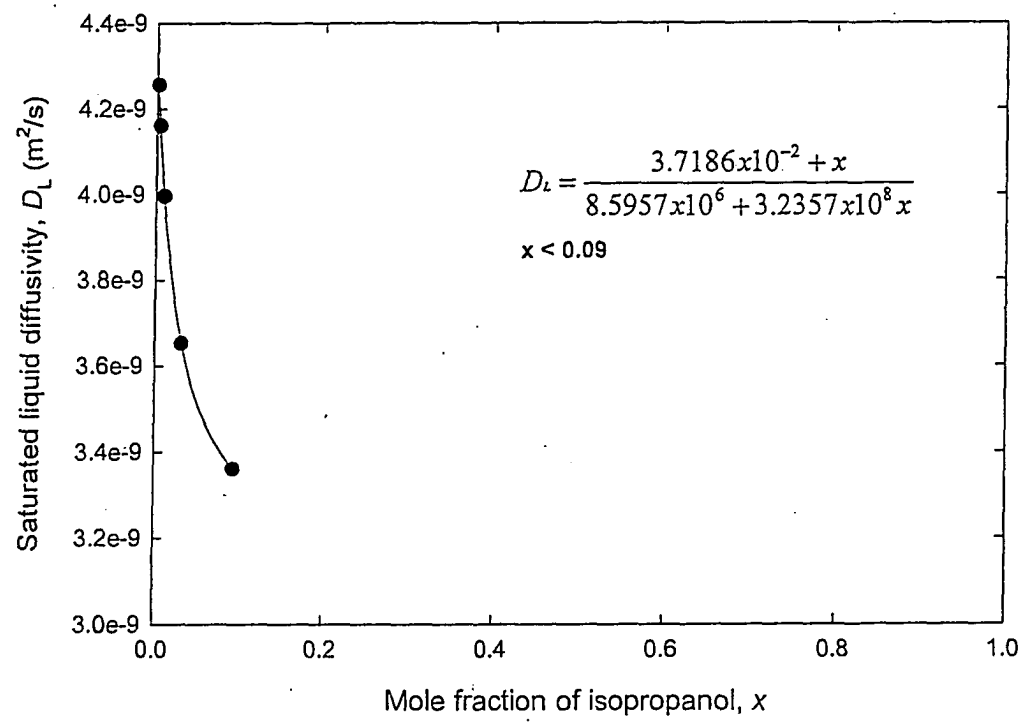

Figure B5.4 Saturated liquid diffusivity as a function of isopropanol concentration (x < 0.09).

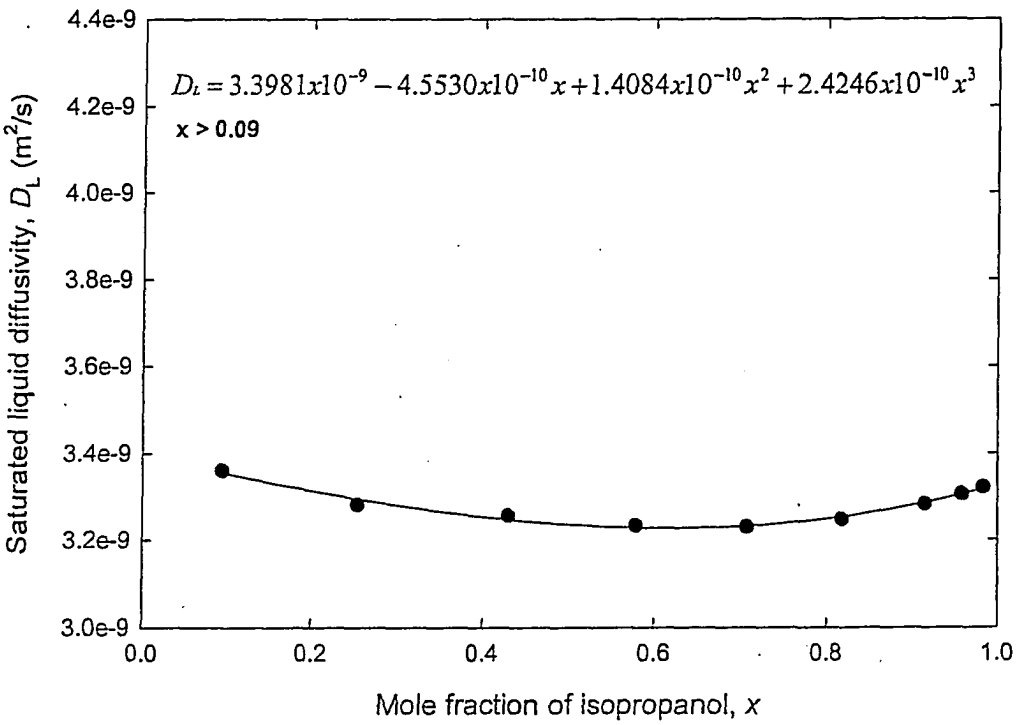

Figure B5.5 Saturated liquid diffusivity as a function of isopropanol concentration (x > 0.09).

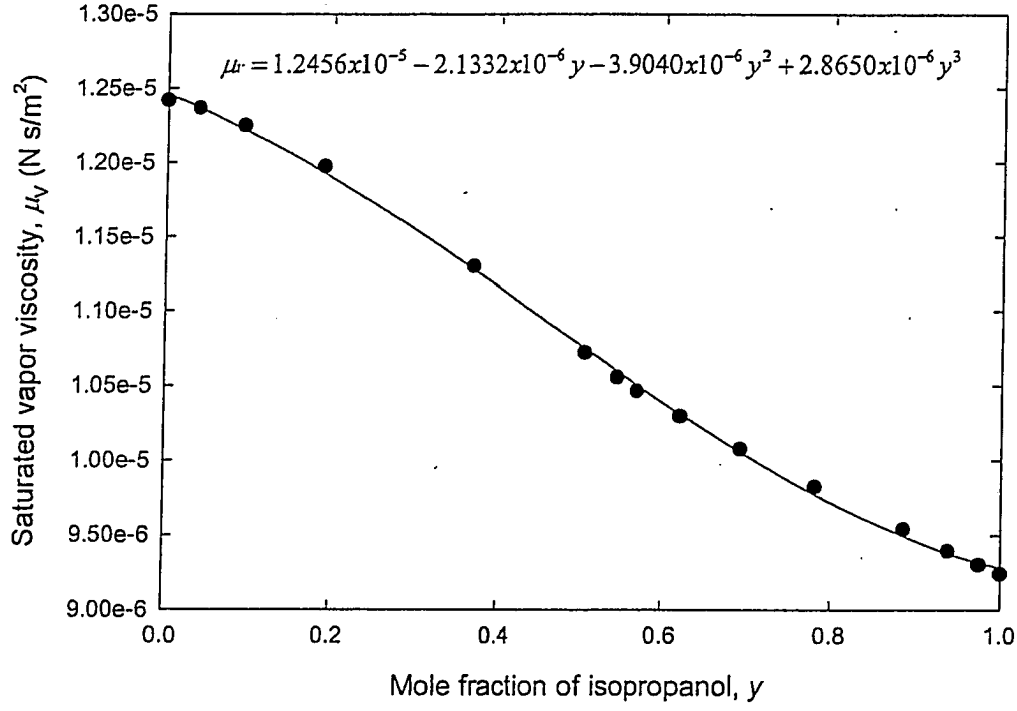

Figure B5.6 Saturated vapor viscosity as a function of isopropanol concentration.

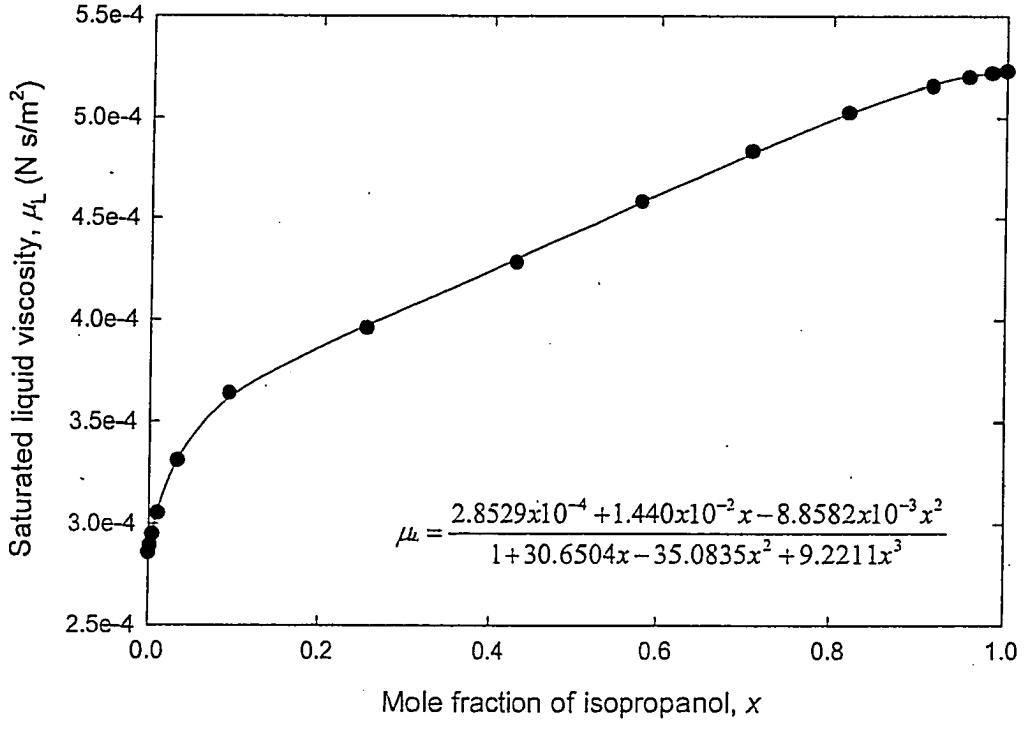

Figure B5.7 Saturated liquid viscosity as a function of isopropanol concentration.

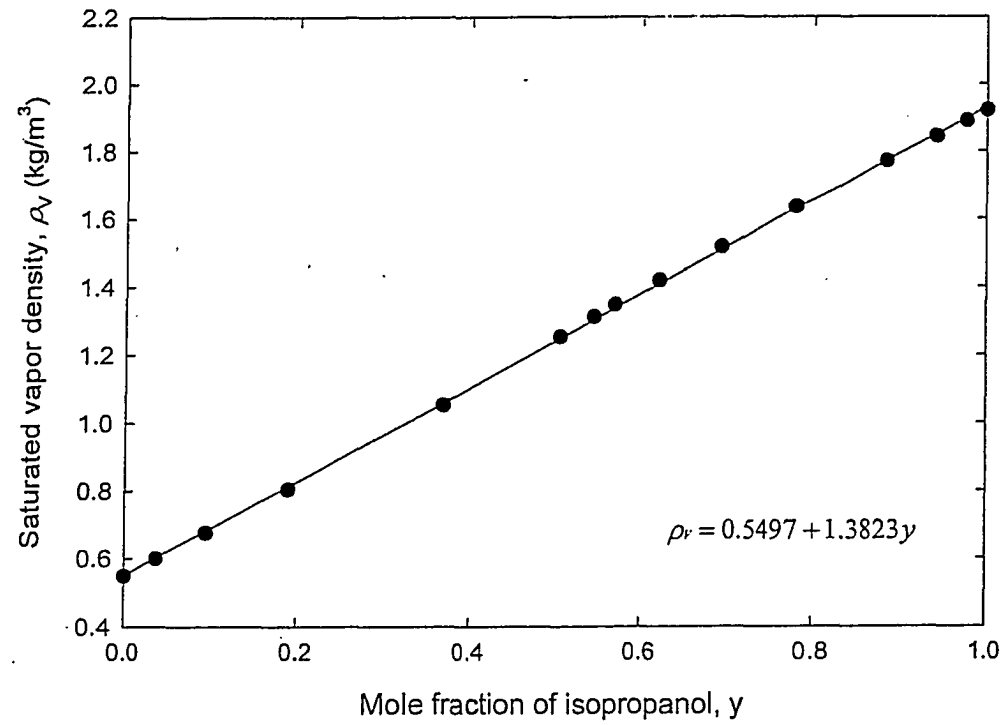

Figure B5.8 Saturated vapor density as a function of isopropanol concentration.

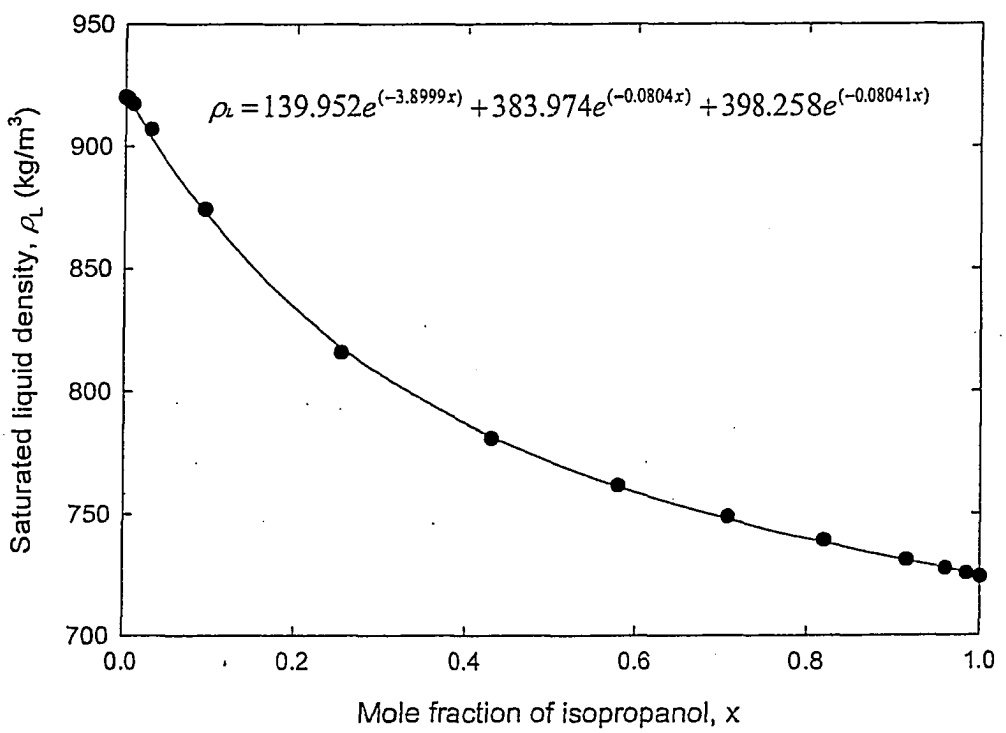

Figure B5.9 Saturated liquid density as a function of isopropanol concentration.

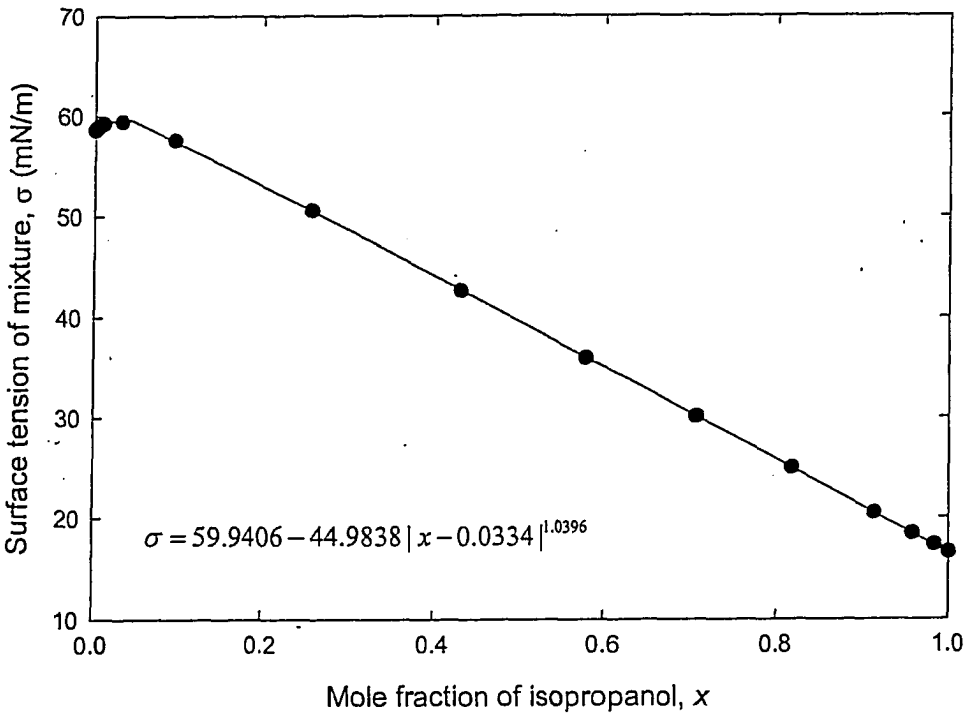

Figure B5.10 Surface tension of the mixture as a function of isopropanol concentration.

Water / Isopropanol

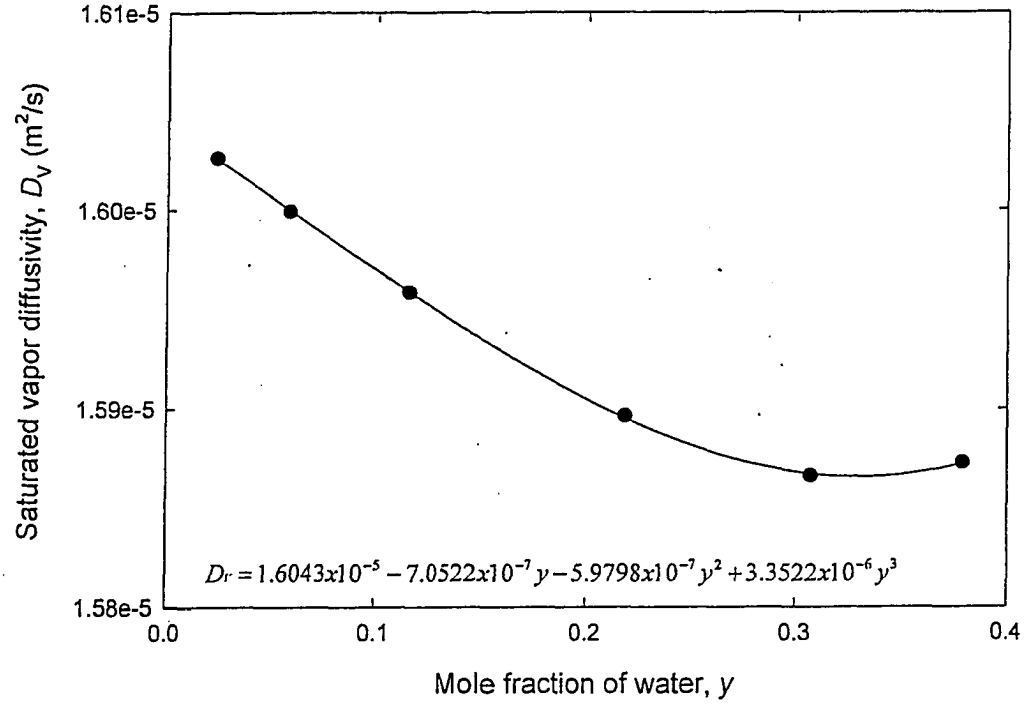

Figure B5.11 Saturated vapor diffusivity as a function of water concentration

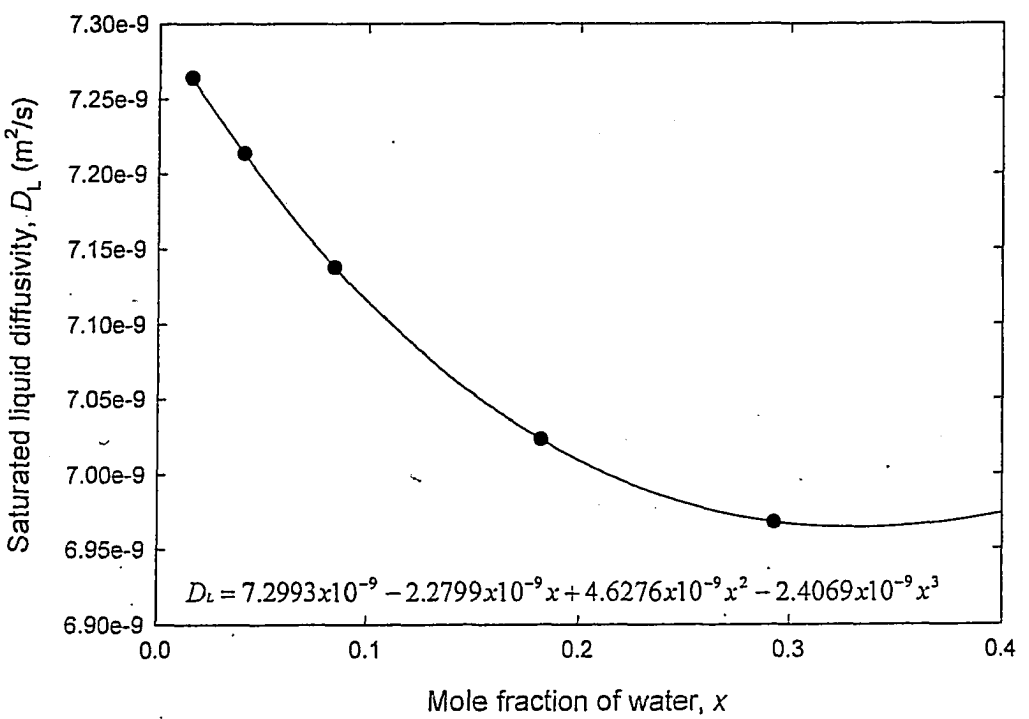

Figure B5.12 Saturated liquid diffusivity as a function of water concentration

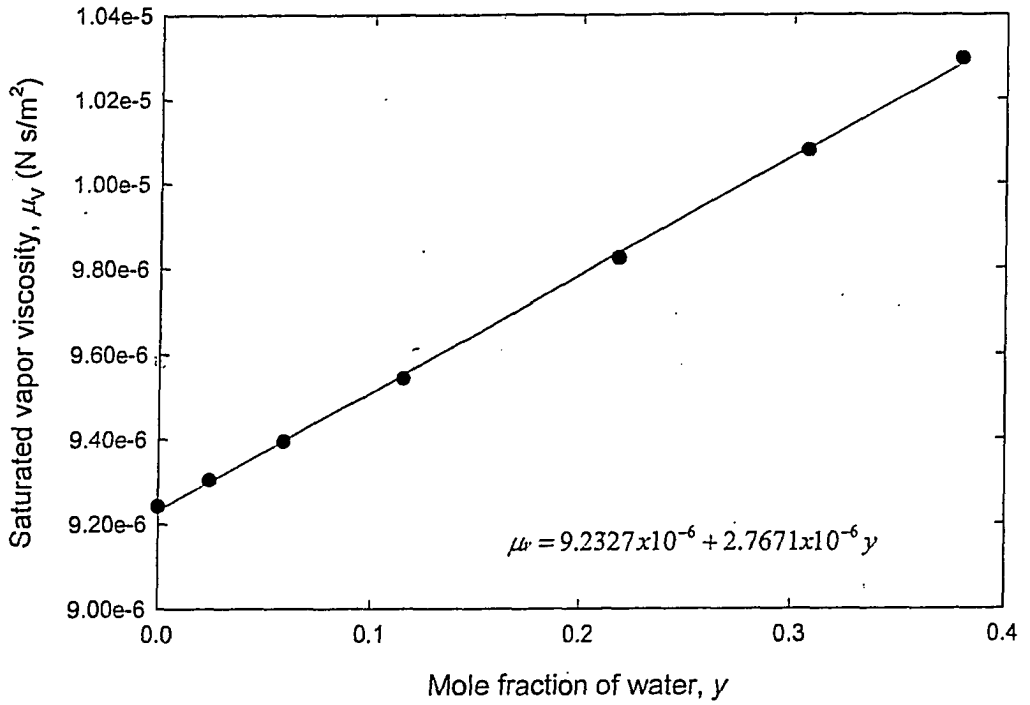

Figure B5.13 Saturated vapor viscosity as a function of water concentration.

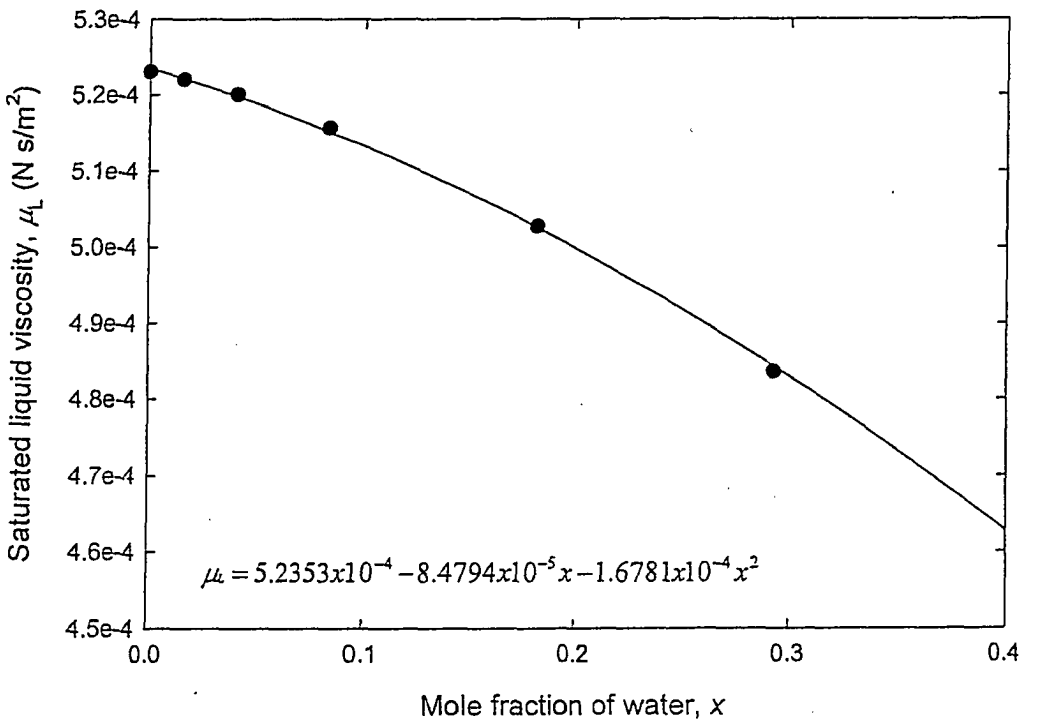

Figure B5.14 Saturated liquid viscosity as a function of water concentration.

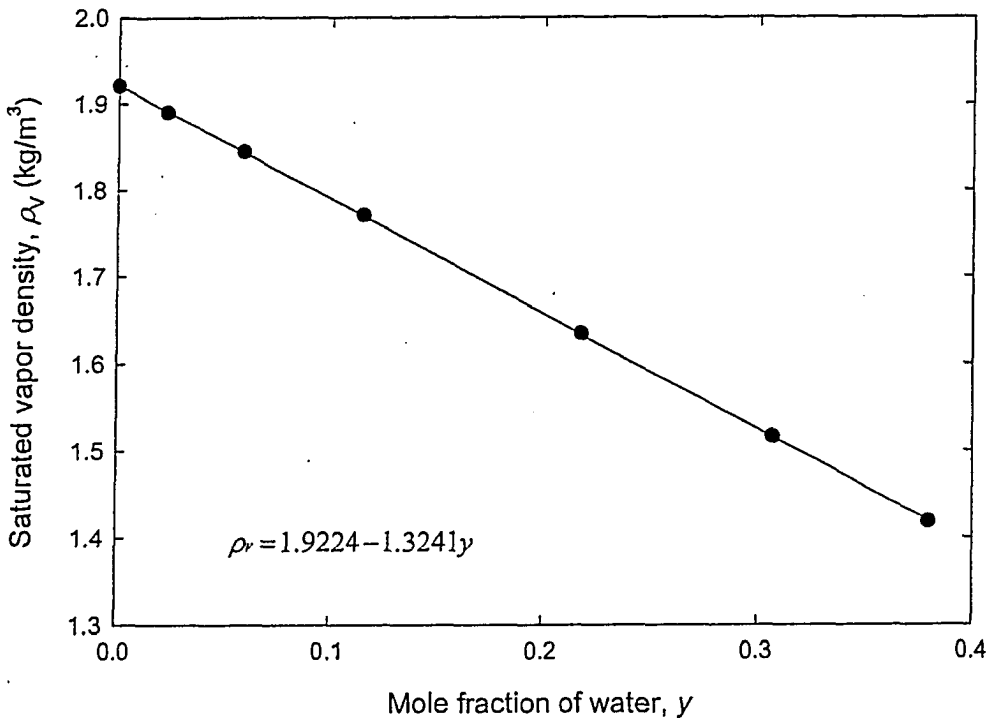

Figure B5.15 Saturated vapor density as a function of water concentration.

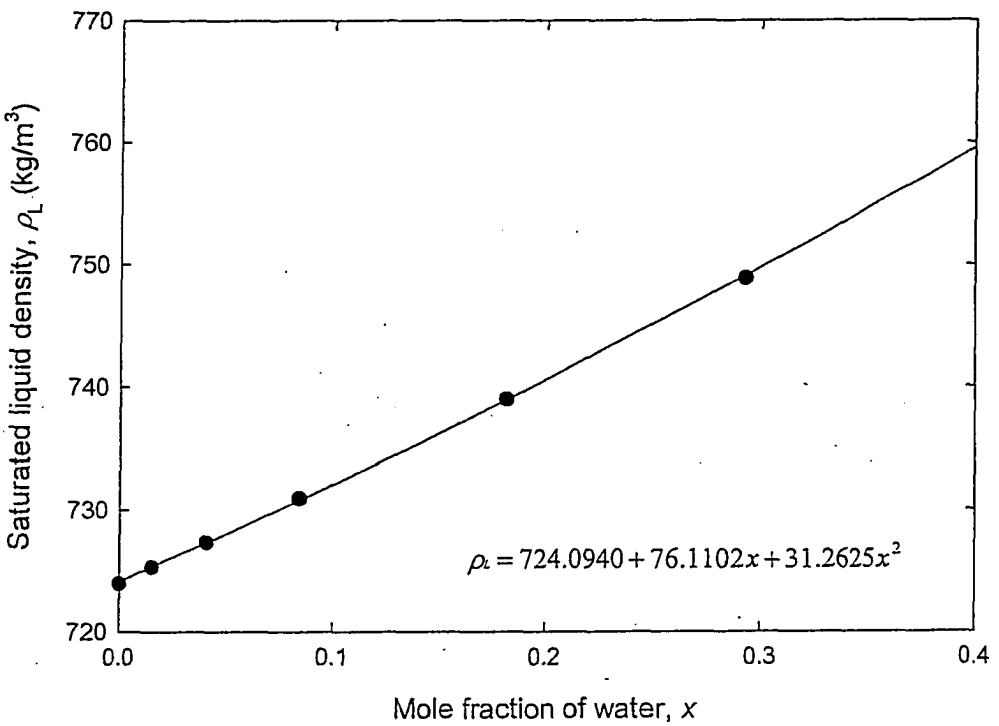

Figure B5.16 Saturated liquid density as a function of water concentration.

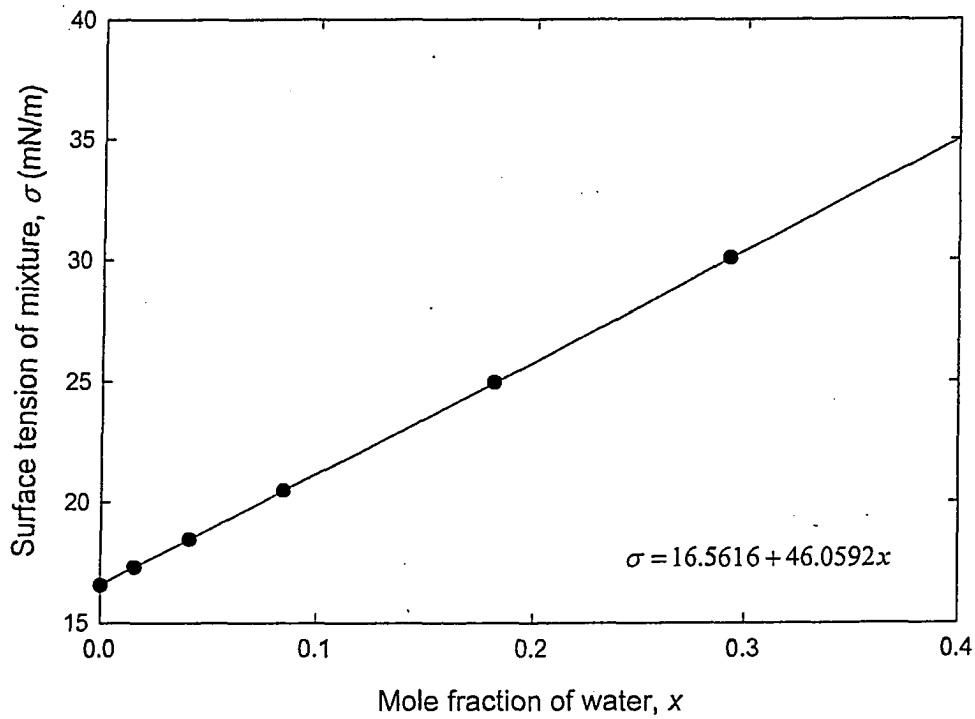

Figure B5.17 Surface tension of the mixture as a function of water concentration.

B6 Saturated system property data for the METHANOL / ISOPROPANOL system determined using the Peng-Robinson Wong-Sandler method

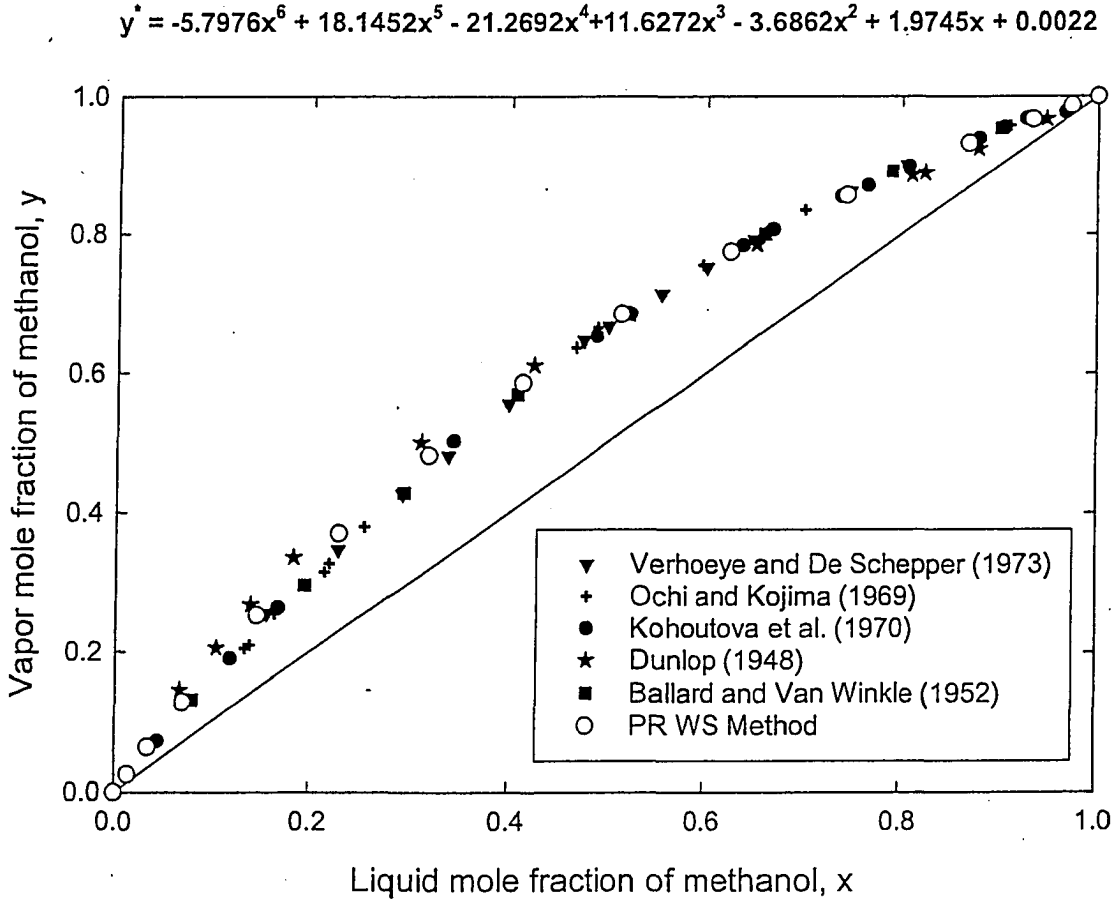

Figure B6.1 Vapor-liquid equilibrium data for the methanol/isopropanol system.

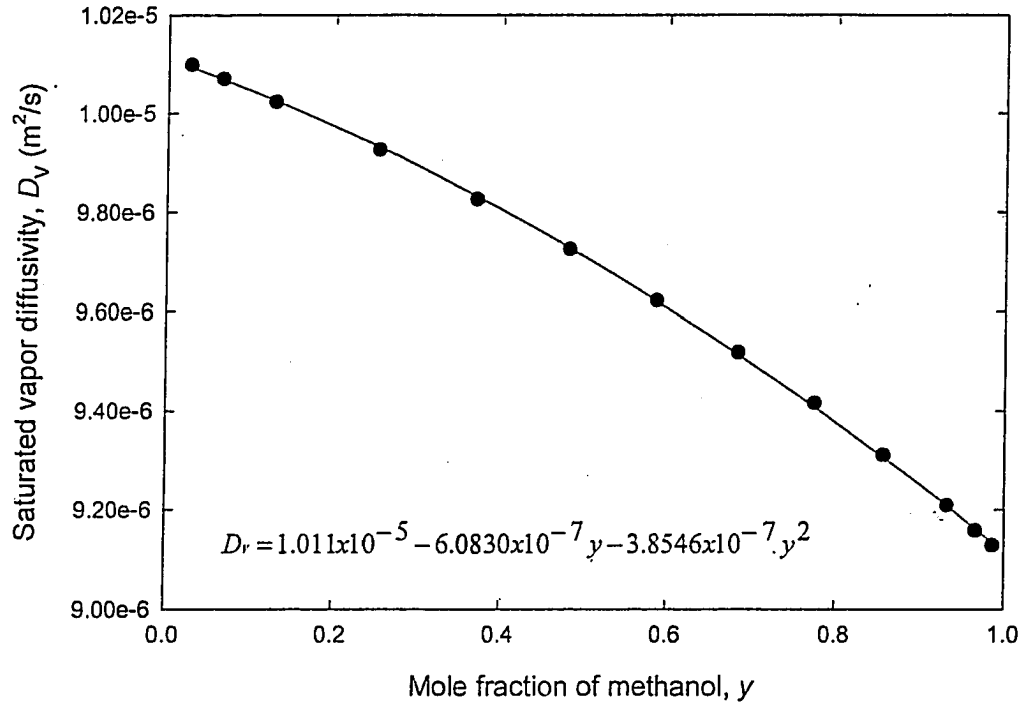

Figure B6.2 Saturated vapor diffusivity as a function of methanol concentration

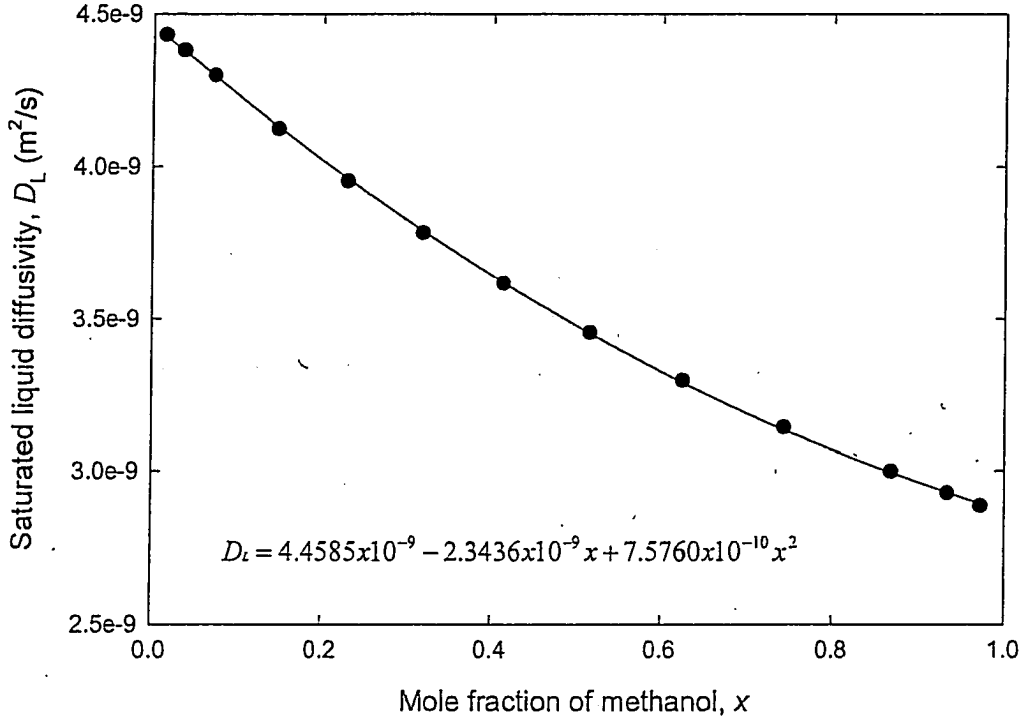

Figure B6.3 Saturated liquid diffusivity as a function of methanol concentration

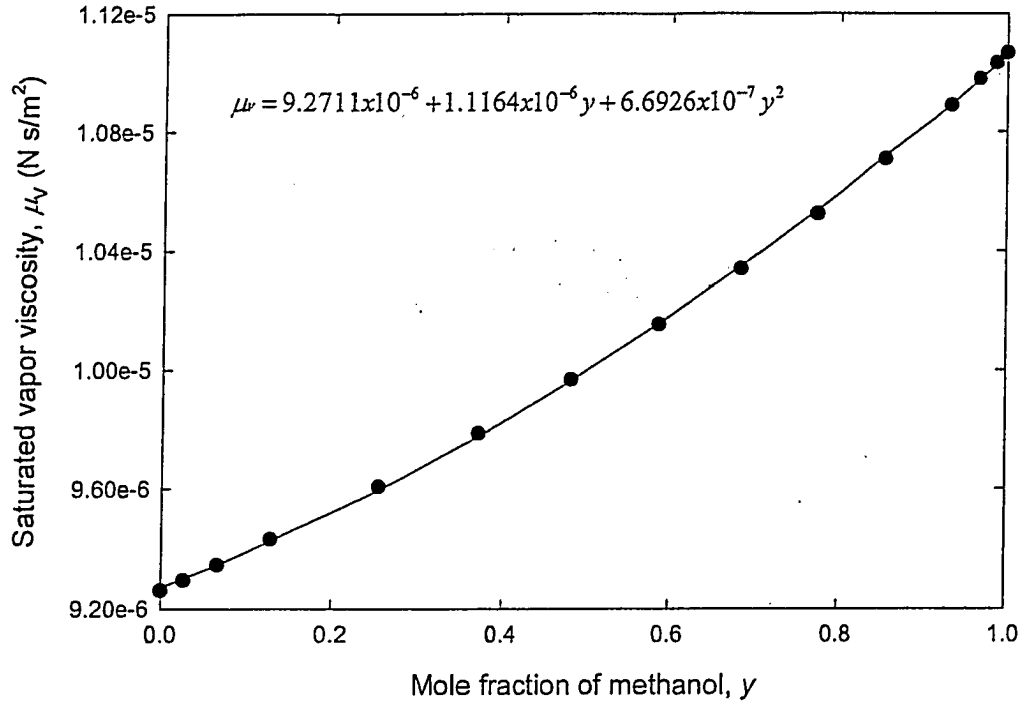

Figure B6.4 Saturated vapor viscosity as a function of methanol concentration.

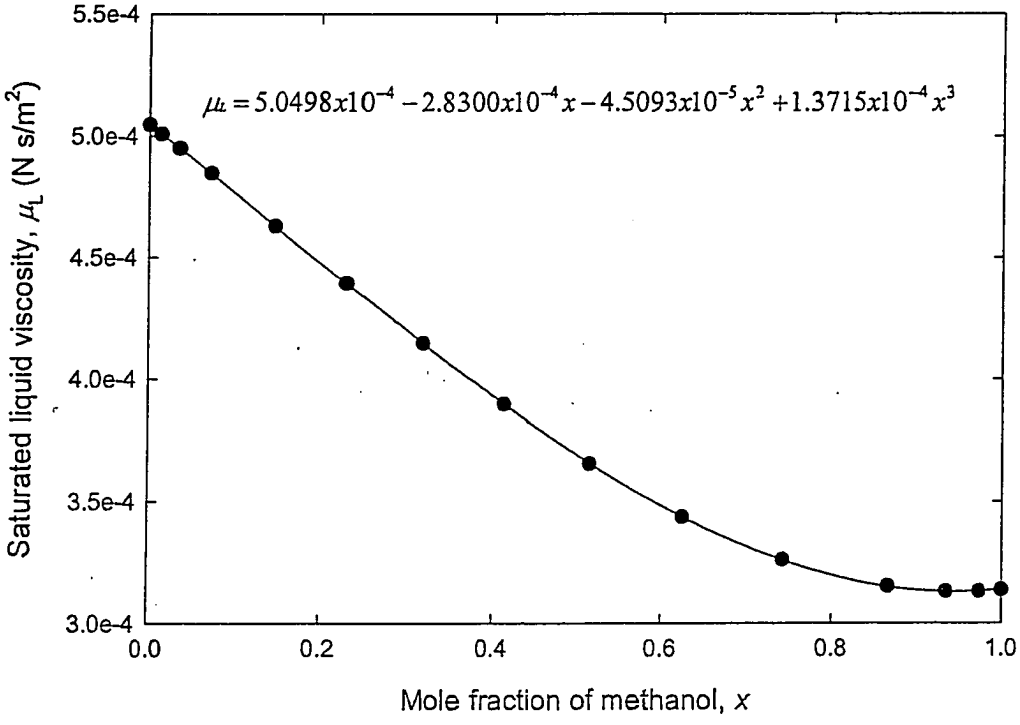

Figure B6.5 Saturated liquid viscosity as a function of methanol concentration.

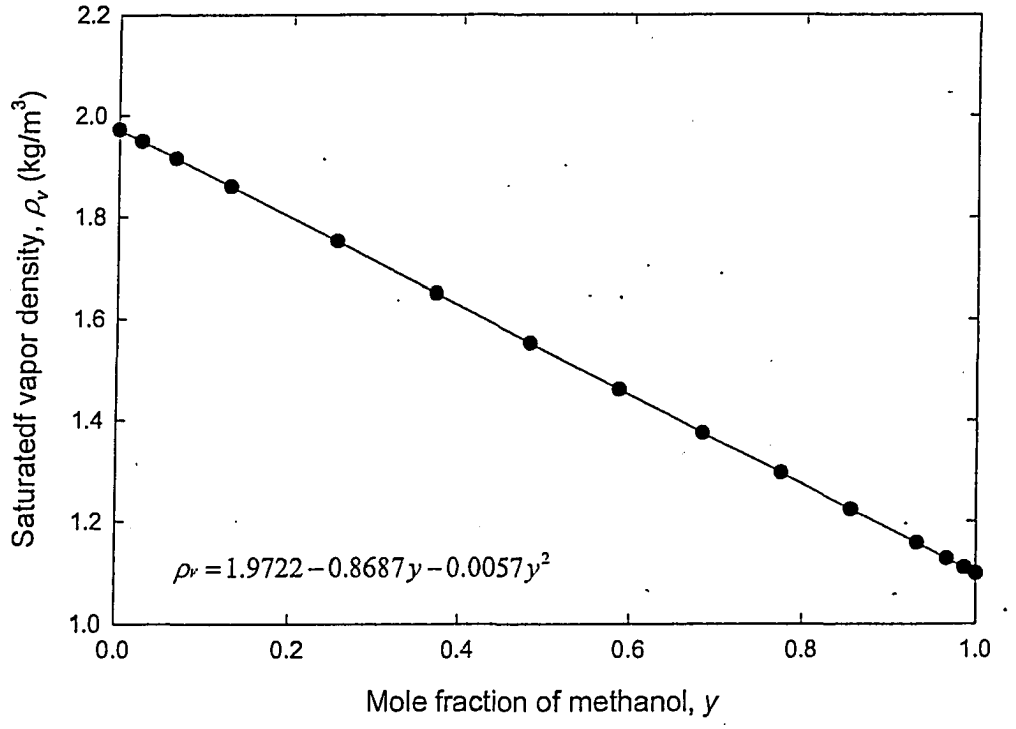

Figure B6.6 Saturated vapor density as a function of methanol concentration.

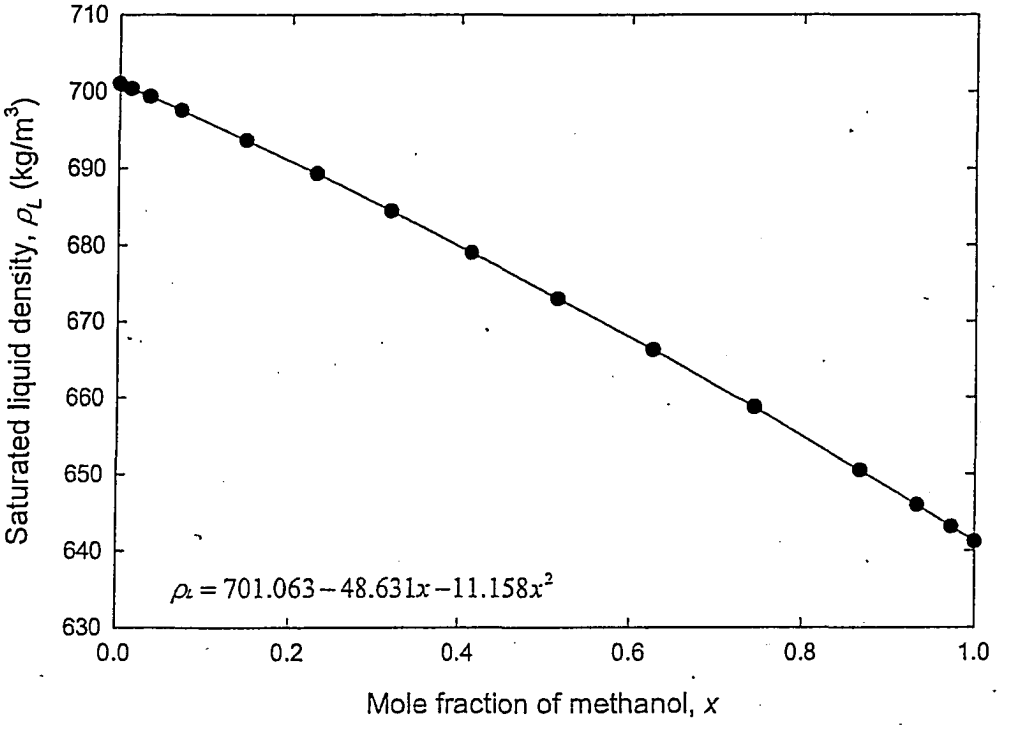

Figure B6.7 Saturated liquid density as a function of methanol concentration.

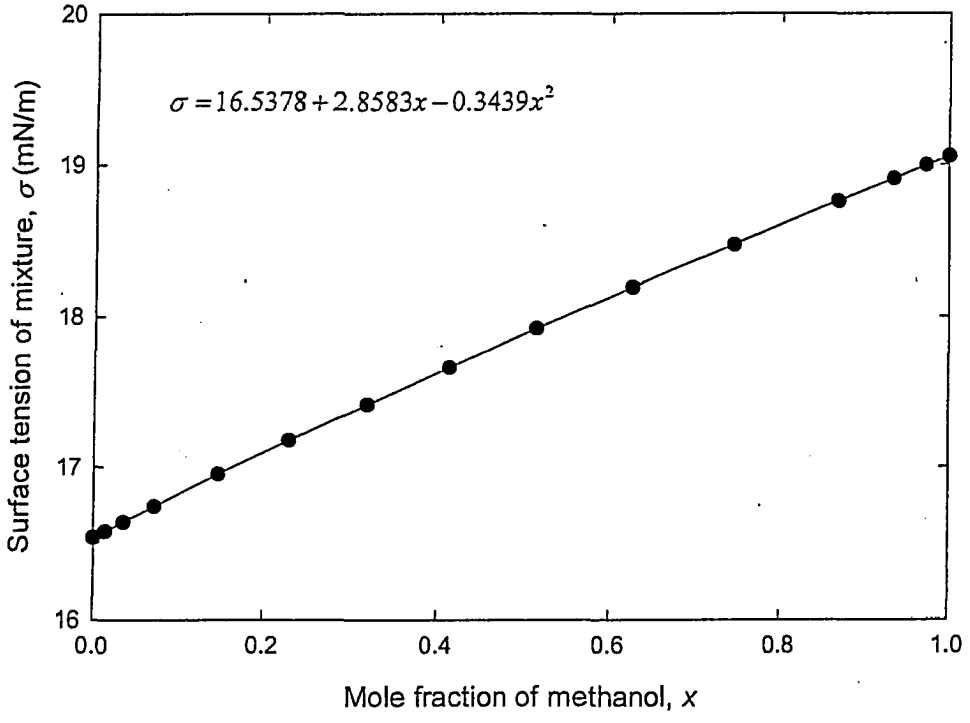

Figure B6.8 Surface tension of the mixture as a function of methanol concentration.

B7 Saturated system property data for the CYCLOHEXANE / n-HEPTANE system determined using the Peng-Robinson Wong-Sandler method

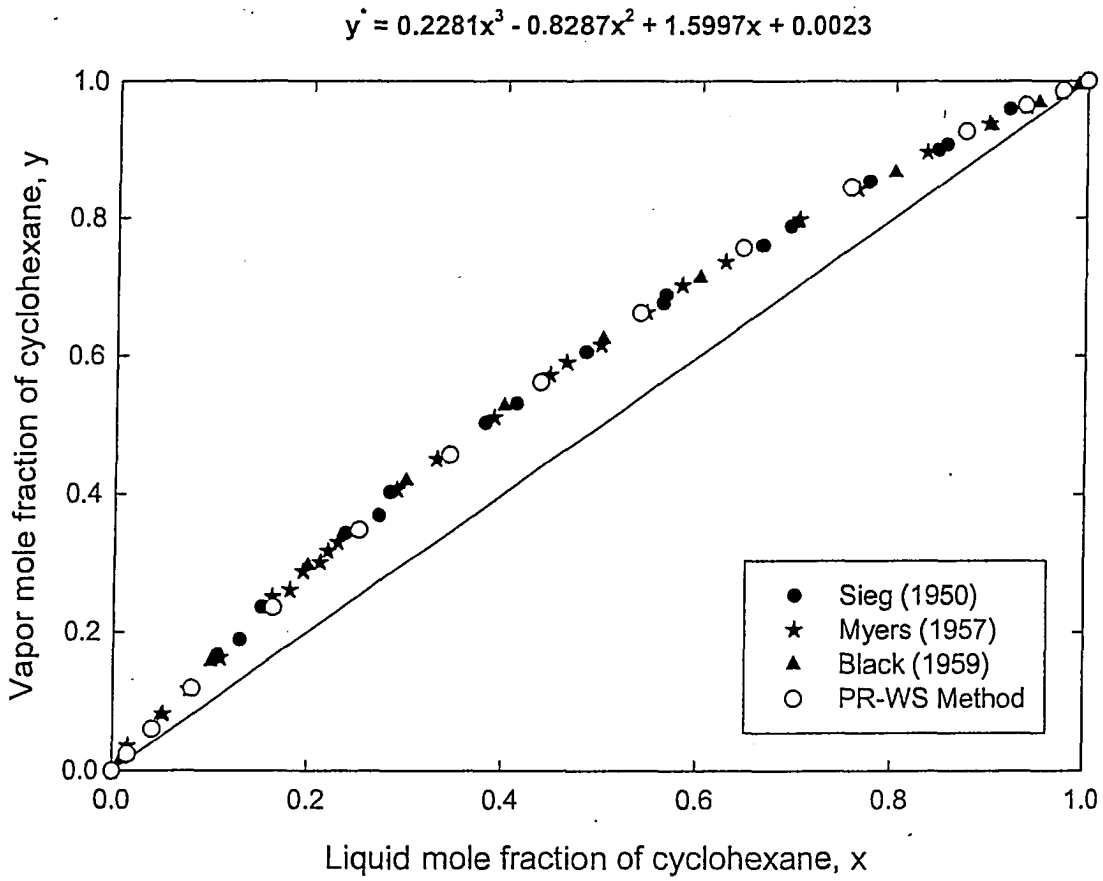

Figure B7.1 Vapor-liquid equilibrium data for the cyclohexane/n-heptane system.

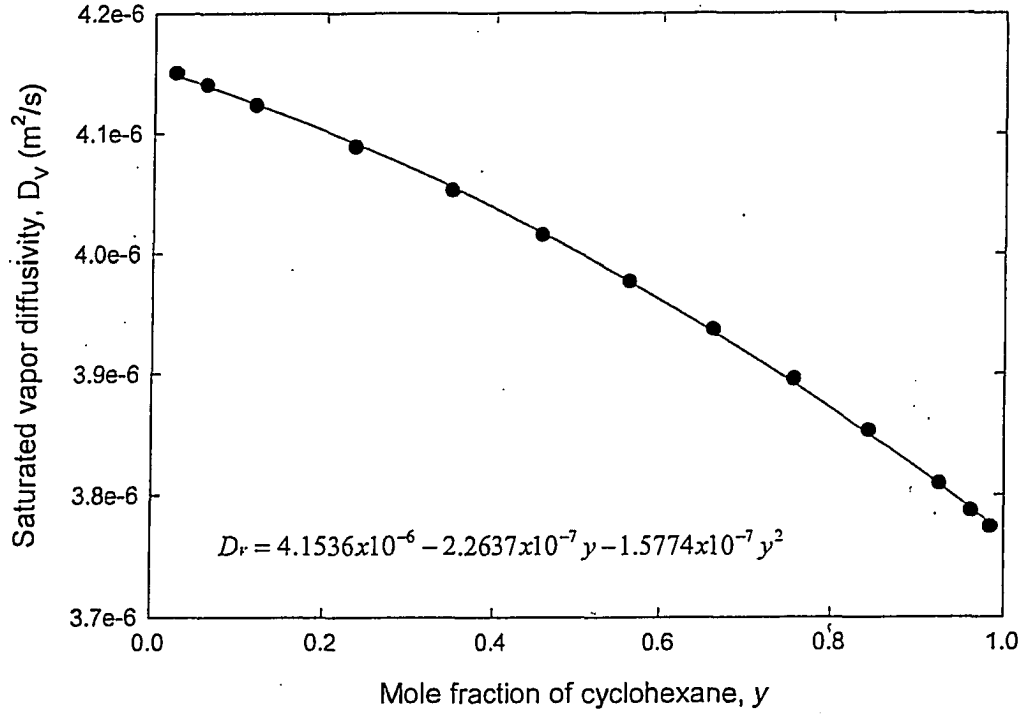

Figure B7.2 Saturated vapor diffusivity as a function of cyclohexane concentration

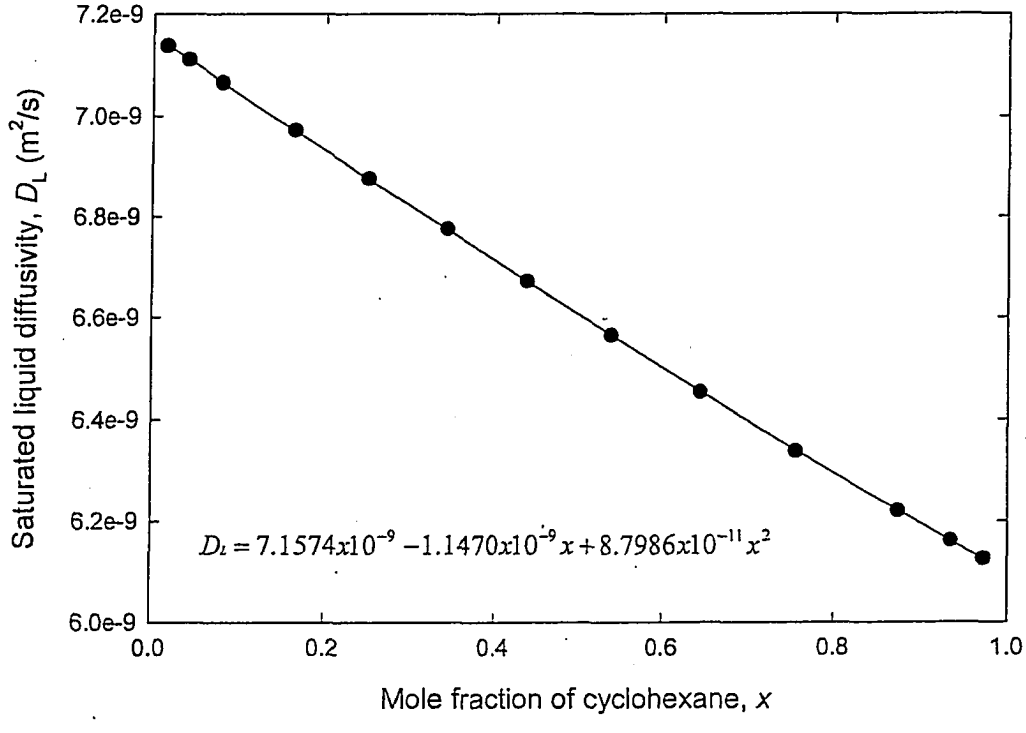

Figure B7.3 Saturated liquid diffusivity as a function of cyclohexane concentration

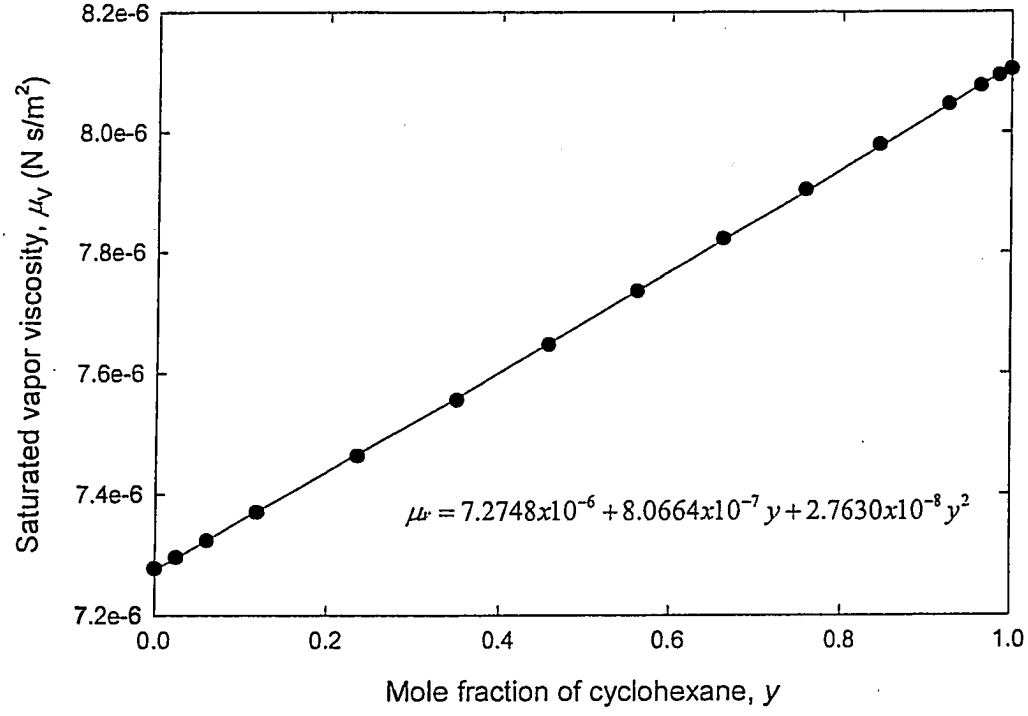

Figure B7.4 Saturated vapor viscosity as a function of cyclohexane concentration.

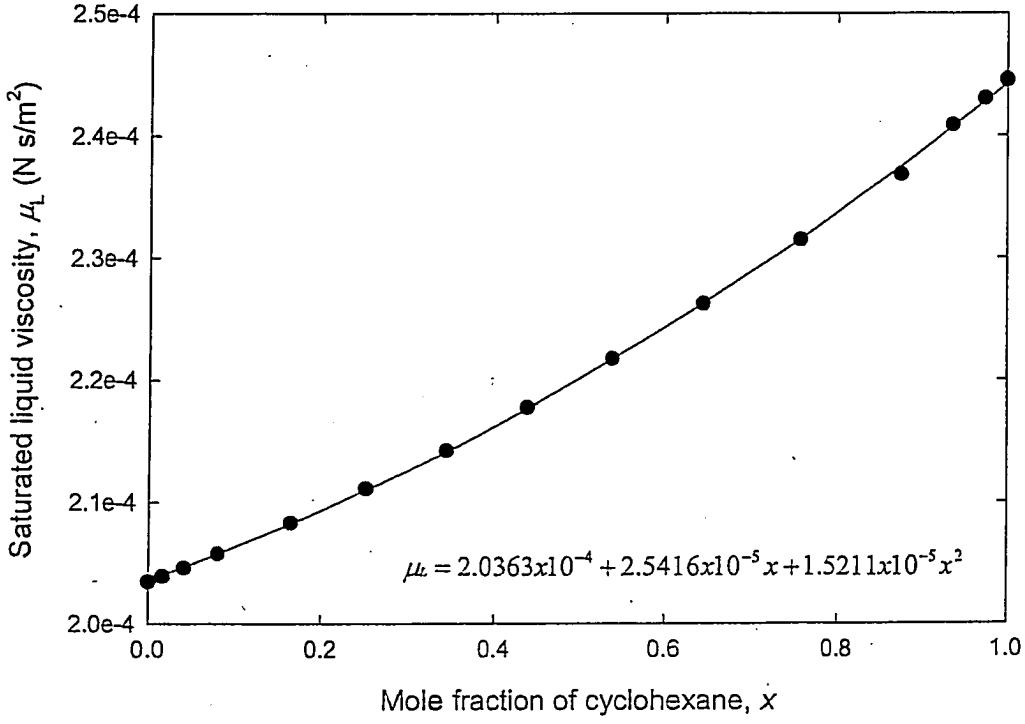

Figure B7.5 Saturated liquid viscosity as a function of cyclohexane concentration.

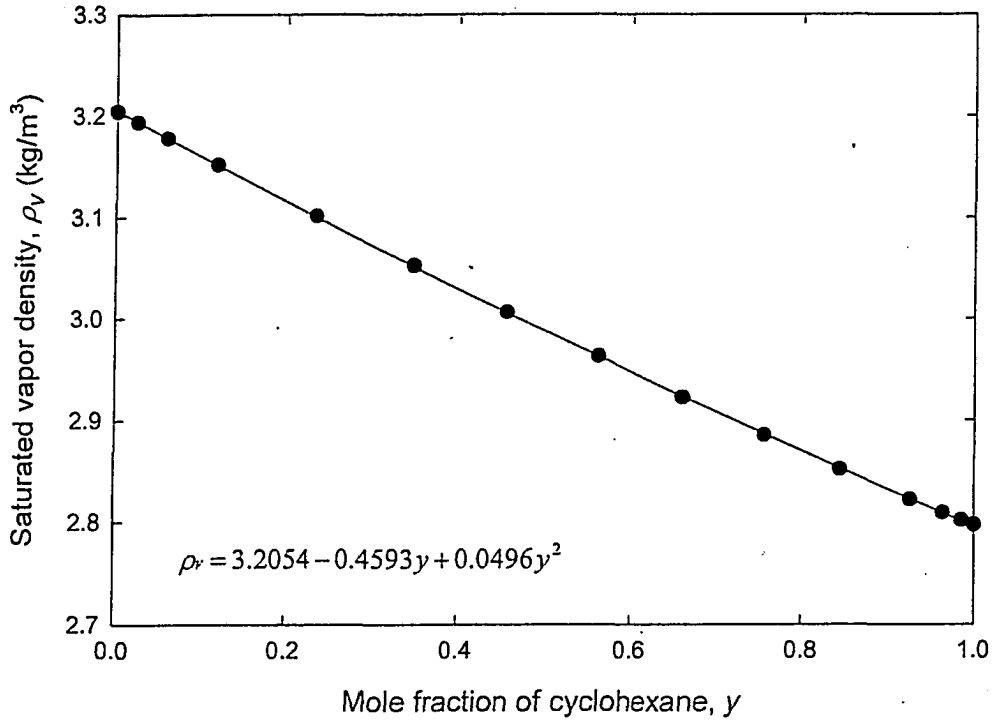

Figure B7.6 Saturated vapor density as a function of cyclohexane concentration.

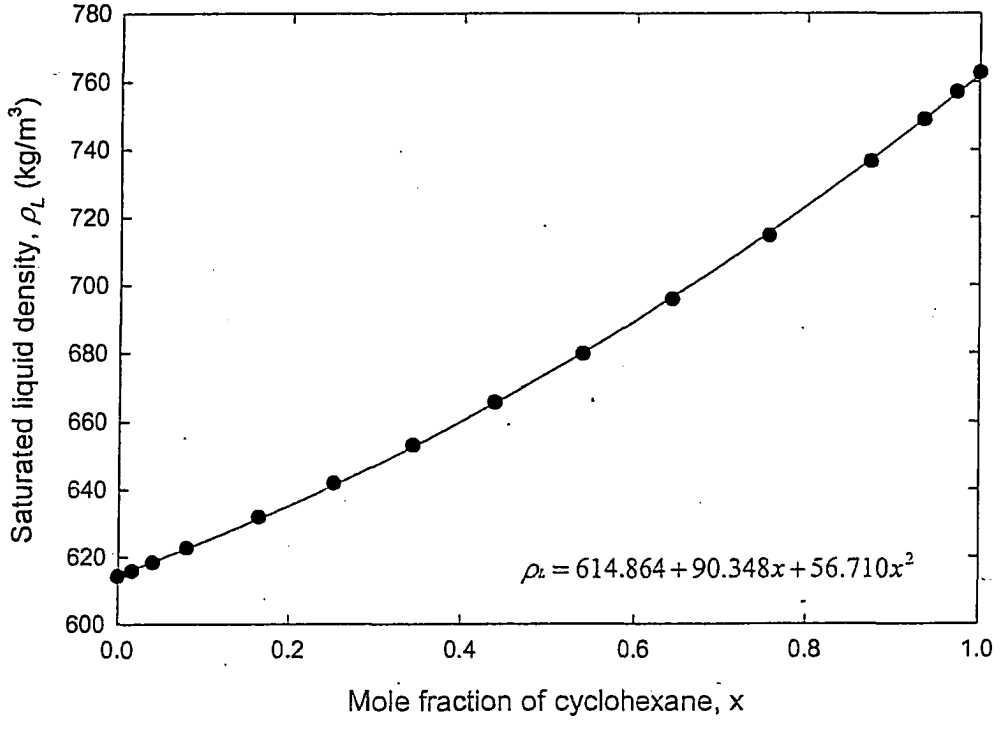

Figure B7.7 Saturated liquid density as a function of cyclohexane concentration.

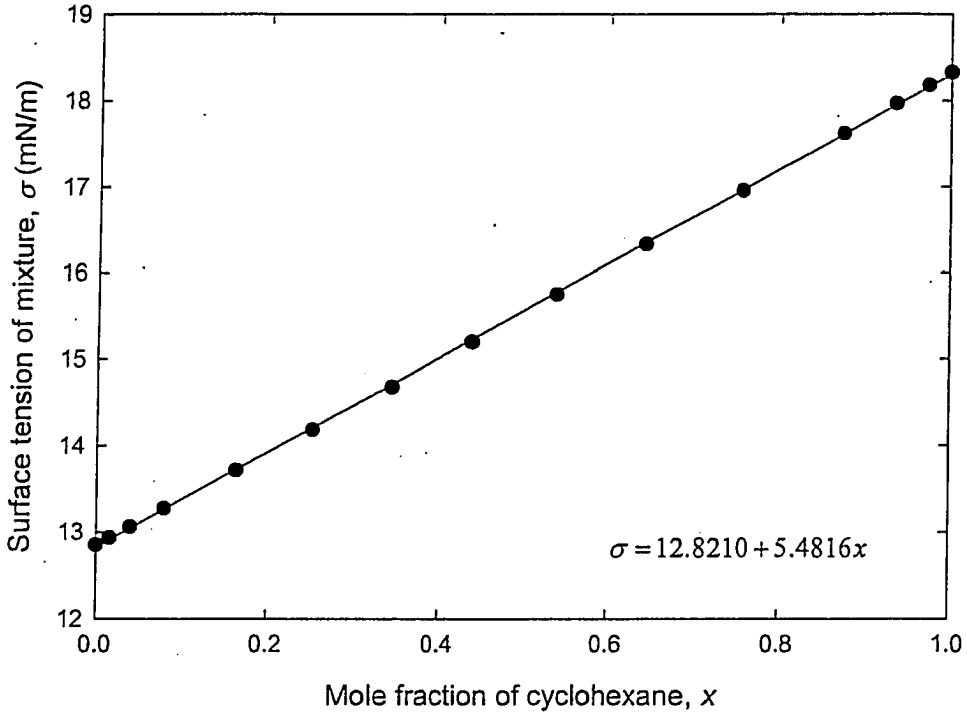

Figure B7.8 Surface tension of the mixture as a function of cyclohexane concentration.

Appendix C

ROTAMETER AND GC CALIBRATION CURVES AND EQUATIONS

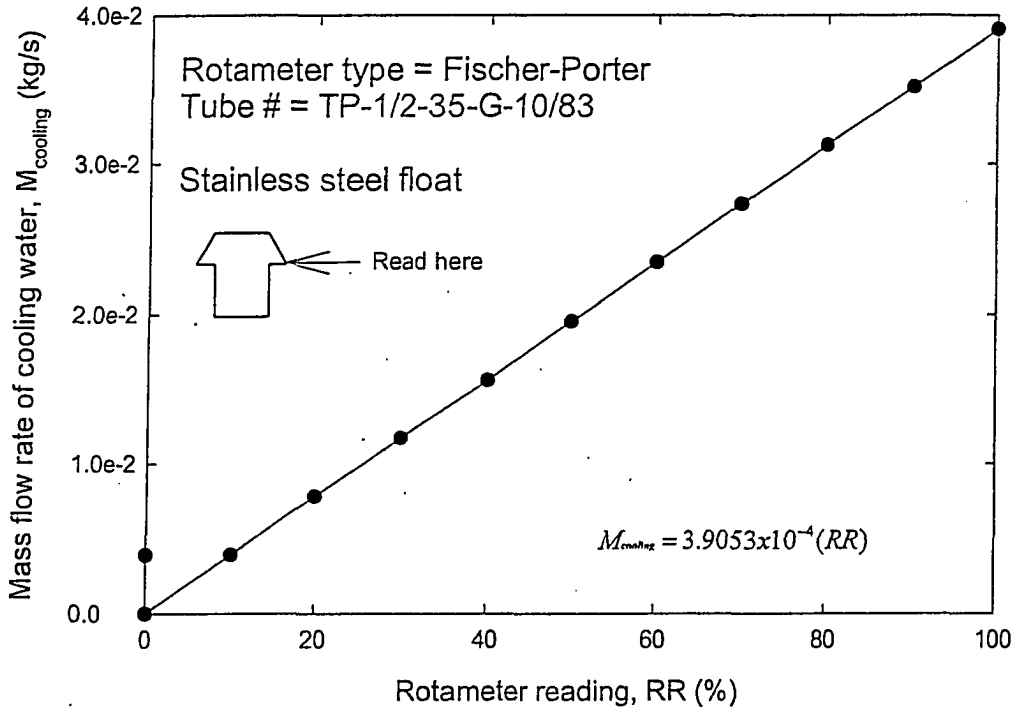

Figure C1 Rotameter calibration curve used to determine the mass flow rate of cooling water.

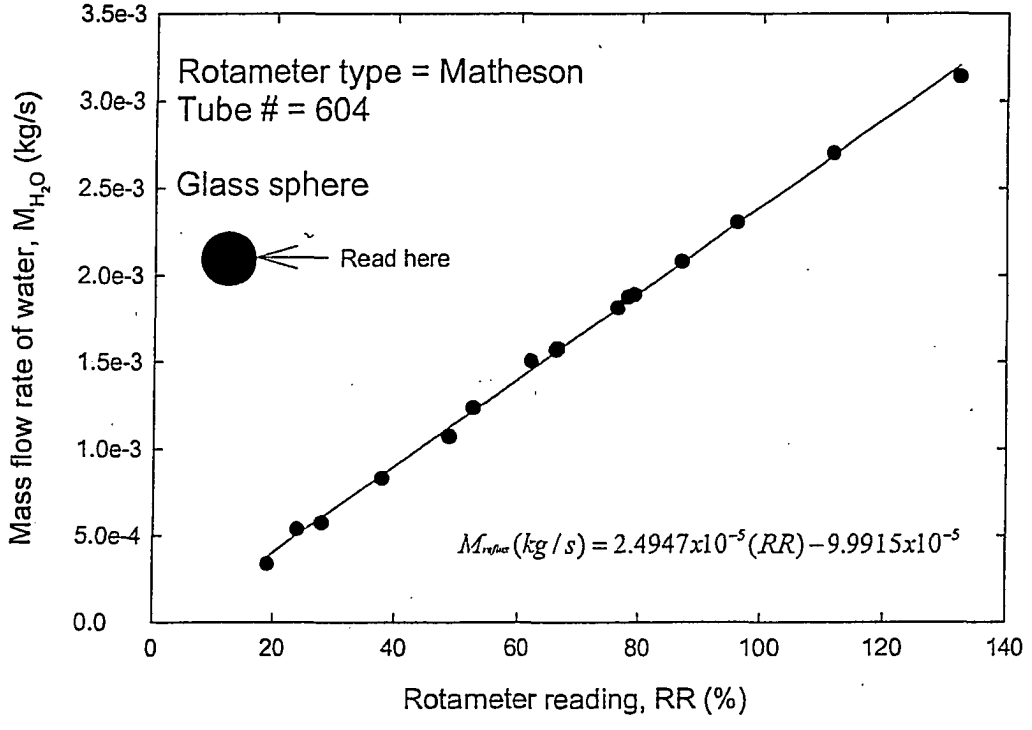

Figure C2 Rotameter calibration curve used to determine the mass flow rate of reflux in terms of mass flow rate of water.

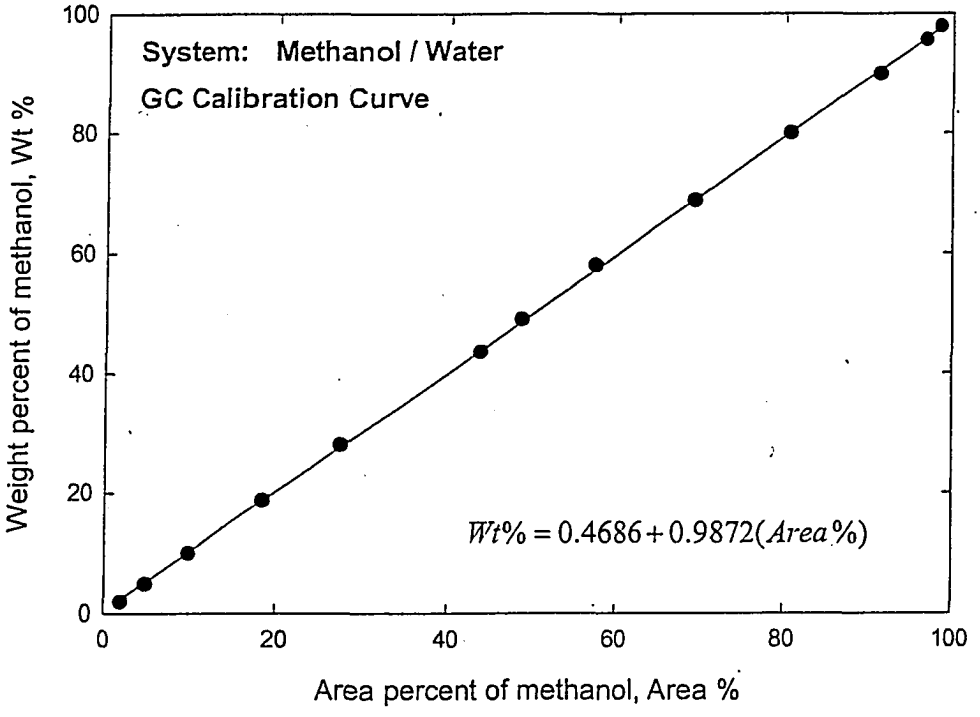

Figure C3 GC calibration curve for the methanol/water system.

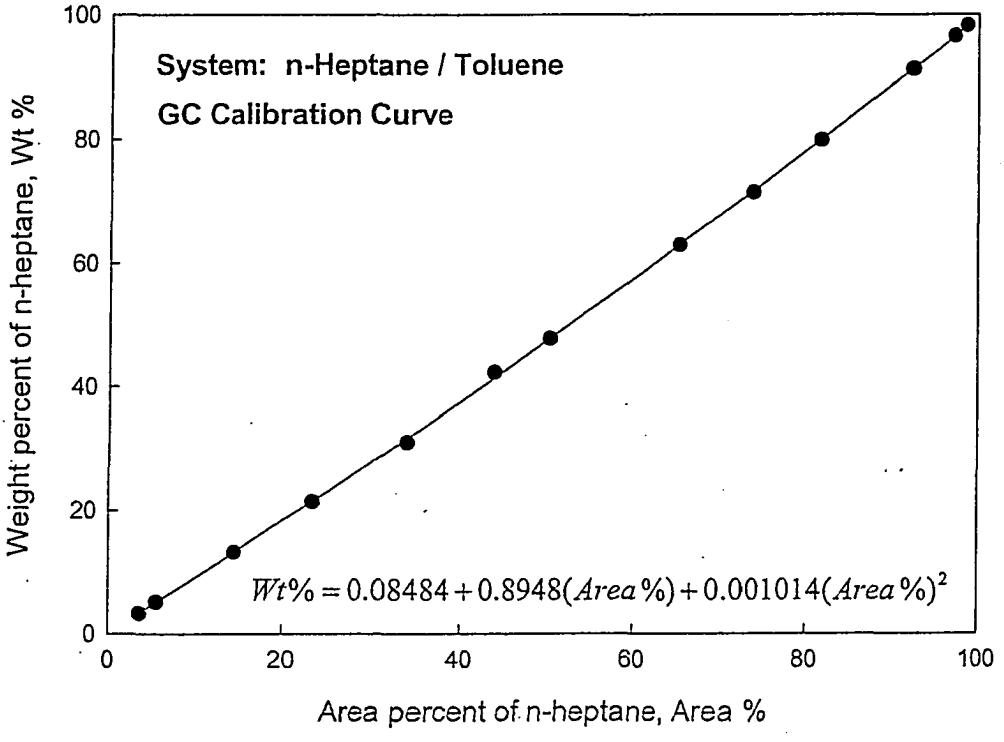

Figure C4 GC calibration curve for the n-heptane/toluene system.

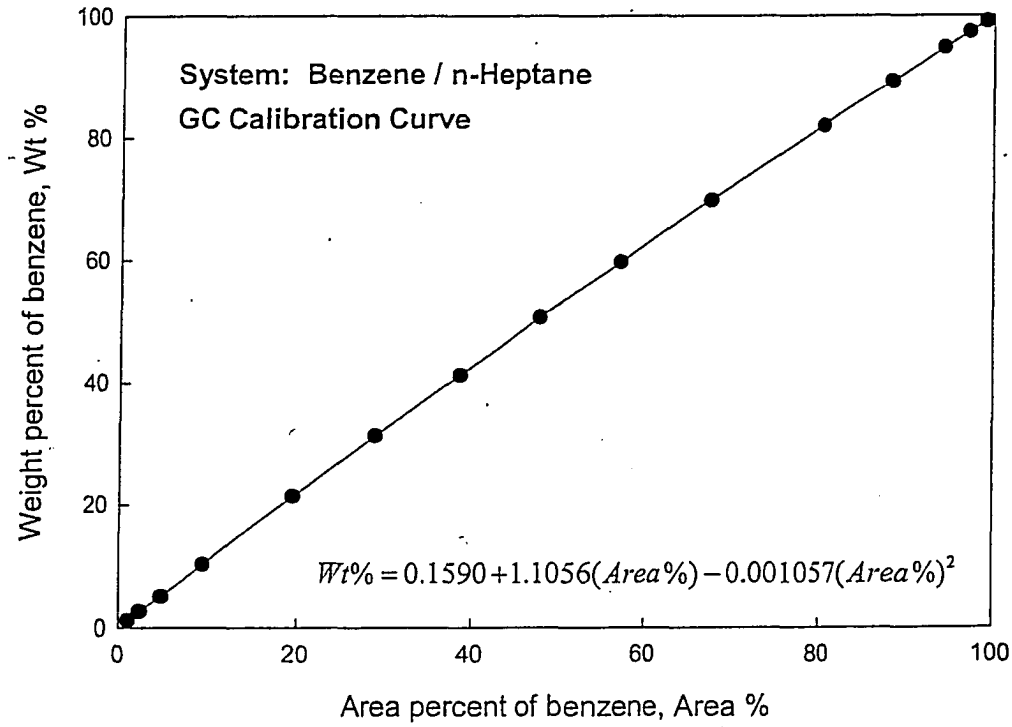

Figure C5 GC calibration curve for the benzene/n-heptane system.

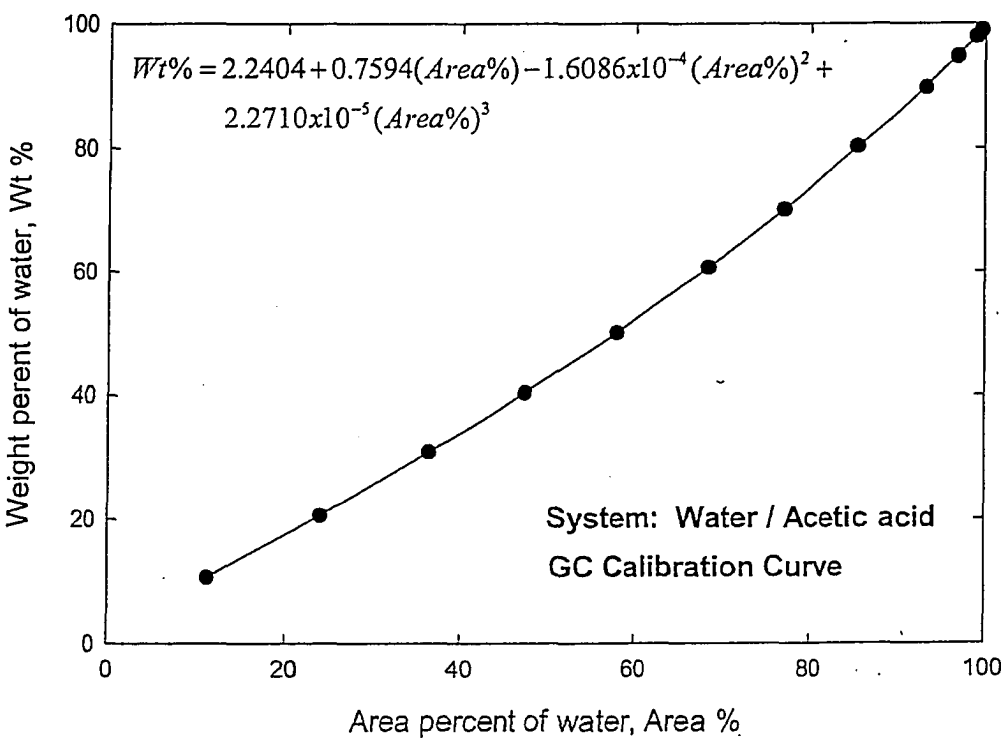

Figure C6 GC calibration curve for the water/acetic acid system

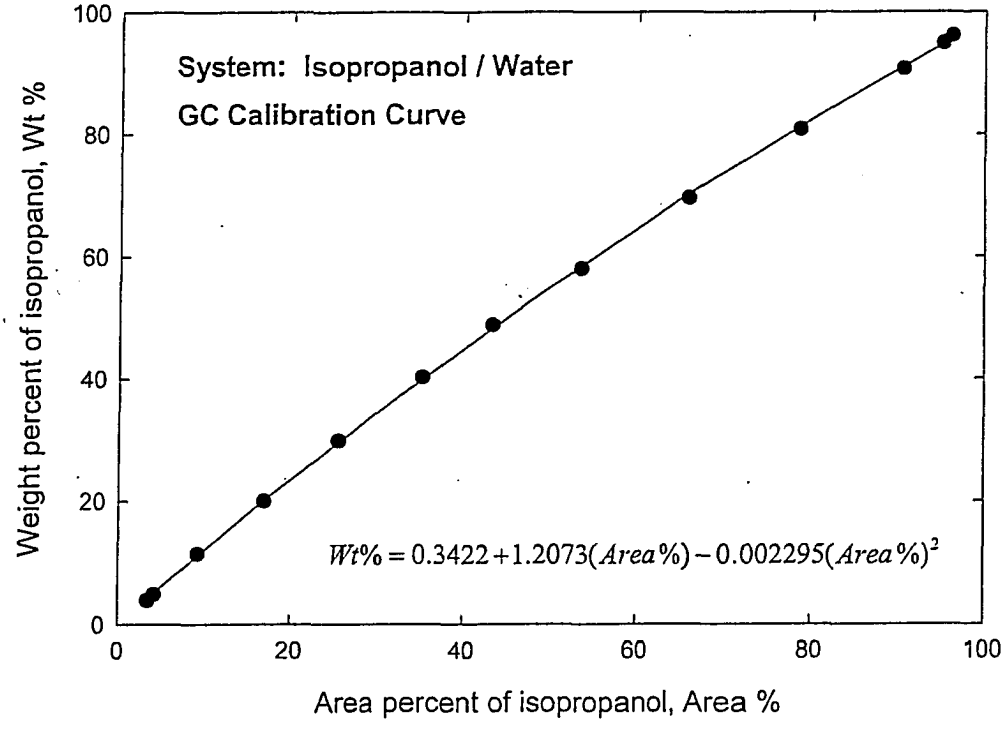

Figure C7 GC calibration curve for the isopropanol/water system.

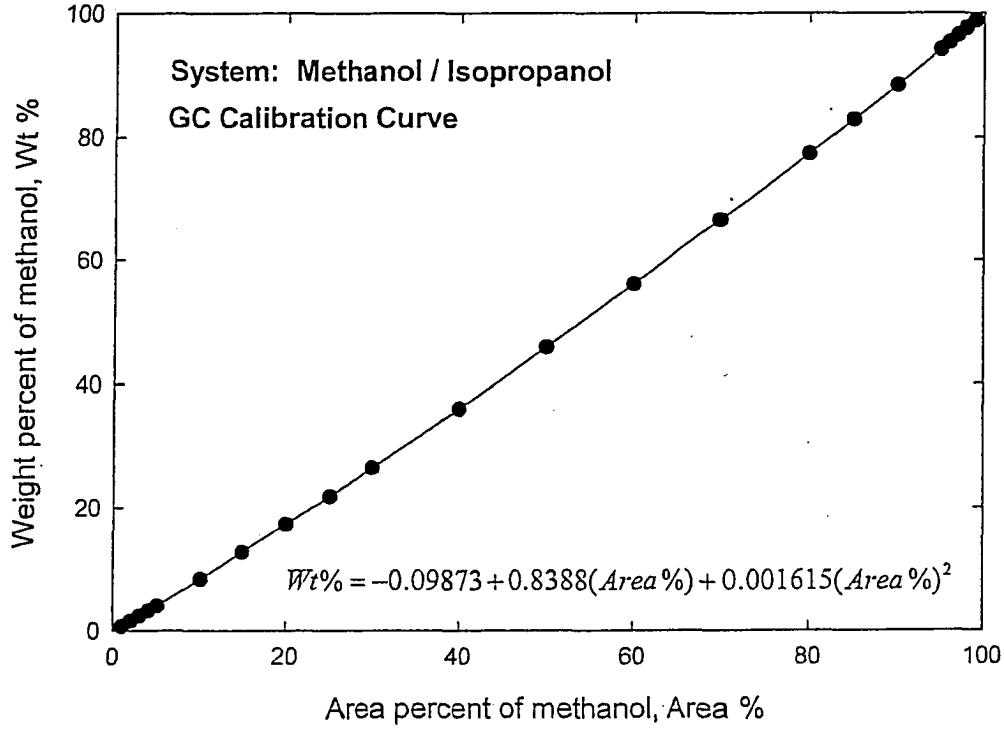

Figure C8 GC calibration curve for the methanol/isopropanol system.

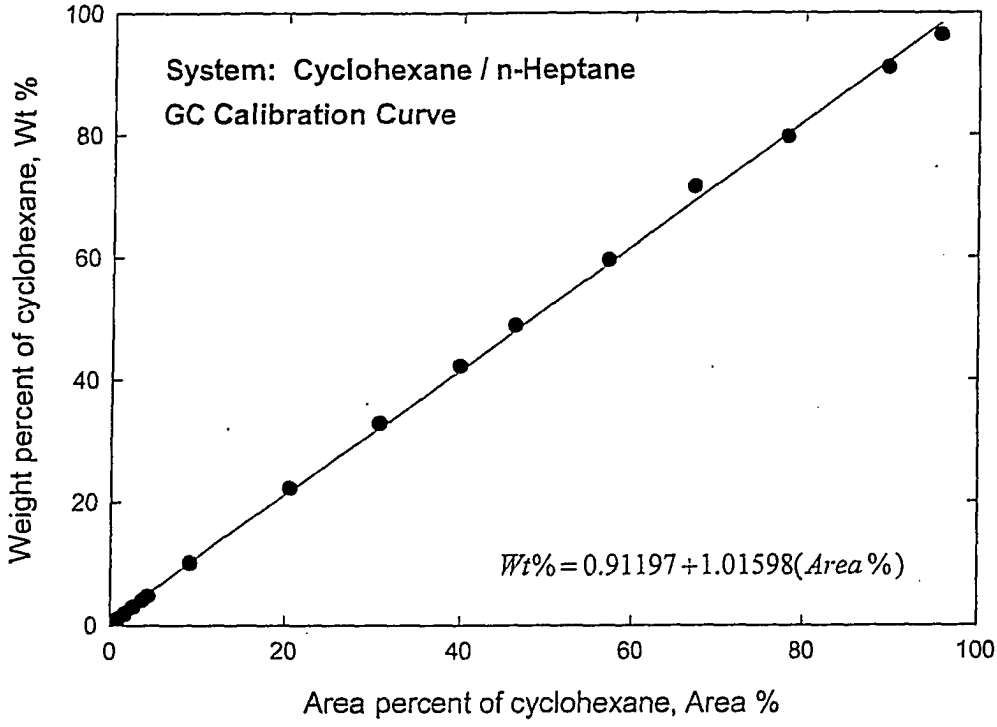

Figure C9 GC calibration curve for the cyclohexane/n-heptane system.

Appendix D

MURPHREE TRAY EFFICIENCY DATA (SYEDA, 2002)

Table D1 Tray efficiency data for the methanol/water system.

Average methanol concentration x_{avg}	Murphree tray efficiency E_{MV}	Height equivalent to a theoretical plate HETP (m)
0.075	0.350	0.143
0.087	0.400	0.125
0.110	0.450	0.111
0.150	0.560	0.089
0.164	0.550	0.091
0.190	0.680	0.074
0.204	0.750	0.067
0.244	0.790	0.063
0.287	0.808	0.062
0.300	0.834	0.060
0.312	0.832	0.060
0.340	0.839	0.060
0.355	0.839	0.060
0.470	0.848	0.059
0.501	0.858	0.058
0.520	0.858	0.058
0.597	0.868	0.058
0.580	0.842	0.059
0.620	0.851	0.059
0.670	0.897	0.056
0.740	0.902	0.055
0.770	0.880	0.057
0.800	0.884	0.057
0.853	0.837	0.060
0.890	0.844	0.059
0.900	0.718	0.070
0.930	0.640	0.078

Table D2 Tray efficiency data for the n-heptane/toluene system.

Average n-heptane concentration x_{avg}	Murphree tray efficiency E_{MV}	Height equivalent to a theoretical plate HETP (m)
0.920	0.385	0.130
0.917	0.504	0.099
0.940	0.440	0.114
0.960	0.400	0.125
0.874	0.583	0.086
0.869	0.511	0.098
0.821	0.622	0.080
0.810	0.650	0.077
0.750	0.583	0.086
0.746	0.679	0.074
0.702	0.726	0.069
0.681	0.660	0.076
0.640	0.660	0.076
0.629	0.705	0.071
0.591	0.696	0.072
0.588	0.659	0.076
0.491	0.749	0.067
0.496	0.660	0.076
0.458	0.730	0.069
0.418	0.718	0.070
0.413	0.627	0.080
0.377	0.682	0.073
0.377	0.580	0.086
0.368	0.747	0.067
0.322	0.607	0.082
0.302	0.714	0.070
0.268	0.545	0.092
0.262	0.623	0.080
0.250	0.572	0.087
0.197	0.600	0.083
0.150	0.520	0.096
0.146	0.480	0.104
0.104	0.508	0.098
0.103	0.450	0.111

Table D3 Tray efficiency data for the benzene/n-heptane system.

Average benzene concentration x_{avg}	Murphree tray efficiency E_{MV}	Height equivalent to a theoretical plate HETP (m)
0.955	0.564	0.089
0.953	0.447	0.112
0.917	0.550	0.091
0.906	0.560	0.089
0.880	0.460	0.109
0.849	0.568	0.088
0.840	0.514	0.097
0.820	0.453	0.110
0.808	0.580	0.086
0.777	0.567	0.088
0.709	0.624	0.080
0.705	0.550	0.091
0.673	0.567	0.088
0.617	0.636	0.079
0.605	0.543	0.092
0.594	0.471	0.106
0.547	0.502	0.100
0.519	0.477	0.105
0.485	0.577	0.087
0.480	0.508	0.098
0.402	0.549	0.091
0.374	0.438	0.114
0.367	0.446	0.112
0.335	0.540	0.093
0.295	0.456	0.110
0.207	0.526	0.095
0.208	0.445	0.112

Table D4 Tray efficiency data for the water/acetic acid system.

Average water concentration x_{avg}	Murphree tray efficiency E_{MV}	Height equivalent to a theoretical plate HETP (m)
0.967	0.309	0.162
0.935	0.336	0.149
0.907	0.385	0.130
0.894	0.436	0.115
0.889	0.425	0.118
0.872	0.344	0.146
0.864	0.352	0.142
0.845	0.428	0.117
0.840	0.376	0.133
0.816	0.381	0.131
0.743	0.389	0.128
0.739	0.321	0.156
0.717	0.352	0.142
0.708	0.293	0.171
0.707	0.295	0.169
0.655	0.390	0.128
0.589	0.363	0.138
0.533	0.312	0.160
0.517	0.300	0.167
0.460	0.350	0.143
0.395	0.289	0.173
0.261	0.299	0.167
0.210	0.250	0.200

Table D5 Tray efficiency data for the methanol/isopropanol system.

Average methanol concentration x_{avg}	Murphree tray efficiency E_{MV}	Height equivalent to a theoretical plate HETP (m)
0.950	0.570	0.088
0.940	0.639	0.078
0.919	0.550	0.091
0.880	0.530	0.094
0.832	0.530	0.094
0.787	0.540	0.093
0.760	0.490	0.102
0.699	0.520	0.096
0.655	0.542	0.092
0.602	0.480	0.104
0.521	0.498	0.100
0.502	0.410	0.122
0.490	0.510	0.098
0.537	0.540	0.093
0.444	0.474	0.105
0.403	0.409	0.122
0.384	0.496	0.101
0.321	0.452	0.111
0.288	0.415	0.121
0.250	0.330	0.151
0.208	0.308	0.162

Table D6 Tray efficiency data for the cyclohexane/n-heptane system.

Average cyclohexane concentration x_{avg}	Murphree tray efficiency E_{MV}	Height equivalent to a theoretical plate HETP (m)
0.935	0.584	0.086
0.928	0.513	0.097
0.916	0.579	0.086
0.904	0.556	0.090
0.889	0.569	0.088
0.861	0.548	0.091
0.857	0.585	0.085
0.818	0.592	0.085
0.816	0.460	0.109
0.774	0.511	0.098
0.747	0.468	0.107
0.747	0.521	0.096
0.732	0.558	0.090
0.655	0.537	0.093
0.646	0.404	0.124
0.577	0.480	0.104
0.504	0.530	0.094
0.490	0.470	0.106
0.452	0.447	0.112
0.411	0.521	0.096
0.386	0.440	0.114
0.383	0.459	0.109
0.330	0.451	0.111
0.318	0.429	0.116

Appendix E

SAMPLE CALCULATIONS

The following sample calculations illustrate how all calculated values were obtained. The data used has been taken from the measured methanol/water data presented in Tables A1.1 and A1.2 of Appendix A.

Once steady state was achieved, liquid samples were taken from sample ports located just below the packed bed, s_1, and at the bottom of the condensate hold-up container, s_2. The samples were analyzed using gas chromatograph (GC). The inlet and outlet cooling water temperatures, reboiler temperature, cooling water and reflux rotameter readings were also recorded. The following data were obtained:

GC Output: Area % MeOH @ s_2 = 95.363
Area % MeOH @ s_1 = 86.164

Cooling water: T_{in} (°C) = 9.70
T_{out} (°C) = 61.80
RR = 25.0 %

Reboiler: T_{reb} (°C) = 77.20

Reflux: RR = 60.0 %

Area % methanol was converted to weight % methanol using the calibration equation given below:

$$Wt\,\%\,MeOH = 0.9872\,(Area\,\%\,MeOH) + 0.4686$$

$$Wt\,\%\,MeOH = 0.9872\,(95.363) + 0.4686 = 94.611$$

Wt % MeOH @ s_2 = 94.611
Wt % MeOH @ s_1 = 85.530

Using the molecular weights for methanol and water, 32.04 g/mol and 18.02 g/mol, respectively, the mole fractions of methanol above and below the packed bed were calculated:

$$Mole\%MeOH = \frac{\frac{Wt\%MeOH}{MW\,MeOH}}{\frac{Wt\%MeOH}{MW\,MeOH} + \frac{(100 - Wt\%MeOH)}{MW\,H_2O}}$$

$$Mole\%MeOH = \frac{\frac{94.611}{32.04}}{\frac{94.611}{32.04} + \frac{(100 - 94.611)}{18.02}} = 90.8$$

Mole fraction of MeOH @ $s_2 = 0.908$ (x_{Top})

Mole fraction of MeOH @ $s_1 = 0.769$ (x_{Bottom})

All equations used to determine the system properties were functions of mole fraction and all system properties were calculated based on the top composition.

The cooling water flow rate was calculated using the following rotameter calibration equation:

$$M_{cooling} = 3.9053x10^{-4}(RR) = 3.9053x10^{-4}(25.0) = 9.7633x10^{-3}\ kg/s$$

The reflux flow rate was first determined in terms of mass flow rate of water using the rotameter calibration equation given below:

$$M_{reflux} = 2.4947x10^{-5}(RR) - 9.9915x10^{-5}$$

$$M_{reflux} = 2.4947x10^{-5}(60.0) - 9.9915x10^{-5} = 1.40x10^{-3}\ kg_{H_2O}/s$$

The reflux flow rate was then converted to mass flow rate of mixture using the following equation:

$$M_{reflux} = \sqrt{\frac{(\rho_{float} - \rho_L)\rho_L}{(\rho_{float} - \rho_{water})\rho_{water}}}$$

where ρ_{float}, ρ_L, ρ_{water} are the float density, mixture liquid density at the reflux temperature (62 °C) and water density at 25 °C (corresponding to 2650 kg/m^3, 752 kg/m^3 and 983 kg/m^3, respectively).

$$M_{reflux} = \sqrt{\frac{(2650-752)752}{(2650-983)983}} = 1.30x10^{-3}\ kg_{mixture}/s$$

In order to determine the *f*-factor, calculation of the superficial vapor velocity was required:

$$Ug = \frac{M_{reflux}}{\rho_V\ A_c}$$

where A_c is the cross sectional area of the column (A_c = 0.00434 m^2) and ρ_V is the saturated mixture vapor density (ρ_V = 1.024 kg/m^3).

$$Ug = \frac{1.4x10^{-3}}{1.024 \cdot 0.00434} = 0.29\,m/s$$

The *f*-factor was then calculated using the equation given below:

$$f-factor = Ug\sqrt{\rho_V} = 0.29 \cdot \sqrt{1.024} = 0.30\ (m/s)(kg/m^3)^{0.5}$$

To determine packing efficiency the number of theoretical trays, N_T, must first be calculated. This requires calculation of the relative volatility at the top and bottom of the packed bed. The relative volatilities were calculated using equilibrium data.

$$\alpha_{Top} = \frac{\frac{y^*}{x_{Top}}}{\frac{(1-y^*)}{(1-x_{Top})}} \qquad \alpha_{Bottom} = \frac{\frac{y^*}{x_{Bottom}}}{\frac{(1-y^*)}{(1-x_{Bottom})}}$$

Where y^* is the vapor concentration that is in equilibrium with the liquid concentration, x, which was obtained using the following equation:

$$y^* = -20.8777x^6 + 72.4933x^5 - 100.3125x^4 + 70.9239x^3 - 27.4288x^2 + 6.1815x + 0.0136$$

$$y^*_{top} = -20.8777(0.908)^6 + 72.4933(0.908)^5 - 100.3125(0.908)^4 + 70.9239(0.908)^3 - 27.4288(0.908)^2 + 6.1815(0.908) + 0.0136 = 0.963\,(mole\ fraction)$$

$$y^*_{bottom} = -20.8777(0.769)^6 + 72.4933(0.769)^5 - 100.3125(0.769)^4 + 70.9239(0.769)^3 - 27.4288(0.769)^2 + 6.1815(0.769) + 0.0136 = 0.897(mole\ fraction)$$

$$\alpha_{Top} = \frac{\frac{y^*}{x_{Top}}}{\frac{(1-y^*)}{(1-x_{Top})}} = \frac{\frac{0.963}{0.908}}{\frac{(1-0.963)}{(1-0.908)}} = 2.66$$

$$\alpha_{Bottom} = \frac{\frac{y^*}{x_{Bottom}}}{\frac{(1-y^*)}{(1-x_{Bottom})}} = \frac{\frac{0.897}{0.769}}{\frac{(1-0.897)}{(1-0.769)}} = 2.63$$

The Fenske (1932) Equation was then used to determine the number of theoretical stages, N_T:

$$N_T = \frac{\log\left[\left(\frac{x_{Top}}{1-x_{Top}}\right)\left(\frac{1-x_{Bottom}}{x_{Bottom}}\right)\right]}{\log\left(\sqrt{\alpha_{Top}\alpha_{Bottom}}\right)}$$

$$N_T = \frac{\log\left[\left(\frac{0.908}{1-0.908}\right)\left(\frac{1-0.769}{0.769}\right)\right]}{\log\left(\sqrt{2.66 \cdot 2.63}\right)} = 1.119$$

Finally, height equivalent to a theoretical tray, HETP, was calculated by knowing the packing height, z (z = 0.0508 m):

$$HETP = \frac{z}{N_T} = \frac{0.0508}{1.119} = 0.045\,m$$

Murphree tray efficiency data, obtained from Syeda (2002), were converted to HETP (tray) using the following equation:

$$HETP\,(tray) = 100 * \frac{S}{E_{MV}}$$

where S (S = 0.050 m) is the tray spacing in meters and E_{MV} is the Murphree tray efficiency in percent (E_{MV} = 75%).

$$HETP\,(tray) = 100 * \frac{0.050}{75} = 0.066\,m$$